Neural Network Modelling and Analysis of Serotonergic System

Chandan Kumar Behera

Faculty of Computing, Engineering, and the Built Environment,

Ulster University

A dissertation submitted in partial fulfilment of the requirements for the degree of

DOCTOR OF PHILOSOPHY

November, 2020

I confirm that the word count of this thesis is less than 100,000 words excluding the title page, contents, acknowledgements, summary, abstract, abbreviations, footnotes, diagrams, maps, illustrations, tables, appendices, and bibliography.

To he who has given me the dreams to look forward to.

Table of Contents

List of Figures

List of Tables

Acknowledgements

This work was carried out at the Intelligent Systems Research Centre (ISRC), School of Computing, Engineering and Intelligent Systems, Faculty of Computing, Engineering and the Built Environment, Ulster University (UU). I owe immense gratitude to my supervisors, Dr. KongFatt Wong-Lin and Prof. Girijesh Prasad, who provided excellent supervision, so that the work became enjoyable to continue. KongFatt guided me starting from the basics of neuroscience to writing up the thesis. Girijesh devoted his generous hours in teaching and advising, every time with extreme patience and wisdom. I would like to thank them for their scientific and personal encouragements and guidance they have given me over the years.

Moreover, I would like to express my gratitude to Prof. Nik Kasabov, who kindly agreed to take over as the Internal Examiner of this thesis, despite his immense workload. I am greatly indebted to all my external collaborators for their significant contributions and help in my work. I want to especially thank Prof. Da-Hui Wang for his valuable guidance during the initial phase of my Ph.D. and for his help in dynamical systems theory. I would like to express my appreciation for my University of Oxford collaborator, Prof. Trevor Sharp for sharing his lab's data, hosting my visits in his lab, and helping to contribute to my research work. I also thank Ruairi O'Sullivan from the Sharp lab for his help in the recording of the electrophysiological data which I have used for my analyses.

Within the ISRC, I wish to express my gratitude to Dr. Jose Sanchez-Bornot for being available and sharing his knowledge in statistical analyses. I also thank Dr. Alok Joshi for sharing his insights in neuroscience. In addition, I thank my fellow lab mates at the ISRC centre, especially Nadim Atiya, Niamh McCombe, Sujit Roy, and Dheeraj Rathee who provided great working atmosphere in the lab so that I can fully concentrate on my research. I sincerely thank Prof. Liam McDaid for his constructive comments on my earlier work, particularly my Ph.D.'s 100-day and Confirmation reports. Special thanks go to Mrs. Hazel Campbell, the administrative officer at UU who has regularly helped me from the

moment I first arrived at UU. With my numerous travel plans attending conferences, meetings and trainings, I thank Ms Louise Gallagher for kindly providing the great research administrative support.

Last but not least, I wish to thank my family and, above all, the Almighty for setting me on this path. I could never have achieved this stage without their indefatigable support.

Abstract

This Ph.D. thesis contributes towards the neural computational modelling and analysis, and functional connectivity analysis of the serotonergic system. The thesis starts with a concise review of the known neurobiological functions of the serotonergic system. Different experimental measurements of the system are described, with focus on electrophysiological, optogenetic and voltammetry recordings. Further, the neuronal signalling of serotonergic systems under reward and punishment tasks are described. This is followed by a brief review on computational modelling of the serotonergic system, with focus on mechanistic and biologically based models. Then, signal processing and data analytical approaches of electrophysiological data are discussed. While reviewing these, research questions are formulated regarding the serotonergic system. It is amply clear from the reviews that, it is not known whether neural circuits encompassing serotonergic neurons can be degenerate (i.e. different structures performing the same functions), and how population of serotonin neurons in the dorsal raphe nucleus interact with themselves and with the cortex.

Following the literature review are three original contributing chapters. In the first contributing chapter, biologically based mean-field network models of serotonergic and dopaminergic neural interactions under reward and punishment tasks are developed and simulated to evaluate the possibility of network structure degeneracy. Non-serotonergic and non-dopaminergic neural populations are considered to evaluate multiple possible indirect serotonin-dopamine connections. The modelling results reveal the possibility that serotonin-dopamine neural circuits can be degenerate, at least under reward/punishment tasks. In the next contributing chapter, the stability of these degenerate neural circuits under tonic and phasic activity modes are evaluated using dynamical systems theory. The analyses show that all the considered degenerate neural circuits are stable in both activity modes. In the third contributing chapter, signal processing and analysis are performed on electrophysiological data (neuronal spike trains and electrocorticography, ECoG) from experimental collaborators. In particular, analyses were conducted on ECoG

activities in the frontal cortices and the visual cortex, and neuronal firing activities from the dorsal raphe nucleus (DRN), a main source of serotonergic neurons. Then coherence-based method is used to identify the functional connectivity among simultaneously recorded neurons in the DRN, and between the DRN neuronal activity and the ECoG activity. The coherence analyses show that interactions of the DRN neurons are generally weak and sparse, and that the slow-firing DRN neurons (putative serotonergic neurons) exhibit relatively stronger interactions with each other. Further, unlike the strong corticocortical ECoG interactions, the DRN neuronal to ECoG interactions are generally weak, and that slow, regular firing DRN (putative serotonergic) neurons have relatively stronger interactions with the right frontal ECoG activity. Finally, this thesis concludes with a discussion on all the chapters and proposed future work.

Note on access to contents

I hereby declare that with effect from the date on which the thesis is deposited in the Research Office of Ulster University, I permit:

The librarian of Ulster University to allow the thesis to be copied in whole or in part without reference to me on the understanding that such authority applies to the provision of single copies made for study purposes or for inclusion within the stock of another library.

The thesis to be made available through the Ulster Institutional Repository and/ or EThOS under the terms of the Ulster eTheses Deposit Agreement, which I have signed.

IT IS A CONDITION OF USE OF THIS THESIS THAT ANYONE WHO CONSULTS IT MUST RECOGNISE THAT THE COPYRIGHT RESTS WITH THE AUTHOR AND THAT NO QUOTATION FROM THE THESIS AND NO INFORMATION DERIVED FROM IT MAY BE PUBLISHED UNLESS THE SOURCE IS PROPERLY ACKNOWLEDGED.

……..... …07.11.2020.

Chandan Kumar Behera Date

Chapter 1
Introduction

The human brain consists of brain cells (neurons) and synapses, constituting neural networks or circuits (Bear et al., 2020). Interactions within local and global neural networks help to mediate multiple brain functions to allow perceptual, cognitive and emotional processing, and behavioural output (Bear et al., 2020; Fröhlich, 2016).

Neural networks are known to be adaptive, depending on the environment and context, allowing the organism harbouring the brain to survive and improve its well-being (Bear et al., 2020; Leotti et al., 2010). Despite this ability, changes in neural networks based only on learning cannot lead to sufficiently fast optimal adaption of novel changes in the environment. This would require alternative mechanism for fast re-configuration of functional network even with the same underlying network structure.

A solution is to have degenerate neural networks, i.e. they consist of different elements and/or structure while performing the same function or yielding the same output (Cropper et al., 2016). However, identifying which degenerate network(s) to "tap" into or activate (or deactivate) would require regulation from endogenous brain chemicals called neuromodulators (Cropper et al., 2016; Marder et al., 2014), which have been shown to modulate neuronal excitability, synaptic efficacy, and hence, network configurations (Kaczmarek and Levitan, 1987; Marder, 2012). Some of these are mediated through their influence on intracellular signalling and gene transcriptions, which controls their neurotransmitter releases and receptors. There are many types of neuromodulators in the brain, and the more highly studied neuromodulators include serotonin, dopamine, norepinephrine (or noradrenaline), acetylcholine, orexin (or hypocretin) and histamine (Halbach and Dermietzel, 2006). These neuromodulator systems are well preserved phylogenetically, and hence influential on neural information processing and behaviour not only in primates but also in more primitive life-forms such as nematode.

In recent years, the serotonergic and dopaminergic systems have recently been studied intensely using state-of-the-art experimental methods (Boureau and Dayan, 2011; De Deurwaerdère and Di Giovanni, 2017; Di Giovanni et al., 2009; Fischer and Ullsperger, 2017). These have led to revealing more detailed information regarding the structure and function of these systems and their underlying constituents (e.g. specific neuronal types). However, despite that, there is still no clear consensus regarding the interactions between these the serotonergic and dopaminergic systems. Moreover, it is unclear whether the neural circuits encompassing the sources of neuromodulators such as serotonin- and dopamine-producing neurons, and their interactions can themselves be degenerate. If this is so, then perhaps stable neuromodulator influences on targeted neural circuits can be achieved. Further, it is still not completely known how the local population of neurons in the serotonergic system together communicate with targeted brain regions such as the cortex.

1.1. Aims and outline of the thesis

This thesis aims to contribute towards the computational modelling, mathematical analysis, and functional connectivity analysis of the serotonergic system. In particular, based on neurobiological data, the serotonergic and dopaminergic systems' interactions will be computationally modelled and the level of degeneracy of these interactions will be systematically investigated. For any set of degenerate interactions, their network stability will be mathematically analysed using dynamical systems theory. Data collected from experimental collaborators will be analysed to uncover the interactions between neurons within the serotonergic system, and their relationships with neural activities in different cortical regions. This is done using coherence based functional connectivity method.

Three contributing chapters (Chapters 4, 5 and 6) will be discussed. These chapters are based on the authors original research works during the research programme, which led to several conference presentations and publications, conference/meeting/travel awards, a manuscript submitted to a journal (Chapters 4 and 5), a paper published and presented at a conference and a manuscript currently in preparation (Chapters 6). Overall, the thesis is organised as follows.

In Chapter 2, the essential literature on the neurobiological functions of the serotonergic system will be discussed. Various types of measurements of the system will also be outlined, although the focus is on electrophysiological, optogenetic and voltammetry recordings. In particular, the neurophysiological and neurochemical identities and neuronal signalling of serotonergic neurons under reward/punishment tasks will be discussed. Interactions with other brain systems will also be discussed, with a focus on the dopaminergic system and the cortex. Importantly, limitations of our current understanding of these interactions and their diversity will be discussed and to be addressed in Chapters 4-6.

In Chapter 3, computational modelling and analytical methods will be discussed. In the first part of this chapter, several types of computational models of the serotonergic system will be discussed, focusing on mechanistic biologically based models. Importantly, the use of a specific modelling approach, the mean-field modelling approach, will be elaborated (for subsequent use in Chapters 4 and 5). Dynamical systems theory is then introduced for investigating stability in neural networks (for subsequent use in Chapter 5). In the second part of this chapter, signal processing and analytical approaches of multi-neuron electrophysiological data and electrocorticographic (ECoG) data, and their interpretations, will be discussed. These methods will be used to analyse new data obtained from a collaborator's lab.

In Chapter 4, mechanistic biologically based neural network models of serotonergic and dopaminergic interactions are developed. In particular, the modelling focuses on the dorsal raphe nucleus (DRN) and ventral tegmental area (VTA) brain regions, which are major sources of serotonin (5-HT) producing neurons and dopamine (DA) producing neurons, respectively. This is achieved by incorporating in the computational models not only 5-HT and DA neurons, but also DRN glutamatergic, DRN GABAergic and VTA GABAergic local (inter)neurons. Hence, direct and indirect connections between the 5-HT neurons in the DRN and DA in the VTA neurons are modelled. The modelling shows that most of the diverse and distributed neuronal activity profiles under reward and aversive conditions, observed in separate experimental studies, can be recapitulated by individual computational models. This provides evidence regarding the possibility of degeneracy within neuromodulator

circuits. However, not all experimental observations can be captured by single models, hence suggesting the possibility of multiple parallel DRN-VTA circuits. Under the same set of conditions, the modelling also shows that there are several (at least 84) different types of DRN-VTA degenerate circuit models. Using computational modelling to mimic dopamine receptor (D2) agonist administration, some of these degenerate DRN-VTA models are then shown to be distinguishable, especially in rewarding condition – a testable prediction.

In Chapter 5, dynamical systems theory is used to understand whether the degenerate DRN-VTA circuit models in Chapter 4 are dynamically stable. First, detailed mathematical derivation for the steady state(s) or fixed point(s) of each network configuration/model is provided. Second, mathematical derivations of the Jacobian matrix and related eigenvalues at the steady state(s) are provided. Then, the steady state values and associated eigenvalues are computed. It is found that all the degenerate model architectures are dynamically stable. This strengthen the findings in Chapter 4, that the 84 identified degenerate DRN-VTA circuit models are all stable in both phasic and tonic states. In particular, degenerate circuit models with fast 5-HT-to-DA connections, mediated by 5-HT_3 receptors, are found to be more stable than the degenerate circuit models without such fast receptors.

In Chapter 6, multi-neuron firing activities of the DRN recorded from several live mice from a collaborator's lab is described. Then coherence-based functional connectivity method is applied to the diverse and noisy data. The results reveal that, at least for this frequency-based approach, the DRN neurons are generally found to be weakly and sparsely correlated with each other. Slow-firing DRN neurons with regular and irregular spiking characteristics, potentially serotonergic neurons, have relatively stronger connectivity than neurons with other spiking characteristics. Data from ECoG recording of three cortical regions (left frontal, right frontal, and right occipital cortex) in several live (anaesthetized) mice from the collaborator's lab is described. Then, coherence-based functional connectivity between slow-wave oscillatory ECoG activities and DRN neuronal firing rate activities are studied. The results show that slow-firing DRN neurons with regular and irregular spiking characteristics are more likely to have stronger frequency-based relationships with the ECoG signals,

especially the frontal cortex. Moreover, specific types of DRN neurons seem to have relatively stronger connectivity with each other and with the frontal cortex.

Chapters 4-6 have led to a series of publications, preprints and conference presentations/papers (Behera at al, 2017; O'Sullivan et al., 2018; Schweimer et al., 2018; Behera et al., 2018; Behera et al., 2019a; Behera et al., 2019b; Behera et al., 2020; Behera et al., 2020).

In Chapter 7, a summary of the work presented in the previous chapters is discussed and new directions for future work are proposed.

Chapter 2
Neurobiology and functions of serotonergic system

This Chapter is a concise review of the essential neurobiology and functionals of the serotonergic system. Parts of the review, especially in section 2.3, are published in a conference paper and archived in a pre-print manuscript.

2.1. Neurobiology and functions of serotonergic system

Serotonin (5-hydroxytryptamine; 5-HT) is a class of endogenous neurochemicals or neurotransmitters, called neuromodulators, and plays a major role in modulating a broad range of physiological and behavioural processes including learning and memory, decision-making, mood, appetite, sleep, pain and motor activity (Müller, Christian P., 2010; Müller and Cunningham, 2020; Smythies, 2005). 5-HT is perhaps one of the oldest neurotransmitters in vertebrates and invertebrates. Dysfunctions in 5-HT systems have been associated with disorders in the nervous systems including psychiatric illnesses (e.g. anxiety disorders, depression and schizophrenia) and behavioural impulse related disorders (e.g. obsessive control, attention deficit disorder, substance abuse, physical violence) Müller and Cunningham, 2020). For further details, the reader is referred to other more comprehensive reviews (Jacobs and Azmitia, 1992; Müller, Christian P., 2010; Muller and Cunningham, 2020; Muller and Jacobs, 2009)In the brain, the majority of 5-HT originates from 5-HT-producing neurons residing in the dorsal and median raphe nuclei (DRN and MRN, respectively) located in the midbrain, the deep region of the brain (Figure 2.1) (Müller and Cunningham, 2020). Although most parts of the brain are affected or within the vicinity of 5-HT innervation, this thesis will focus on the DRN, given the latter's extensive projections to the forebrain, which is known for its important role in various cognitive

and emotional processing, and behaviours (Azmitia and Segal, 1978; Azmitia and Gannon, 1986;; Müller and Cunningham, 2020).

The DRN consists of about 8000 and 91000 5-HT neurons in mice and humans, respectively. This represents around 30-56% of 5-HT neurons in the brain, depending on the species (Jacobs and Azmitia, 1992; Thévenot et al., 2003). The DRN also contains neurons producing gamma aminobutyric acid (GABA), catecholamines (dopamine, noradrenaline/norepinephrine), thyrotropin releasing hormone, growth hormone, growth hormone-releasing hormone, nitric oxide, substance P, galanin, cholecystokinin, neurotensin, somatostatin, vasoactive intestinal peptide, leu-enkephalin, metenkephalin, gastrin and glutamate, potentially in combination with a variety of neuropeptides, such as corticotropin-releasing factor (Fu et al., 2010; Jacobs and Azmitia, 1992; Köhler and Steinbusch, 1982; Michelsen et al., 2007). Moreover, there is mounting evidence of co-transmissions of 5-HT with glutamate (El Mestikawy et al., 2011; Prouty et al., 2017; Sengupta et al., 2017; Trudeau and El Mestikawy, 2018; Wang et al., 2019), but their computational principles remain to be fully identified. Thus, the DRN consists of a rather complex mix of neurochemicals.

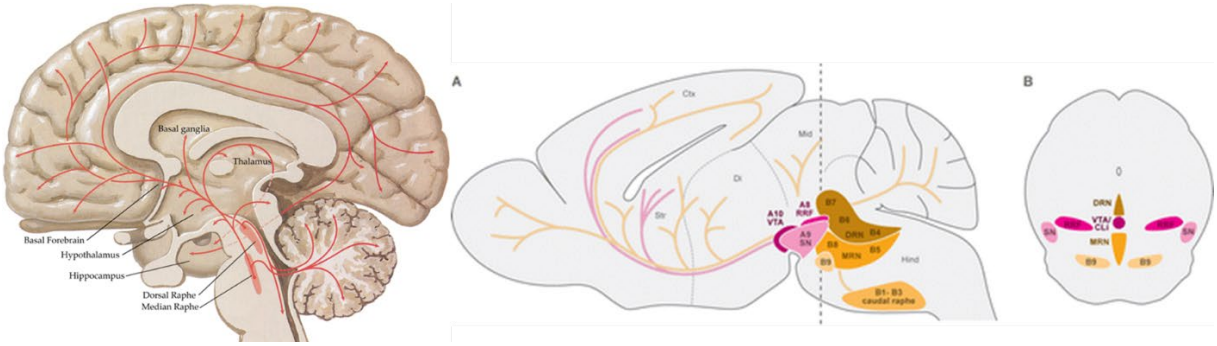

Figure 2.1. Location and projection of the dorsal and median raphe nuclei in the human and rodent brains. Sagittal view of the human (left) and rodent (right, A) brains; (right, B): coronal view of rodent brain. Dorsal raphe nucleus (DRN). Median raphe nucleus (MRN). Left: Adopted with permission from Scarr et al. (2013). Right: Adopted with permission from (Niederkofler et al., 2015).

To add to the complexity, it is now known that there are seven general 5-HT receptor classes, 5-HT1-7, which are further divided into a total of 14 different 5-HT receptor subtypes (5-HT1A5-HT1B, 5-HT1D, 5-HT1E, 5-HT1F, 5-HT2A, 5-HT2B, 5-HT2C, 5-HT3, 5-HT4, 5-HT5A, 5-HT5B, 5-HT6, 5-HT7) (Palacios, 2016; Sharp and Barnes, 2020). All of them are metabotropic based G-protein coupled receptors (GPCRs)

except 5-HT3 receptors which comprise of fast ligand-gated ion channels(Beliveau et al., 2017; Hoyer et al., 1994). An exemplar example is the prefrontal cortex, in which different subtypes of 5-HT receptors are distributed differentially across the cortical layers (Celada et al., 2001; Puig and Gulledge, 2011). With regards to neuronal circuits, these 5-HT receptors can modulate neuronal firing and synaptic changes, which in turn can influence the release of several other neurotransmitters, which include glutamate, dopamine, GABA, epinephrine, norepinephrine, and acetylcholine, as well as several hormones, including prolactin, oxytocin, cortisol, vasopressin, corticotropin, and substance P, among others (Müller and Cunningham, 2020). This is done mainly through intracellular second messenger mechanisms (Masson et al., 2012; Palacios, 2016; Wong-Lin et al., 2017; Sharp and Barnes, 2020; Joshi et al., 2020).

Several natural and pharmaceutical compounds acting on the receptors of 5-HT result in a variety of behavioural responses. In fact, this is the major driving force for 5-HT research over the decades – its use as pharmacological therapeutics for psychiatric illnesses and as psychedelics. For instance, the psychedelic effects of lysergic acid diethylamide (LSD; also known as acid) arise through its binding actions to some 5-HT receptors (Muller and Jacobs, 2009). It is also known that acute administration of selective serotonin reuptake inhibitor (SSRI) or monoamine oxidase inhibitor can enhance 5-HT function to treat clinical depression (Berendsen and Broekkamp, 1994; Müller and Cunningham, 2020), while acute decreases of 5-HT functions via autoreceptors like 5-HT1A or 5-HT1B, are anxiolytic (McDevitt and-Neumaier, 2011). More recently, due to the multiple secondary pathways that 5-HT-receptor based drugs can target, these drugs are also suggested for treating neurological diseases such as Parkinson’s disease and Alzheimer’s diseases (Joshi et al., 2020; Ohno et al., 2015).

Finally, 5-HT might affect different receptor subtypes differently, yet the second messenger pathways mediated by these receptor subtypes might cross paths and influence each other (Joshi et al., 2020; Wong-Lin et al., 2017). Different 5-HT receptor subtypes are also distributed differently across different brain structures (Masson et al., 2012; Muller and Jacobs, 2009; Müller and Cunningham, 2020).

2.2. Measuring and quantifying serotonergic activities

To understand serotonergic functions, various forms of serotonergic activities have been measured and quantified. Electrophysiological properties are fundamental towards understanding neurobiological functions. There are several ways to measure the electrophysiological properties of 5-HT neurons. For many years, the most basic type of measurement is the use of microelectrodes to record the neuronal spiking activity and its derived electrophysiological measures, e.g. neuronal firing rate and coefficient of variation (CV) (Aghajanian et al., 1978, 1970; Allers and Sharp, 2003; Dayan and Abbott, 2001; Mlinar et al., 2016; Sprouse and Aghajanian, 1987). So far, it has been found, particularly in anesthetized brain and brain slices, that most DRN 5-HT neurons exhibit clock-like firing properties, with a smaller proportion of neurons with bursting properties (Hajos et al., 1995; Hajós et al., 1996).

To identify whether the electrophysiologically recorded neurons are 5-HT-containing, traditional methods include classification based on broad actional potentials (~1.8 ms), slow after-hyperpolarization (AHP) (with an amplitude of around ~10-20 mV and slow recovery over ~200-800 ms), and slow tonic spiking/firing rate (between ~0.5 Hz to 5 Hz, depending on brain state) (Aghajanian and Vandermaelen, 1982; Hajós et al., 1996; Allers and Sharp, 2003; Kirby et al., 2003; Judge and Gartside, 2006; Hajos et al., 2007; Ranade and Mainen, 2009; Cohen et al., 2015; Li et al., 2016). However, when it comes to awake or behaving animals, there exist a wide variety of spiking patterns from DRN neurons (e.g. Ranade & Mainen, 2009) and it is not immediately clear which ones can be classified as 5-HT neurons without more precise labelling (see below).

Another classical method to identify 5-HT neurons is through drug-mediated enhancement (via “agonists”) or inhibition (via “antagonists”) of 5-HT1A autoreceptors since it is known that 5-HT neurons can self-regulate their activities through such “autoinhibitions”(Sprouse and Aghajanian, 1987;McDevitt and Neumaier, 2011). However, this is difficult in more intact brains as these drugs do not distinguish 5-HT1A autoreceptors from heteroreceptors or post-synaptic receptors – neuronal firing rate

enhancement of suppression could be due to neuronal circuitry feedback effects and not purely to single neuronal effects.

Such issues can partially be resolved using more accurate labelling such as juxtacellular recording technique which labels the neuron recorded extracellularly (Duque and Zaborszky, 2006; Pinault, 1996), which validates that the electrophysiological characteristics between the classical regular-spiking and bursting 5-HT neurons are quite similar (Kirby et al., 2003). In fact, some DRN neurons even exhibit both regular and spike “doublets” within a single recording (Hajós et al., 1996). Juxtacellular labelling method also shows that bursting or slow AHP neurons in DRN are reliably identified to be 5-HT-containing neurons (Kirby et al., 2003; Hajós et al., 2007). However, the neuronal electrophysiological properties are found to be generally heterogeneous across 5-HT and non-5-HT neurons (Calizo et al., 2011; Kirby et al., 2003; Marinelli et al., 2004). Importantly, it should be noted that these experiments are neither definitive nor convenient during *in vivo* preparations.

At the neuronal population level, DRN activities can be measured based on local field potentials or calcium imaging (Kocsis et al., 2006; Li et al., 2016; Ren et al., 2018). However, the use of multi-electrode arrays (MEA) in brain slice tissues and multi-unit recordings in alive/behaving animals have yet to be utilized as much in 5-HT/raphe research. My experimental collaborators have recently performed single electrode, tetrode and ter 4multi-unit recordings in the DRN (see Chapter 6). However, it should be noted that each electrode may detect multiple cells and also that many electrodes may record the spiking activity of the same cell. Hence, the typical approach is to utilise spike sorting algorithms and methods (e.g. Lefebvre et al., 2016). We will devote a concise discussion on these algorithms and methods in Chapter 3. Analysis of such data may shed light on the effective or functional connectivity among neurons. To elucidate the structural connectivity between neurons, anterograde or retrograde tracing have traditionally been used (Muzerelle et al., 2016).

Optogenetics is a relatively recent approach that not only could precisely label genetically similar neurons, including 5-HT neurons, but also study the causal relationship of these neurons in (transgenic) animal behaviour by direct precise perturbation of these labelled neurons via specific light wave frequency (Bi et al., 2006; Boyden, 2005; Guru et al., 2015; Kim et al., 2017; Lima and Miesenböck, 2005;

Marcinkiewcz et al., 2016; Zhang et al., 2015). The chemical equivalent to optogenetics, chemogenetics (Roth, 2016), has also been developed, which involves designed receptors exclusively activated by designer drugs (DREADDS), i.e. drugs targeting specific receptor-tagged neurons.

The combination of optogenetics/chemogenetics approach with other complementary methods can often lead to deeper insights into the neuronal circuit function and behaviour (Kim et al., 2017; Marcinkiewcz et al., 2016; Niederkofler et al., 2016; Ogawa et al., 2014; Pollak Dorocic et al., 2014; Ren et al., 2018). These often reveal another layer of complexity in the neurobiology, such as heterogeneity and mixed functions. More recent work using molecular genetic, genomic and functional methods has also indicated that the electrochemical, morphological, anatomical and neurochemical properties of 5-HT neurons are not homogenous in the raphe (Okaty et al., 2019; Ren et al., 2019).

In sum, various characteristics and heterogeneity of DRN neuronal activity have been reported in recent literature (Dorocic et al., 2014; Ogawa et al., 2014; De Deurwaerdère and Di Giovanni, 2017; Ogawa and Watabe-Uchida, 2018; Okaty et al., 2019; Ren et al., 2019, 2018; Müller and Cunningham, 2020). Firstly, DRN neurons are observed to respond differently to various external (and internal) events (rewards, punishments, sensory stimuli, etc.), which suggests that afferent inputs to the DRN are wide in range and variety. Secondly, different populations of DRN neurons (e.g. residing in different spatial locations of the raphe) may receive different inputs from other brain regions, thus, leading to differential responses. Thirdly, there are different sub-types of neurons, including 5-HT neurons in the raphe, which may respond differently to events such as rewards and punishment. Some of these will be discussed in the next subsection.

To complete our discussion, it should first be noted that higher (e.g. 5-HT) neuronal firing rate often leads to higher transmission of extracellular (e.g. 5-HT) neurotransmitters (Bunin et al., 1998; Bunin and Wightman, 1998; Hashemi et al., 2009; Dankoski and Wightman, 2013), which can in turn modulate the targeted neurons and circuits. To evaluate the amount of release of extracellular 5-HT neurotransmitters, we can directly measure it using *in vivo* microdialysis and *in vitro* high-performance liquid chromatography (HPLC), with time resolution in the minutes

(Szeitz and Bandiera, 2018; Yang et al., 2013) or indirectly but with much higher temporal resolution (in subseconds) using (fast-scan) voltammetry method (Dankoski and Wightman, 2013; Moran et al., 2018).

In humans, 5-HT receptors and transporters can use non-invasive specific positron emission tomography (PET) or single-photon emission computed tomography (SPECT) imaging tracers (Beliveau et al., 2017; Huang et al., 2010; Saulin et al., 2012; Scheffel et al., 1994; Spies et al., 2015; Visser et al., 2011). Also, functional magnetic resonance imaging (fMRI) has been used to detect changes in raphe activity and functional connectivity of the raphe albeit its poor (~second) temporal resolution and indirect measurement of neuronal activity (Beliveau et al., 2017, 2015; Wittmann et al., 2020).

2.3. Structural and functional relationships with other brain regions

Several studies have shown that the 5-HT system can interact with many brain regions simultaneously (e.g. amygdala, prefrontal cortex, hippocampus), forming a complex neuronal network (Dayan and Huys, 2009; Dorocic et al., 2014; Ogawa et al., 2014; De Deurwaerdère and Di Giovanni, 2017; Ogawa and Watabe-Uchida, 2018; Müller and Cunningham, 2020). The densest innervations of 5-HT outside the DRN are normally found in the substantia nigra reticulata (SNr), ventral tegmental area (VTA) and the ventral striatum, inclusive of the nucleus accumbens (NAc) (De Deurwaerdère et al., 1998; Fitoussi et al., 2013) and in terms of the cortex, the prefrontal cortex (PFC) (Celada et al., 2013).

5-HT-producing neurons from the DRN are known to innervate the cortex, providing dense projection to the frontal cortex (Celada et al., 2013). Electrical stimulation of the DRN releases 5-HT that modulates both the frequency and amplitude of cortical slow-wave oscillations in the PFC (Celada et al., 2013, 2008; Gartside et al., 2000; Totah et al., 2018) (Figs. 2.1 and 2.2). This slow-wave activity is normally present during natural sleep but can also be induced by certain anaesthetics like urethane (Crook and Lovick, 2016). It has also been found that 5-HT_{1A} receptors mediate decrease in the firing rate of fast spiking interneurons in the PFC, whereas 5-HT_{2A} receptors

mediate increase in the firing rate of fast-spiking inhibitory interneurons in the PFC (Puig et al., 2010), but overall increase the signal power of cortical slow-wave oscillations (Celada et al., 2013).

At the other end of the PFC-DRN circuit, the DRN receives several inputs from various parts of the brain (Pollak Dorocic et al., 2014; Ranade and Mainen, 2009) including from the prefrontal cortex (PFC) (Celada et al., 2013, 2001; Challis and Berton, 2015; Hajós et al., 1998; Heidbreder and Groenewegen, 2003). There are evidences that indicate the prefrontal corticoraphe projection could be mediated by glutamatergic synapses (Challis and Berton, 2015; Geddes et al., 2016). Further, high frequency stimulation of pyramidal neurons in the PFC is shown to inhibit 5-HT activities in the DRN (Celada et al., 2001; Shaw, 1981). More precise state-of-the-art optogenetic stimulation of the PFC has shown potent effects on the DRN activity and behaviour (Geddes et al., 2016; Warden et al., 2012), which may have implications in brain disorders, especially the dysfunctions in mood regulation and stress processing (Geddes et al., 2016; Srejic et al., 2016; Warden et al., 2012), as also reflected in abnormal neural activity oscillatory patterns (Basar and Guntekin, 2008).

In (Schweimer et al., 2011), it reveals that most DRN 5-HT neurons, including those with clock-like and bursting firing activities, are found to have significant coherence with cortical oscillations. Specifically, these neurons typically fire more frequently during the inactive phase (trough) of the slow cortical oscillation. Interestingly, almost 50% of the bursting 5-HT neurons do not show any significant coherence with cortical rhythms. In contrast, the non-5-HT neurons in the DRN fire at a higher rate during the active phase (peak) of the slow cortical waves. Hence, within the DRN, electrophysiologically and neurochemically distinct neuronal groups exhibit distinct relations to cortical activity.

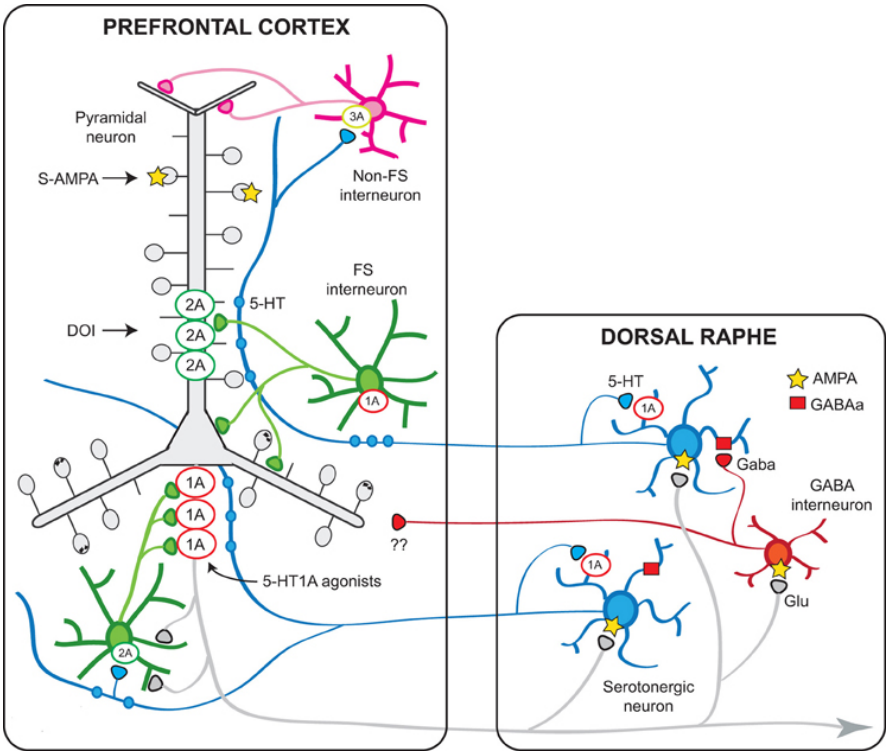

Figure 2.2. Schematic diagram of the interactions between the (medial part of the) prefontal cortex (PFC) and the dorsal raphe nucleus (DRN) (involving 5-HT1A and 5-HT2A receptors). Pyramidal neurons in the mPFC project densely to the DRN and modulate the activity of 5-HT neurons via direct and indirect influences, while 5-HT modulates pyramidal cell activity through the activation of various receptors expressed in the neocortex, of which 5-HT_{1A} and 5-HT_{2A} receptors play a major role. Obtained with permission from Pau Celada et al., 2013.

Overall, the abovementioned evidences seem to indicate a tight reciprocal relationship between the cortex, especially the PFC, and the DRN. However, most of the studies typically involved single-cell recordings and/or focused on slow-wave cortical activity. Moreover, previous studies did not take into account several cortical regions in parallel. Thus, it is not clear how the DRN neuronal population as a whole work in concert with the cortex, and how different cortical regions are comparatively associated with the DRN activity. This will be addressed in Chapter 6 of this thesis.

5-HT can also interact with other neurotransmitters, which may in turn co-modulate cognition and behaviour (Fig. 2.3a). For instance, 5-HT neurons in the DRN can interact with other neurotransmitters (e.g. orexin/hypocretin, norepinephrine/noradrenaline) regulating wakefulness and circadian rhythms (Joshi et al., 2017, 2011). Generally, based on several neurochemical, electrophysiological, genetic and pharmacological studies, 5-HT is found to promote wakefulness and

inhibit REM sleep (Monti, 2010), while also regulating the mammalian circadian clock via the suprachiasmatic nucleus (Glass et al., 2003; Sprouse et al., 2004).

A particular interest of this thesis is the investigation of the plausible direct and indirect interactions between the 5-HT neurons in the DRN and dopamine (DA) neurons in the VTA. In fact, there is increasing evidence for direct synaptic interactions between these two neuromodulators, particularly at the level of the VTA (Boureau and Dayan, 2011; De Deurwaerdère and Di Giovanni, 2017; Di Giovanni et al., 2009). At the functional level, DA and 5-HT are known to play a critical role in reward and punishment (Li et al., 2016). For example, there is strong evidence that DA neuronal activity signals reward prediction error (difference between predicted and actual reward outcome) to guide reinforcement learning (Doya, 2002). Specifically, DA neurons are phasically excited upon unexpected reward outcome or reward-predictive cues, and inhibited upon unexpected reward omission or punishment (Schultz et al., 1997; Cohen et al., 2012; Watabe-Uchida et al., 2017), although there is heterogeneity amongst DA neurons in this regard (Cohen and Uchida, 2012; de Jong et al., 2019; Kremer et al., 2020; Lammel et al., 2014, 2013; Morales and Margolis, 2017).

In comparison to DA neurons, DRN 5-HT neurons exhibit greater complexity in function, with recent studies reporting that 5-HT neuronal activity encodes both reward and punishment. For instance, Cohen et al., 2015 found that certain 5-HT neurons (labelled “Type I”) were phasically activated only by reward predicting cues, but not punishment in a classical conditioning paradigm. On the other hand, another population of 5-HT neurons (“Type II”) signalled both expected reward and punishment with sustained elevated activity towards reward outcome (Cohen et al., 2015). The latter study also found that baseline firing of Type-I 5-HT neurons was generally higher in rewarding than punishment trials, and this effect lasted across many trials, suggesting information processing over a long timescale. Moreover, DA neurons did not exhibit this property. Similar 5-HT neuronal responses to reward and punishment were reported in other rodent (Liu et al., 2014a; Li et al., 2016; Matias et al., 2017; Zhong et al., 2017) and non-human primate (Hayashi et al., 2015; Wittmann et al., 2020) studies. This differential responding of DA and 5-HT neurons to reward and punishment is not easy to reconcile within a simple model of two opposing neuromodulatory systems as proposed previously (Boureau and Dayan, 2011).

Other studies reveal further complexity in reward/punishment processing, specifically in the form of altered activity of non-5-HT/DA midbrain neurons. For example, DRN neurons utilising gamma-aminobutyric (GABA) were tonically inhibited during reward-waiting with further inhibition during reward acquisition, but phasically activated by aversive stimuli (Li et al., 2016). In contrast, GABAergic neuronal activity in the VTA exhibited sustained activity upon rewarding cue onset but no response to the presence or absence of actual reward outcome (Cohen et al., 2012). Further, other studies found that VTA GABAergic neuronal activity was potently and phasically activated by punishment outcome, which in turn inhibited VTA DA neuronal activity (Tan et al., 2012; Eshel et al., 2015). Another study showed that glutamatergic (Glu) neurons in the DRN reinforced instrumental behaviour through VTA DA neurons (McDevitt et al., 2014a).

This complexity of signalling within the DRN-VTA system in response to reward and punishment may reflect the DRN and VTA having shared afferent inputs (Ogawa et al., 2014; Dorocic et al., 2014; Beier et al., 2015; Tian et al., 2016; Watabe-Uchida et al., 2017; Ogawa and Watabe-Uchida, 2018). Another possibility is that the DRN and VTA interact with each other. Indeed, a growing number of studies have suggested that there are direct and indirect interactions among distinctive neuronal types between and within the DRN and VTA (Beier et al., 2015; Boureau and Dayan, 2011; De Deurwaerdère and Di Giovanni, 2017; Di Giovanni et al., 2009; Li et al., 2019; McDevitt et al., 2014b; Ogawa et al., 2014; Valencia-Torres et al., 2017; Wang et al., 2019; Watabe-Uchida et al., 2012; Xu et al., 2017). Taken together, information of reward and punishment signalled by neuronal activities within the DRN and VTA seems to be diverse, heterogeneous, distributed and mixed. Some of these signalling responses are illustrated in Fig. 2.3b. This led to the following questions (Fig. 2.3a). First, can these experimental findings from separate studies be reconciled and understood in terms of a single neural circuit model encompassing both the DRN and VTA? Second, can there be degenerate DRN-VTA neural circuits? Third, can these degenerate circuits, if they exist (theoretically), be identifiable, at least in principle, e.g. through pharmacological means. These questions will be addressed in Chapter 4 of this thesis. Another question would be whether the degenerate neural circuits are dynamically stable. This question will be addressed in a mathematical analysis using dynamical systems in Chapter 5.

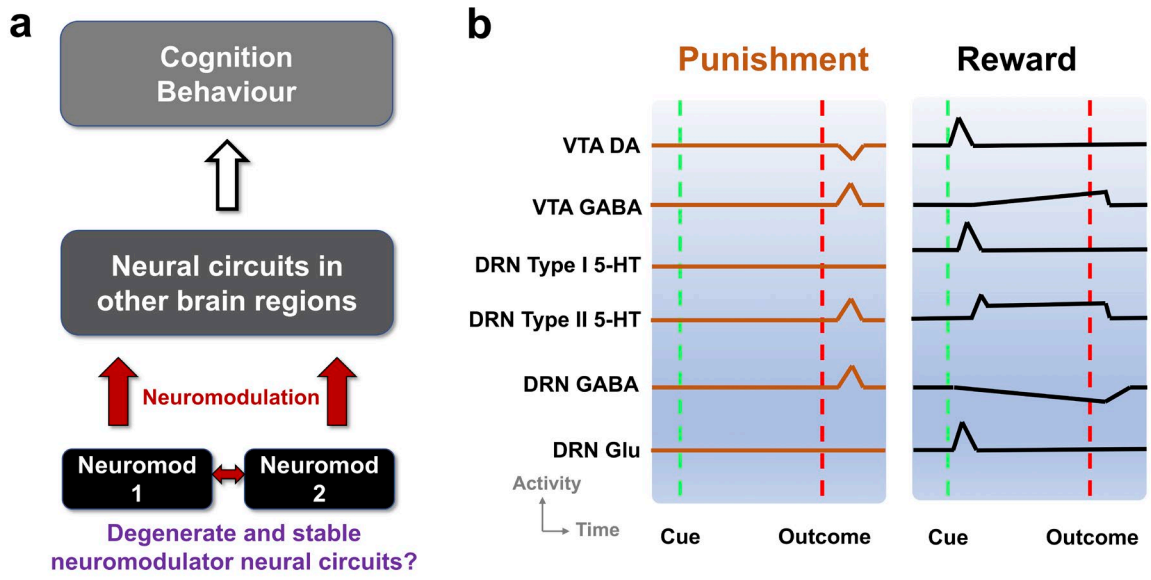

Figure 2.3 Co-modulation of neural circuits and cognition/behaviour, and potential degenerate neuromodulator circuits constrained by stereotypical signalling a, Multiple neuromodulators that influence neural circuits, cognition and behaviour. Such circuits may also be embedded within degenerate neural circuits. Neuromod: Specific neuromodulator type. **b,** Schematic of DRN and VTA activity profiles in reward (black colour lines) and punishment (orange colour lines) tasks. Activities (firing rates) aligned to timing of unexpected punishment outcome (left, vertical red dashed lines) and learned reward-predictive cue (right, vertical green dashed lines) and reward outcome (right, vertical red dashed lines). Top-to-bottom: VTA DA neural activity exhibits phasic excitation (inhibition) at reward-predictive cue (punishment) outcome (e.g. Cohen et al (2012), Tan et al. (2012)). VTA GABAergic neural activity shows phasic excitation upon punishment (e.g. Tan et al. (2012), Eshel et al. (2015)), while exhibiting post-cue tonic activity which is not modulated by the presence/absence of actual outcome (e.g. Cohen et al. (2012)). DRN Type-I 5-HT neurons shows phasic activation by reward-predicting cue (right) but not punishment (left). DRN Type-II 5-HT neurons signal punishment outcome (left) and sustained activity towards expected reward outcome (right) (e.g. Cohen et al. (2015)). DRN GABAergic neurons have phasic activation upon punishment but have tonic inhibition during waiting and reward delivery (e.g. Li et al. (2016)). DRN glutamatergic neurons deduced to be excited by reward-predicting cue, in line with VTA DA neural activation (McDevitt et al., 2014), and assumed not to respond to punishment outcome. Baseline activity for Type-I 5-HT DRN neurons are higher in reward than punishment tasks (e.g. Cohen et al. (2015)).

Chapter 3
Neural computational modelling and data analytical approaches

This chapter provides a focused review on the methodologies adopted in this thesis work in computational modelling and analysis of electrophysiological data of serotonergic system. Parts of this review are published in a conference paper and archived in a pre-print manuscript.

3.1. Computational models of serotonin neurons and neuronal networks

Computational or mathematical modelling approaches can complement experimental neuroscience approaches by providing deeper or more systemic understanding on the complex 5-HT functions. Currently, computational modelling of 5-HT systems or its functions can be categorized into two general types: probabilistic/reinforcement-learning type and neurobiologically/mechanistic type. This subsection will focus on the latter, and in particular, on computational modelling of 5-HT based neural circuits. For more comprehensive reviews on the field of computational neuromodulation and modelling serotonergic systems/functions, the reader is referred to other published reviews (Boureau and Dayan, 2011; Doya, 2002; Fellous and Linster, 1998; Wong-Lin et al., 2017).

3.1.1. Spiking and biophysical neuronal models

The basic constituent in neuronal network modelling is the neuronal model. Tuckwell and Penington (2014) developed a biophysical single-compartmental 5-HT neuronal model that included various channel currents, using the Hodgkin-Huxley formalism (Dayan and Abbott, 2001; Hodgkin and Huxley, 1990). The model could account for a variety of electrophysiological properties of 5-HT neurons (e.g. spontaneous periodic spiking, subthreshold neuronal membrane potential humps, etc.). On the other hand,

without modelling specific ion channels that describes neuronal membrane dynamics, simpler spiking neuronal models such as integrate-and-fire neuronal models can instead be used (Benuskova and Kasabov, 2010; Espinosa-Ramos et al., 2019). An even simpler spiking Izhikevich-type neuronal model, conducive for rigorous mathematical analysis and computational simulation efficiency, could still replicate the experimentally observed spiking and subthreshold membrane potential profiles of 5-HT neurons (Flower and Wong-lin, 2014; Wong-Lin et al., 2012, 2011). A similar approach was used to model 5-HT neurons using exponential integrate-and-fire neuronal model (Joshi, 2014). Tuckwell and colleagues (Tuckwell and Penington, 2014) subsequently also developed reduced 5-HT spiking neuronal models. Biophysical neuronal models of 5-HT modulation of non-5-HT neuron had also been modelled. They include the modelling of 5-HT modulation on sensory neuron and burster neuron of simple organisms(Baxter and King, 1999; Bertram, 1994; Bertram and Che, 1993) and cortical neurons (Cano-Colino et al., 2014). These often involved modelling the changes of specific ion channels.

At the neuronal microcircuit level, computational models with spiking neurons could be used to describe 5-HT targeted brain regions. For example, the leaky integrate-and-fire neuronal model was used to describe prefrontal cortical neurons modulated by 5-HT (Cano-Colino et al., 2014, 2013), without modelling 5-HT neuronal activity explicitly. Computational models of neural network type could also describe the source of 5-HT, especially neuronal microcircuit activities in the raphe. So far, there is only one model that describes the heterogeneous microcircuit activities of the DRN (Flower and Wong-lin, 2014; Wong-Lin et al., 2012, 2011). This model, constrained by known electrophysiological properties (neuronal membrane potential dynamics), could account for raphe neuronal activities in behaving non-human primates (Bromberg-Martin et al., 2010) while demonstrating the importance of fast inhibition from DRN's non-5-HT GABA to heterogeneous 5-HT neurons. The models also predicted the presence of emergent slow theta-band oscillation.

3.1.2. Neural population and mean-field models

To allow better model scalability and computational simulation efficiency, simpler population-based firing-rate or mean-field models are required. These modelling

techniques bridge from spiking neuronal network models to population firing rates (Renart et al., 2004; Wilson and Cowan, 1973, 1972; Wong and Wang, 2006). In the context of neuromodulation, sufficiently realistic population-based neural network modelling approach that takes into account the nonlinear input-output functions modulated by 5-HT, and the release-and-reuptake dynamics of the neuromodulator (including 5-HT) based on voltammetry measurements have been developed (Joshi et al., 2017, 2011). Importantly, Joshi et al. (2017) developed a general computational modelling framework to describe the interactions among multiple sources of neuromodulators. This modelling framework was subsequently adopted to model the direct and indirect interactions between 5-HT in the DRN and dopamine in the ventral tegmental area (VTA) in Chapters 4 and 5.

Specifically, the instantaneous firing rate for a (homogeneous) population of neurons can be described by:

$$\tau_i \frac{dr_i}{dt} = -r_i + F_i(I_i) \tag{3.1}$$

$$\boldsymbol{I_i = \sum_i w_{ij} r_j + I_{i,ext}} \tag{3.1}$$

where r_i is the mean firing rate for the i^{th} population, I_i is the total input current into a neuron in the i^{th} population, w_{ij} is the synaptic weight, and F_i is its (generally nonlinear) input-output (transfer) function (Wilson and Cowan, 1972). For a simple "threshold-linear" input-output (transfer) function, *F*,

$$\tau_i \frac{dr_i}{dt} = -r_i + F_i(I_i) = -r_i + [I_i - \theta_i]_+ \tag{3.2}$$

For $I_i > \theta_i$,

$$\tau_i \frac{dr_i}{dt} = -r_i + \sum_i w_{ij} r_j + I_{i,ext} \tag{3.4}$$

If we assume quasi-steady state for the neural population firing rate (e.g. when the neural system is dominated by relatively slow dynamics, as with e.g. slow

neuromodulator effects), the averaged firing rate of a population neurons, can be described, by its quasi-instantaneous activities:

$$r_i = F_i(I_i) \tag{3.5}$$

In electrophysiological experiments, the input-output functions of 5-HT and dopaminergic neurons have been observed to be approximately of the threshold-linear type (Richards et al., 1997; Crawford et al., 2010), which can be mathematically described by (Jalewa et al., 2014; Joshi et al., 2017):

$$F = g[I - I_0]_+ \tag{3.6}$$

where g is the slope of the linear function and I_0 some threshold current, and with $[I]_+ = I$ if $I \geq 0$, and 0 otherwise.

Generally, I is the summed currents which includes neuromodulator-induced currents I_x's and ionotropic receptor-based currents. A neuromodulator induced current, I_x, which can be effectively excitatory or inhibitory (depending on experimental findings), can be described by

$$\tau_x \frac{dI_x}{dt} = -I_x + \frac{k_x}{1+e^{-g_x([x]-[x]_0)}} \tag{3.7}$$

where x is some neuromodulator, τ_x the associated time constant, k_x some constant that determined the current amplitude, and constants g_x and $[x]_0$ that control the slope and offset of the nonlinear function on the right-hand-side of Equation (3.7), respectively.

The dynamics of the averaged extracellular neuromodulator concentration level $[x]$ is regulated to some extent by the release-and-uptake dynamics, and is described by:

$$\frac{d[x]}{dt} = [x]_p r_x - \frac{V_{max,x}[x]}{K_{m,x}+[x]} \tag{3.8}$$

for some neuromodulator x, where $[x]$ is the concentration of x, $[x]_p$ the release per neural firing frequency (Joshi et al., 2017), and constants $V_{max,x}$ and $K_{m,x}$ are constants determined from voltammetry measurements (see Chapter 2). We can see that the

release depends on the firing rate of neural populations containing that neuromodulator x (first term on right-hand-side of Eq. (3.8)).

This completes the closed-loop modelling from neuromodulator source activity (neural firing rates), to release and uptake of extracellular neuromodulator, which in turn affect the currents of targeted neural populations (which can include the neuromodulator source, via autoreceptors). This modelling framework can be summarised in Fig. 3.1

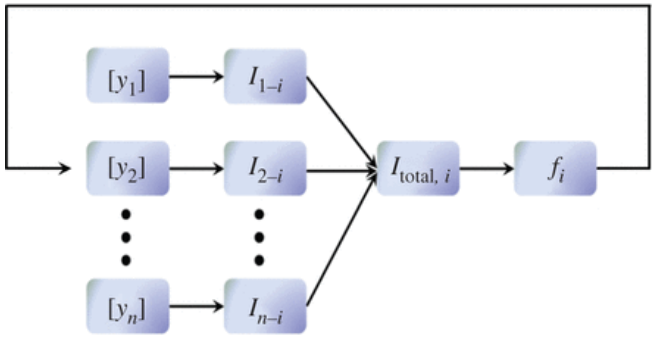

Figure 3.1. Neuromodulator circuit modelling framework. $[y_i]$ represents the concentration of i^{th} brain region. $I_{j\text{-}i}$ is the induced current at j^{th} region due to neuromodulator from i^{th} region, $I_{total,i}$ is the total current and f_i is the firing rate in the region i. Adapted from Joshi et al. (2017) with permission.

Using even simpler firing-rate models, direct and indirect connections between two sources of neuromodulators (5-HT in DRN and orexin/hypocretin in lateral hypothalamus) has also been developed (Jalewa et al., 2014). Similarly, simplified mean-field model has been developed to demonstrate that 5-HT and DA can simultaneously co-modulate prefrontal cortical rhythms in nonlinear, unintuitive and complex ways (Wang and Wong-Lin, 2013). However, there is no explicit neural circuit model that has investigated the direct and indirect interactions between 5-HT neurons in the DRN and dopaminergic neurons in the VTA especially during reward- or punishment-based conditioning tasks. Chapters 4 and 5 will address this, while aiming to reconcile various recent separate studies, especially those utilising a combination of optogenetics, electrophysiological, tracing and behavioural approaches.

3.2. Dynamical stability analysis of network models

As can be inferred above, the dynamics of the above neural network models are described by (continuous) dynamical equations, i.e. differential equations. Hence, to determine the stability of a network model essentially requires applying dynamical systems theory (Haykin, 2010; Strogatz, 2018). Specifically, how (locally) stable a dynamical system is will depend on the response(s) of the system upon (local) perturbations.

More technically, the stability of a set of dynamical equations can be determined through finding their Jacobian matrix. The eigenvalues of the Jacobian matrix at some steady state (or fixed point) determine whether the system of equations is stable, unstable, metastable, etc. In particular, if the real part of all the eigenvalues are negative, then the system is said to be stable at that fixed point.

The following steps can be used to find the Jacobian matrix for systems involving any number of variables and parameters. For illustrative purposes, supposed we have a system described by two first order coupled differential equations:

$$\dot{x} = f(x, y) \tag{3.9}$$

$$\dot{y} = g(x, y) \tag{3.10}$$

Step 1: Find the values of the fixed points x^* and y^*. This is done by setting Eqns. (3.9) and (3.10) to be zero and their solutions will provide these fixed-point values.

Step 2: For each set of fixed points (x^*, y^*), we introduce small perturbations $\hat{x}(t)$ and $\hat{y}(t)$ such that

$$x(t) = x^* + \hat{x}(t) \tag{3.11}$$

$$y(t) = y^* + \hat{y}(t) \tag{3.12}$$

Step 3: To find out how the perturbations evolve with time, substitute Equations (3.11) and (3.12) back into the original differential equations (Equations (3.9) and (3.10)) remembering that $\dot{x}^* = 0$ and $\dot{y}^* = 0$, since the fixed points are time-independent. For example, for the x variable we find

$$\dot{x} = \dot{\hat{x}} = f(x^* + \hat{x}, y^* + \hat{y}) \tag{3.13}$$

Using Taylor series expansion up to first order, we have

$$\dot{\hat{x}}(t) = f(x^*, y^*) + \hat{x}(t)\frac{\partial f}{\partial x} + \hat{y}(t)\frac{\partial f}{\partial y} + \text{higher order terms}$$

$$\Rightarrow \dot{\hat{x}}(t) = \hat{x}(t)\frac{\partial f}{\partial x} + \hat{y}(t)\frac{\partial f}{\partial y} + \text{higher order terms} \quad (3.14)$$

using the fact that, by definition, $f(x^*, y^*) = 0$. The higher order terms which have been neglected are of the quadratic and higher order terms. Note that $\partial f/\partial x$ and $\partial f/\partial x$ are evaluated at $x = x^*$ and at $y = y^*$.

Similar steps can be performed for the y variable, i.e.

$$\dot{\hat{y}}(t) = \hat{y}(t)\frac{\partial g}{\partial x} + \hat{y}(t)\frac{\partial g}{\partial y} + \text{higher order terms} \quad (3.15)$$

Step 4: Linear stability analysis, as its name implies, consists of ignoring the higher order terms in Eqns. (3.14) and (3.15). This then leads to the following equations, in matrix form:

$$\frac{d}{dt}\begin{pmatrix}\hat{x}(t)\\ \hat{y}(t)\end{pmatrix} = \begin{pmatrix}\frac{\partial f}{\partial x} & \frac{\partial f}{\partial y}\\ \frac{\partial g}{\partial x} & \frac{\partial g}{\partial y}\end{pmatrix}_{FP}\begin{pmatrix}\hat{x}(t)\\ \hat{y}(t)\end{pmatrix} \quad (3.16)$$

where the subscript FP denotes the matrix evaluated at the fixed point. The above 2 × 2 matrix is called the Jacobian matrix, and is simply a matrix of numbers:

$$M_{Jacobian} = \begin{pmatrix}\frac{\partial f}{\partial x} & \frac{\partial f}{\partial y}\\ \frac{\partial g}{\partial x} & \frac{\partial g}{\partial y}\end{pmatrix}_{FP} = \begin{pmatrix}J_{11} & J_{12}\\ J_{21} & J_{22}\end{pmatrix} \quad (3.17)$$

To carry out linear stability analysis, we determine the eigenvalues of $M_{Jacobian}$, and if the real parts of all the eigenvalues are negatives, then the fixed point is dynamically (locally) stable. Detailed analyses for specific neuromodulator circuits are provided in Chapter 5.

3.3. Electrophysiological data processing and coherence analysis of neuronal firing and ECoG activities

Often, biophysical models require data from electrophysiological experiments to develop or validate. They typically come in the form of neuronal membrane potential dynamics including trains of spiking activities and characteristics of spike waveforms, and their derived forms, e.g. firing rates, CV, and ISI (see Chapter 2). However, as mentioned in section 2.2, parallel electrophysiological recordings of multiple neurons in the DRN of alive/behaving animals have yet to be performed.

As part of the original research collaborative programme, an initial set of multi-unit data was recorded from experimental collaborators at the University of Oxford. The data consisted of extracellular single unit recordings of neurons in the DRN of anaesthetized rodents while ECoG were recorded around the frontal cortex. These recordings were made simultaneously in the DRN and cortex. The goal was to use data analytical and signal processing methods to determine the relationship between spike waveform (derivative of neuronal action potential filtered by extracellular medium), spike train (and its derivatives e.g. firing rate) and brain (oscillation) state from ECoG (Chapter 6).

The data analysis method was structured in such a way that in the end we could understand the interactions between various DRN neurons, the three ECoG signals and also the mutual interactions between the spiking activities of DRN neurons and ECoG signals. The interactions can be judged through measures of coherence (Nylen and Wallisch, 2017) in frequency domain signals or correlation analysis in time domain signals (see below). For such analysis the data must be of the same length, which was the case as simultaneous recordings of DRN and cortex were performed within the same duration of time. If features of the data at various frequency components play important roles in deciding the research question, then frequency domain approach is used. Whereas, if temporal features of the data play important roles in analysing the research question then time domain analysis method is preferred. In our data, as described in Chapter 6, we focus on frequency domain analysis to understand the

interactions across a range of neural oscillatory frequencies in anaesthesized rodent brains. Below we will discuss the processing and the various analyses of such electrophysiological data.

3.3.1. Electrophysiological data processing

Electrocorticography (ECoG) is typically used to monitor brain state (e.g. wakefulness) of humans and animals. In the experiment presented in Chapter 6, my collaborators performed multi-site/channel cortical ECoG recordings of anaesthesized rodents. Three ECoG signals are recorded in 3 cortical regions, namely, left frontal, right frontal and right occipital. In addition, extracellular signals were recorded within the DRN simultaneously. Single units were recorded in the DRN and the spike trains of neurons were recorded for a sustained period of time. Signal processing on such data is typically required. For instance, raw neuronal spiking data can be filtered and single units can be identified automatically using Kilosort (Pachitariu et al., 2016) and verified by manual clustering using the software package Phy (Rossant et al., 2016). Spike trains can also be further analysed to reveal spike waveform characteristics, firing rate and firing rate regularity. The estimation of Inter Spike Interval (ISI) distribution is commonly used to study neuronal variability (Dayan and Abbott, 2001). This ISI distribution of a particular spike train can be broad or sharply peaked. In order to quantify the width of the ISI distribution for a particular spike train, the Coefficient of Variance (CV) is calculated. The CV of the ISI can be calculated, using e.g. Elephant toolbox in Python 3.0 (Yegenoglu et al., 2015), for every spike train (see below). This is regarded in the Elephant toolbox as the COV.

Study of ECoG signals are typically limited to certain frequency bandwidth (Nylen and Wallisch, 2017). ECoG signals can be converted into frequency domain using Fast Fourier Transform (FFT). This allows to study the characteristics of the data at different frequency ranges, which is important in structuring the methods for the data analysis. For instance, if we need to study the interactions between the instantaneous firing rates (IFRs) of the DRN and the slow wave oscillations in the ECoGs, then it can be done through frequency domain analysis (see Chapter 6). The Butterworth high pass filter (Butterworth, 1930) can be used for such filtering process. In Chapter 6, a lower frequency bandwidth using a 5^{th} order Butterworth high-pass filter was used, because previous studies have indicated low-frequency neural oscillations in the DRN (e.g.

Kocsis et al. (2006)) (also low frequencies are typically present in anaesthetized brain state). This is also confirmed in post-hoc analysis in Chapter 6 (from the power spectral density analysis of the ECoG signals). Notably, the maximal signal power of the ECoG signals in our data is found to be concentrated at low frequency components of around 1 Hz in all the mice (Chapter 6). These ECoG signals can then be concatenated for further analysis (see below).

The IFR of a neuron can be obtained from a spike train using an appropriate time bin with the following equation (Dayan and Abbott, 2001):

$$r(t) = \int_{-\infty}^{+\infty} d\tau \, w(\tau) \, \rho(t - \tau) \tag{3.18}$$

$$w(\tau) = \frac{1}{\sqrt{2\pi}\sigma} \exp\left(\frac{\tau^2}{2\sigma^2}\right) \tag{3.19}$$

where the window function w(τ) is the Gaussian filter, also called the filter kernel, specifies how the neural response function and kernel, evaluated at time t − τ contributes to the firing rate approximated at time t. σ controls the temporal resolution of the resulting rate. In the study in Chapter 6, the IFRs were derived from the corresponding neuronal spike trains using non-overlapping time bins of 5 ms, using the Elephant toolbox in Python 3.0 (Yegenoglu et al., 2015).

Statistical features such as CV and ISI derived from spike trains can also be obtained using the Elephant toolbox. Specifically, from a train of spikes, the CV can be obtained using the following equation (Dayan and Abbott, 2001):

$$\mathrm{CV} = \frac{\sigma}{\langle \tau \rangle} \tag{3.20}$$

where σ is standard deviation and $\langle \tau \rangle$ is the mean ISI and the ISI, from the equation (Dayan and Abbott, 2001):

$$\langle \tau \rangle = \int_0^{+\infty} d\tau \, \tau \, r \exp(-r \, \tau) = \frac{1}{r} \tag{3.21}$$

where r is the instantaneous firing rate, the probability of not firing a spike for period τ is $\exp(-r \, \tau)$.

Specifically, in the study in Chapter 6, when single-unit firing rates were less than 5 spikes per second or Hz, the spiking activities were categorised as “slow” firing, but above which were labelled as “fast” firing. With regards to the CV, if the spiking activities were less than 0.7, the firing activities were categorised as “regular” firing, but above which were labelled as “irregular” firing. Based on the above mentioned prescribed firing rate and ISI criteria, the spiking activities of neurons can then be categorised e.g. as slow and regular, slow and irregular, fast and regular, and fast and irregular. Within the literature on 5-HT neurons in the raphe, they are typically known to be slow and regular firing, with very occasional bursting behaviour (see Chapter 2).

3.3.2. Correlation in spike trains

Correlation is a measure of the relationship between two signals. The first set of observations of spiking activity in groups of neurons in the 1960s and 1970s established that the spiking activity is correlated across neurons (Gerstein and Clark, 1964; Boureau and Dayan, 2011; Snyder et al., 2015). Subsequent studies have shown that these spike correlations of neurons can depend on the similarity of preferred stimuli, distance between neurons, motion direction of a stimulus and may even change during the performance of cognitive tasks (Kreiter and Singer, 1996; Michalski et al., 1983; Kruger and Aiple, 1988; Snyder et al., 2015). Importantly, spike correlation can offer a glimpse into the underlying nature of interactions of neurons within a neuronal circuit (Cohen and Kohn, 2011).

The Pearson’s correlation coefficient has been used to quantify the correlation between spike counts neurons or single units. One of the simplest and widely used measures of correlated activity is the pairwise correlation coefficient ρ_{xy} (De La Rocha et al., 2007; Greenberg et al., 2008; Perkel et al., 1967; Shea-Brown et al., 2008). It is defined as the covariance of spike counts normalized by the standard deviations of individual neurons, and is described mathematically as follows:

$$\rho_{xy} = \frac{\mathrm{Cov}\,(x,y)}{\sigma_x \sigma_y} \qquad (3.22)$$

where ρ_{xy} is the Pearson product-moment correlation coefficient, $\mathrm{Cov}(x, y)$ is the covariance of variables x and y, σ_x the standard deviation of x, and σ_y the standard deviation of y.

A correlation coefficient is used to evaluate the strength of the spike correlation (De La Rocha et al., 2007). If two signals have a high degree of similarity, the magnitude of the computed correlation coefficient is large. If there is little or no linear relationship between two signals, the magnitude of the coefficient is small (De La Rocha et al., 2007; Cutts and Eglen, 2014). At the extremes, the correlation coefficient is equal to one if the spike trains are identical, and it is zero if the occurrence of a spike at one time is independent of the occurrence of spikes at other times, both within the spike trains from single neurons and across spike trains from multiple neurons. This is not overly surprising given the potential interconnections among neurons, either directly or indirectly, and their potential shared afferent inputs. The presence of these correlations has led to the proposal that they might form a key element of the neural code (De La Rocha et al., 2007; Cutts and Eglen, 2014). However, correlations among DRN neurons are yet to be well determined. This will be addressed in Chapter 6. Although useful for measuring low-level neuronal/single-unit relationships, spike correlations can have difficulty extending to higher, neuronal population level relationships or between different levels of neural activities (e.g. between neuronal firing rate and ECoG).

3.3.3. Coherence analyses of neural signals

As opposed to time-domain data analytical approaches, spectral analysis is a method of transforming signals into the frequency spectra which quantify the relative contributions of these components (Nylen and Wallisch, 2017). It can identify specific bands of frequencies (more specifically, frequency powers) that stand out in the noisy signal. Frequency bands of interests can be specifically focussed by filtration techniques. Power spectral analysis can show the bands of frequencies where the signal power is maximum. Several pre-processing techniques e.g. average referencing can be used but care must be taken that such methods do not impart spurious results, especially when it's a low density recording and the sensors are not too close to each other.

Within the frequency-domain analytical approaches, the cross-spectrum (the Fourier transform of the cross-covariance function) is a complex spectral measure between two signals normalized by the product of the auto-spectra (Mitra and Pesaran, 1999). The magnitude squared coherence, is generally considered to be a measure of the linear dependency of the phase differences between two signals (An et al., 2019; Mitra and Pesaran, 1999). At the extremes, if two signals correspond to each other perfectly at a given frequency, the magnitude of coherence will be 1, but if they are totally unrelated, the coherence will be 0. Specifically, the coherence function, COH, at each given frequency x is mathematically described by

$$COH(x) = \frac{|S_{AB}(x)|^2}{S_{AA}(x)\, S_{BB}(x)} \tag{3.23}$$

where $|S_{AB}(x)|$ is the cross-spectrum between signals A and B, $S_{AA}(x)$ is the autospectrum of signal A, and $S_{BB}(x)$ is the autospectrum of signal B. Thus, similar to time-domain correlation measures, coherence measures the correlation between a pair of signals but expressed as a function of frequency using coherence coefficients instead of product-moment correlation coefficients. This COH measure is suitable for conditions when the sensors for acquiring the neural (source) activities were neither too many in number nor were they spatially close to each other, as volume conduction may not present a serious issue. Otherwise, other more sophisticated techniques are required (see e.g. Sanchez-Bornot et al. (2018)). Moreover, in Chapter 6, this measure will be used to identify relationships among DRN neuronal firing rates (as continuous variables, not spike trains), and between DRN neuronal firing rates and ECoG activities.

In summary, this chapter has discussed some of the methods in computational neural modelling and neural data analyses. These methods will be utilised in the following contributing Chapters of 4, 5 and 6. In particular, Chapter 4 will make use of the mean-field modelling in section 3.1.2, while Chapter 5 will apply the stability analysis in section 3.2. Finally, Chapter 6 will utilise the neural signal processing and analytical methods in section 3.3.

Chapter 4
Computational modelling of degenerate DRN-VTA circuits

This contributing chapter uses computational modelling to demonstrate the plausibility of degeneracy in the serotonergic and dopaminergic neural circuits. Parts of this review are archived in a pre-print manuscript.

4.1. Introduction

The nervous system can be modulated by a group endogenous chemical messengers, often called neuromodulators (Kaczmarek and Levitan, 1987). Neurons or synapses, and hence neural circuits, that succumb to neuromodulation often change circuit configuration and function (Marder, 2012; Marder et al., 2014). However, neural circuits can also be degenerate, that is, circuits consisting of different elements and/or structure while performing the same function or yielding the same output (Cropper et al., 2016). This can allow robust maintenance of functions and behaviour in the face of changes in the underlying structure (Edelman and Gally, 2001; Whitacre, 2010). Although it has been shown that neuromodulators can selectively regulate degenerate neural circuits (Cropper et al., 2016; Marder et al., 2014) it is unclear whether neural circuits with neuromodulator-containing neurons can themselves be degenerate, which could in turn provide stable widespread neuromodulator influences on targeted neural circuits (Fig. 1.3a).

In this theoretical study, the plausibility of degenerate and stable neuromodulator circuits is investigated by focusing on the neural circuits in the midbrain which are the source of ascending pathways of two highly studied monoaminergic neuromodulators, serotonin (5-HT) and dopamine (DA). These neuromodulators have major roles in modulating

various cognitions, emotions and behaviours, and are linked to the pathogenesis and pharmacological treatment of many common neuropsychiatric and neurological disorders (Müller and Cunningham, 2020). The majority of 5-HT-producing neurons are found in the dorsal and median raphe nuclei (DRN and MRN), while most DA-producing neurons reside in the ventral tegmental area (VTA) and substantia nigra compacta (SNc) (Müller and Cunningham, 2020). Importantly, as discussed in Chapter 2, there is increasing evidence for direct and indirect interactions between these two neuromodulators both structurally and functionally (Fig. 1.3a). This can be reflected in the observed complexity of neuronal signalling within the DRN-VTA system in response to reward and punishment (Fig. 1.3b). It may also reflect shared afferent inputs to neurons in the system. In Chapter 2, three questions have been posed, which are re-iterated here: (i) Can experimental findings from separate studies be reconciled and understood in terms of a single neural circuit model encompassing both the DRN and VTA? (ii) Can there be degenerate DRN-VTA neural circuits, which are stable? (iii) Can some of these degenerate circuits be identifiable, for example, through pharmacological means?

To address these questions, a biologically plausible DRN-VTA computational neural circuit model based on a previous multiscale modelling framework was developed (Joshi et al., 2017; Wong-Lin et al., 2017) (Chapter 3.1.2). The modelling took into account known direct and indirect pathways between DRN 5-HT and VTA DA neurons, as discussed above. Upon simulating the model under reward and punishment conditions, it was found that many, but not all of the experimental findings, could be captured in a single DRN-VTA model. Further, several distinct model architectures could replicate the same neural circuit activity response profile, hence demonstrating degeneracy. Applying dynamical systems theory, it was found that all these circuits were dynamically stable. To distinguish the degenerated models, drug effects of DA D2-receptor based agonist was simulated and was able to distinguish between sub-groups of these seemingly degenerate model architectures. Overall, this study demonstrated the plausibility of degeneracy and stability of neural circuits of neuromodulators.

4.2. Computational modelling of the DRN-VTA circuits

To develop the DRN-VTA neural circuit models, the dynamic mean-field (neuronal population-based) modelling framework (Joshi et al., 2017) for neuromodulator interactions was used. The modelling approach was constrained by data from known electrophysiological, neuropharmacological and voltammetry parameters (see Chapter 3.1.2). Each neural circuit model architecture investigated consisted of DRN 5-HT, VTA DA, VTA GABA, DRN GABA, and DRN Glu neuronal populations. Direct and indirect interactions among these five neuronal populations were then explored. The main aim of this work was to evaluate the plausibility of neuromodulator circuit degeneracy and stability rather than replicate every neuronal populations in these brain regions. Thus, DRN DA neurons were not considered in the model due to the lack of studies in standard reward/punishment conditioning tasks. VTA Glu neurons were also not considered as they constituted a lower proportion (2-5%) of cells in this region (Yamaguchi et al., 2015).

4.2.1. Input-output functions of neural population firing rates

The computational models developed were based on a previous mean-field, neural population based modelling framework for neuromodulator circuits (Joshi et al., 2017), in which the averaged concentration releases of neuromodulators (e.g. [5-HT]) were monotonic functions of the averaged firing rate of (e.g. 5-HT) neuronal populations via some neuromodulator induced slow currents. All 5 neural populations' firing rates were described by threshold-linear functions (general form in Eqn. (3.6)) (Jalewa et al., 2014; Joshi et al., 2017):

$$F_{5-HT} = g_{5-HT}\,[I_{5-HT} - I_{0,5-HT}]_+ \tag{4.1}$$

$$F_{DA} = g_{DA}\,[I_{DA} - I_{0,DA}]_+ \tag{4.2}$$

$$F_{Glu} = g_{Glu}\,[I_{Glu} - I_{0,Glu}]_+ \tag{4.3}$$

$$F_{GABA-DRN} = g_{GABA-DRN}[I_{GABA-DRN} - I_{0,GABA-DRN}]_+ \quad (4.4)$$

$$F_{GABA-VTA} = g_{GABA-VTA}\,[I_{GABA-VTA} - I_{0,GABA-VTA}]_+ \quad (4.5)$$

where $[x]_+ = x$ if $x \geq 0$, and 0 otherwise. The threshold input values for $I_{0,DA}$ was -10 (a.u.) for DA neurons, and $I_{0,5-HT}$ was 0.13 (a.u.) for 5-HT neurons, to allow spontaneous activities mimicking *in vivo* conditions. 5-HT neurons had a threshold-linear function with gain value g_{5-HT} of about 1.7 times higher than that for DA neurons, and so DA and 5-HT neurons were set to be 0.019 and 0.033 (Hz), respectively (Challis & Berton, 2015; Crawford et al., 2010; Richards et al., 1997; Wong-Lin et al., 2012). For simplicity, the same current-frequency or input-output function were assumed in either tonic or phasic activity mode (Jalewa et al., 2014; Joshi et al., 2017).

4.2.2. Afferent currents and connectivity

The afferent current, I, for a neural population consisted of summed contributions from external excitatory inputs I_{ext} including those induced by reward or aversive stimuli, and recurrent interactions with other neural populations (see below) e.g. $I_{5-HT,DA}$ for effective DA-induced currents in 5-HT neurons. Additionally, for a neuromodulator population, autoreceptor-induced current, I_{auto}, was included.

Due to limited experimental evidences, and to reduce the parameter search space, the following connections were not considered, from: (i) DRN GABA to VTA DA neurons; (ii) DRN GABA to VTA GABA neurons; (iii) VTA GABA to DRN Glu neurons; (iv, v) DRN Glu to DRN GABA neurons, and vice versa; and (vi) VTA DA to DRN Glu neurons. Then the total (population-averaged) afferent input currents to DA and 5-HT neurons were, respectively, described by

$$I_{DA} = -I_{DA,auto} \pm I_{DA,5-HT} + I_{DA,Glu} - I_{DA,GABA-VTA} + I_{DA,ext} \quad (4.6)$$

$$I_{5-HT} = -I_{5-HT,auto} + I_{5-HT,DA} + I_{5-HT,Glu} - I_{5-HT,GABA-DRN} - I_{5-HT,GABA-VTA} + I_{5-HT,ext} \quad (4.7)$$

where the first terms on the right-hand sides of Eqns. (4.6) and (4.7) were autoreceptor-induced self-inhibitory currents, the second terms were the 5-HT-to-DA (labelled with subscript $DA, 5-HT$) and DA-to-5-HT (with subscript $5-HT, DA$) interactions, the third terms were excitatory interactions from DRN Glu neurons, the fourth/fifth terms were inhibitory interactions from local DRN/VTA GABAergic neurons, and the last terms were additional external constant biased inputs from the rest of the brain and the influence of behaviourally relevant stimuli (due to rewards or punishments; see below). 5-HT neurons have a possible additional negative interaction from VTA GABA neurons (second last term on right-hand-side) (Li et al., 2019). Negative or positive sign in front of each term indicated whether the interaction was effectively inhibitory or excitatory. The $\pm$ sign indicated effectively excitatory $(+)$ or inhibitory $(-)$ interactions. Both signs were investigated given their mixed findings in the literature (see also Eqns. (4.8-4.10)). This form of summed currents was consistent with some experimental evidence that showed different afferents modulating the tonic and phasic activation (Floresco et al., 2003; Tian et al., 2016). Similarly, the total (population-averaged) afferent current to the glutamatergic (Glu), and VTA and DRN GABAergic neurons, can respectively be described by

$$I_{Glu} = I_{self,Glu} \pm I_{Glu,5-HT} + I_{Glu,ext} \tag{4.8}$$

$$I_{GABA-DRN} = -I_{self,GABA-DRN} \pm I_{GABA-DRN,5-HT} + I_{GABA-DRN,DA} - I_{GABA-DRN,GABA-VTA} + I_{GABA-DRN,ext} \tag{4.9}$$

$$I_{GABA-VTA} = -I_{self,GABA-VTA} + I_{GABA-VTA,5-HT} \pm I_{GABA-VTA,DA} + I_{GABA-VTA,ext} \tag{4.10}$$

where, the subscript Glu denoted DRN Glu neural population, and subscripts $GABA-VTA$ and $GABA-DRN$ denoted GABAergic neural populations in the VTA and DRN, respectively. The subscript $self$ denoted self-connection. These connections were visually summarised in Fig. 4.1.

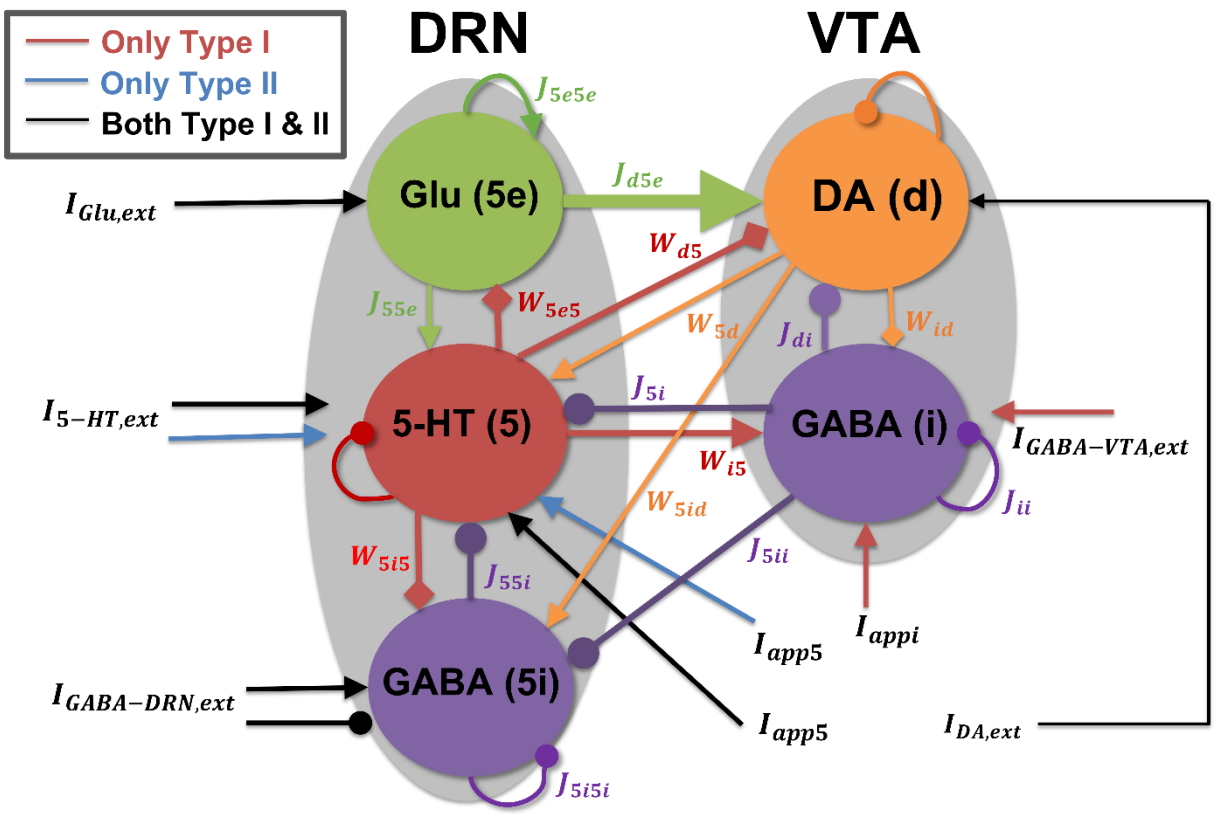

Figure 4.1. Detailed connectivity and labelling for the highly connected DRN-VTA. Grey: brain region. Coloured circle: neuronal population. Legend: network's afferent inputs. Input currents are labelled with I's, and relative weights of connectivity with W's and J's, W's if 5-HT/DA-mediated connections associated; J's if glutamatergic/GABA-mediated connections. Colours of connectivity are based on sources of the connectivity (bright red arrows if Type I; blue arrows if Type II; black arrows denote common inputs for reward/punishment task for both Types). Thicker arrows denote stronger connectivity; the range of values of the relative weights are found in Table 4.1. Ionotropic receptor mediated self-connection strengths within DRN Glu, DRN GABA and VTA GABA neurons are fixed for all simulations; however, in drug simulations, DA neuronal self-connection (auto-inhibition) is increased.

The averaged synaptic currents of non-5-HT/DA ionotropic glutamatergic & GABAergic neurons, namely, $I_{DA,Glu}$, $I_{5-HT,Glu}$, $I_{DA,GABA-VTA}$, $I_{5-HT,GABA-VTA}$, $I_{5-HT,GABA-DRN}$, $I_{self,Glu}$, $I_{self,GABA-DRN}$, $I_{self,GABA-VTA}$ and $I_{GABA-DRN,GABA-VTA}$ were typically faster than currents induced by (metabotropic) 5-HT or DA currents. Thus, the former currents were assumed to reach quasi-steady states and described (Jalewa et al., 2014) and represented by

$I_{e/i} = \pm J_{e/i}\, F_{e/i}$, where the subscript e/i denoted excitatory/inhibitory synaptic current, J the connectivity coupling strength, F the presynaptic firing rate for neural population e/i, and the sign $\pm$ for excitatory or inhibitory currents. This also reduced the number of free model parameters. Along a similar line of argument, we also ignored the relatively faster neuronal membrane dynamics. Further, dimensionless coefficients or relative connectivity weights, $W's$ (with values ≥ 0), were later multiplied to the above neuromodulator induced current terms (right-hand-side of terms in Eqs. (4.6-4.10)). Both the $J's$ and $W's$ were allowed to vary to fit the network activity profiles of Fig. 2.3b within certain tolerance ranges (see below) while exploring different neural circuit architectures (a-l*) (see Table 4.1 for specific values). The self-connection weights $J's$ within the DRN Glu, DRN GABA and VTA GABA neurons were set at 0.5, 0.5, and 10 respectively, for all network activity's response profiles.

For simplicity, fast co-transmission of neurotransmitters was only considered in one modelling instance (e.g. co-release of 5-HT and glutamate via fast 5-HT_3 and ionotropic receptors) based on findings by (Wang et al., 2019). From a modelling perspective, the DRN (Type I) 5-HT and Glu neuronal populations, which have rather similar activity profiles could also be effectively grouped and considered as a single 5-HT neuronal population that "co-transmit" both 5-HT and Glu to DA neurons (Wang et al., 2019).

	a	b	c	d	e	f	g	h	i	j	k	l*
J_{55e}	10	6	5	5	5	5	5	5	5	5	5	5
J_{5i}	0-1	0	0	0	0	0	0	0	0	0	0	0
J_{55i}	0-0.1	0-0.1	0-0.1	0-0.1	0-0.1	0-0.1	0	0	0	0	0	0.1
W_{5d}	0-30	0-10	0-10	0-10	0-10	0	0	0-10	0	0	0	0-10
J_{d5e}	100	100	100	100	100	100	100	100	100	100	100	100
J_{di}	25	25	25	25	25	25	25	25	25	25	25	25
W_{d5}	0-1	0-1	0-1	0-1	0	0	0	0	0-2	0-2	0	0-1
W_{5e5}	0-0.1	0-0.1 5HT to Glu (ex): 0-1	0	0	0	0	0	0	0	0	0	0-0.1
W_{i5}	0-20	0-20	0-20	0-20	0-20	0-20	0-20	0-20	0-20	0-20	0-20	0-20
W_{id}	0-2	0-2	0-2	0	0	0	0	0	0	0	0	0-2
W_{5i5}	p: 0-0.2 r:0-4	0-4	0-4	0-10	0-10	0-10	0-10	0-10	0-10	0-10	0-10	p: 0-4 r:0-3
W_{5id}	p:0-10 r:0-20	0-10	0-10	0-10	0	0	0-20	0	0	0	0	0-10
$J_{self,Glu}$	0.5	0.5	0.5	0.5	0.5	0.5	0.5	0.5	0.5	0.5	0.5	0.5
$J_{self,GABA-DRN}$	0.5	0.5	0.5	0.5	0.5	0.5	0.5	0.5	0.5	0.5	0.5	0.5
W_{5ii}	p:0.4 r:0.1	0	0	0	0	0	0	0	0	0	0	0.4
$J_{self,GABA-VTA}$	10	10	10	10	10	10	10	10	10	10	10	10

$J_{auto,DA}$	1	1	1	1	1	1	1	1	1	1	1	1
$J_{auto,5-HT}$	1	1	1	1	1	1	1	1	1	1	1	1

Table 4.1. Summary of model parameter values of internal connections considered for the degenerate DRN-VTA circuit models. Column: Model architectures; row: connection strength. For connection labels, refer to Fig. 4.1, while for model architectures, refer to Fig. 4.4. These values reflect either single values used or a range of values such that their corresponding neural activity profiles fit within the degeneracy criteria. These values are used with Type I or II 5-HT neuronal model, punishment or reward unless specified with p or r, respectively, and excitatory or inhibitory connections unless specified with $+$ or $-$, respectively. Self-connections are not shown as they are constants except for the DA neurons during D_2 agonist drug simulation cases.

Autoreceptor-induced currents were known to trigger relatively slow G protein-coupled inwardly-rectifying potassium (GIRK) currents (Tuckwell and Penington, 2014). For 5-HT_{1A} autoreceptors, the inhibitory current $I_{5-HT,auto}$ could be described by (Ritter et al., 2008; Tuckwell and Penington, 2014;Joshi et al., 2017):

$$\tau_{auto,5-HT}\frac{dI_{auto,5-HT}}{dt} = -I_{auto,5-HT} + \frac{k_{auto,5-HT}}{1+e^{-g_{auto,5-HT}([5-HT]-[5-HT]_0)}} \quad (4.11)$$

and similarly, for DA autoreceptor induced inhibitory current $I_{auto,DA}$:

$$\tau_{auto,DA}\frac{dI_{auto,DA}}{dt} = -I_{auto,DA} + \frac{k_{auto,DA}}{1+e^{-g_{auto,DA}([DA]-[DA]_0)}} \quad (4.12)$$

where $\tau_{auto,5-HT}$ was set at 500 ms (Joshi et al., 2017) and $\tau_{auto,DA}$ at 150 ms (Benoit-Marand et al., 2001; Courtney et al., 2012; Cullen and Wong-Lin, 2015). The threshold values $[5-HT]_0$ and $[DA]_0$ were set at 0.1 μM. These parameters can be varied to mimic the effects of autoreceptor antagonists/agonist (Joshi et al., 2017). The gains $g_{auto,5-HT}$ and $g_{auto,DA}$ were set at 10 μM^{-1} each, and $k_{auto,5-HT} = k_{auto,DA} = 80$ a.u.. These values were selected to allow reasonable spontaneous neural firing activities and baseline neuromodulator concentration levels (see below), and similar to those observed in experiments.

Similarly, we assumed sigmoid-like influence of $[5-HT]$ ($[DA]$) on DA (5-HT) neural firing activities between the DRN and VTA populations such that the induced current dynamics could be described by (Joshi et al., 2017; Wang and Wong-Lin, 2013):

$$\tau_{DA,5-HT}\frac{dI_{DA,5-HT}}{dt} = -I_{DA,5-HT} + \frac{k_{DA,5-HT}}{1+e^{-g_{DA}([5-HT]-[5-HT]_1)}} \tag{4.13}$$

$$\tau_{5-HT,DA}\frac{dI_{5-HT,DA}}{dt} = -I_{5-HT,DA} + \frac{k_{5-HT,DA}}{1+e^{-g_{5-HT}([DA]-[DA]_1)}} \tag{4.14}$$

with the time constants $\tau_{5-HT,DA} = 1$ s, and $\tau_{DA,5-HT} = 1.2$ s (Aman et al., 2007; Haj-Dahmane, 2001). We set $k_{5-HT,DA} = k_{DA,5-HT} = 0.03$ a.u. and $g_{5-HT} = g_{DA} = 20$ μM^{-1}, $[5-HT]_1 = 0.3\text{nM}, [DA]_1 = 0.1$ nM such that the neural firing activities and baseline neuromodulator concentration levels were at reasonable values (see below) and similar to those in experiments (e.g. Bunin and Wightman (1998) and Hashemi et al. (2011)). For simplicity, we assumed Eqns. (4.13) and (4.14) to be applied equally to all targeted neural populations, but with their currents multiplied by their appropriate weights $w's$ (see above).

4.2.3. Release-and-reuptake dynamics of neuromodulators

The release-and-reuptake dynamics of 5-HT followed the form of a Michaelis-Menten equation (Bunin and Wightman, 1998; Hashemi et al., 2011; Joshi et al., 2017, 2011; Samaranayake et al., 2016):

$$\frac{d[5-HT]}{dt} = [5-HT]_p\, R_{5-HT} - \frac{V_{max,5-HT}\,[5-HT]}{K_{m,5-HT} + [5-HT]} \tag{4.15}$$

where $[5-HT]_p = 0.08$ nM was defined as the release per firing frequency (Joshi et al., 2011; Flower and Wong-Lin, 2014; Joshi et al., 2017) (value selected to fit to reasonable baseline activities (Hashemi et al., 2011; see below), and the Michaelis-Menten constants $V_{max,5-HT} = 1.3$ μM/s (maximum uptake rate) and $K_{m,5-HT} = 0.17$ μM (substrate

concentration where uptake proceeds at half of maximum rate) were adopted from voltammetry measurements (Hashemi et al., 2011).

Similarly, the release-and-reuptake dynamics for DA was described by

$$\frac{d[DA]}{dt} = [DA]_p \, R_{DA} - \frac{V_{max,DA}\,[DA]}{K_{m,DA} + [DA]} \tag{4.16}$$

where $V_{max,DA} = -0.004$ μM/s and $K_{m,DA} = 0.15$ μM (May et al., 1988). $[DA]_p = 0.1$ nM to constrain the ratio $[DA]_p/[5-HT]_p = 1.25$ according to May et al. (1988), Bunin et al. (1998), and Hashemi et al. (2011). For simplicity, Eqns. (4.15) and (4.16) were assumed to be applied equally to all targeted neural populations.

4.2.4. Reward and punishment conditions with Type-I and Type-II 5-HT neurons

The focus will be on the classical, fully learned reward conditioning task, and unexpected punishment task. For each trial or realisation of simulation within a set of condition (reward/punishment, excitatory/inhibitory connection), the cue onset time was set at 4.5 s (to allow the network to stabilise substantially). The within-trial protocol for the external input current, I_{ext}, was implemented as a function of time t as followed, depending on the simulated conditions. Note that all external input currents were assumed to be excitatory, regardless of reward or punishment task, unless stated.

For reward task with Type-I 5-HT neurons: (i) constant input currents $I_{5-HT,ext}$ and $I_{DA,ext}$ to 5-HT and VTA DA neurons, respectively, of amplitude $50\ a.u.$ to simulate long-term reward; (ii) brief 0.2 s pulse $I_{Glu,ext}$ to DRN Glu neurons of amplitude $1000\ a.u.$ at 4.5 s; (iii) constant step input current $I_{GABA-VTA,ext}$ to VTA GABAergic neurons with amplitude $200\ a.u.$ from 4.5 to 5.7 s to simulate sustained activity; and (iv) no external input $I_{GABA-DRN,ext}$ to DRN GABAergic neurons. For punishment task with Type-I 5-HT neurons: (i) no external input to VTA DA, 5-HT neurons and DRN Glu neurons; (ii) brief 0.2 s pulse to VTA (I_{app}) and DRN GABAergic (I_{app5i}) neurons with amplitude $1000\ a.u.$ at 5.7 s.

For reward task with Type-II 5-HT neurons: (i) constant input current to 5-HT and VTA DA neurons with amplitude 50 a.u. to simulate long-term reward; (ii) additional step input current to 5-HT neurons with amplitude 100 a.u. from 4.5 to 5.7 s to simulate sustained activity; (iii) brief 0.2 s pulse to DRN Glu neurons of 1000 a.u. at 4.5 s; (iv) no external input to VTA and DRN GABAergic neurons. For punishment task with Type-II 5-HT neurons: (i) no external input to VTA DA and GABAergic neurons, and DRN Glu neurons; (ii) brief 0.2 s pulse to DRN GABAergic and 5-HT neurons with amplitude of 1000 a.u. at 5.7 s.

In addition, for transient inputs, multiplicative exponential factors $\exp(-t/\tau)$ with τ of 50 ms were used to smooth out activity time courses (e.g. afferent synaptic filtering), but they did not affect the overall results. To simulate long-term, across-trial reward/punishment signalling, we assumed a higher constant excitatory input to both 5-HT and DA neurons in reward than punishment trials. When searching for the neural circuit architecture using either Type I or II 5-HT neurons, we limited ourselves as much as possible to the same internal DRN-VTA circuit structure. This also reduced the complexity of the parameter search space.

4.2.5. Baseline neural activities and acceptable deviations

We define the neural circuit activities under baseline condition (right before cue onset) to follow that in Figs. 4.2a and 4.2b. Namely, the baseline firing rates for 5-HT, DRN GABA, DRN Glu, DA and VTA GABA neurons in punishment task were 3.0, 21.5, 4.1, 4.8 and 13.5 Hz, respectively, and those in reward task were 4.5, 19.4, 4.1, 4.8 and 16.3 Hz, respectively. The baseline $[5-HT]$ and $[DA]$ levels were constrained to be at 10 and 1.5 nM, respectively. However, it is known that these activities can vary widely across subjects, species and studies. Hence, while searching for degenerate neural circuit architecture, we had to define acceptable ranges of neural activities in which we could claim that the variant neural circuit still behaved similarly to that of the model in Fig. 4.2. Specifically, based on multiple experimental studies (Table 4.2), we set an inclusion criterion that

permitted maximal deviations of the 5-HT, DRN GABA, DRN Glu, DA and VTA GABA neural populations to be less than 10%, 17%, 10%, 10% and 17% from their above defined baseline activities, respectively.

Brain region & neuronal type	***Firing rate***	***Reference***
VTA DA neurons	~ 4 - 6 Hz	(Cheer et al., 2003; Li et al., 2012; Stauffer et al., 2016; Tian et al., 2016; Ungless et al., 2004)
VTA GABA neurons	~ 12 - 17 Hz	(Cohen and Uchida, 2012; Steffensen et al., 2009, 1998)
DRN 5-HT neurons	~ 3 - 5 Hz	(Allers and Sharp, 2003; Cohen et al., 2015; Hajós et al., 2007; Judge and Gartside, 2006; Li et al., 2016; Ranade and Mainen, 2009; Srejic et al., 2016)
DRN GABA neurons	~ 15 - 25 Hz	(Allers and Sharp, 2003; Challis et al., 2013; Hernández-Vázquez et al., 2019; Li et al., 2016; Sakai, 2011)
DRN Glu neurons	~ 3 - 5 Hz	(Taylor et al., 2019)

Table 4.2. Baseline firing rates of DRN and VTA neurons. Firing rate ranges estimated based on relevant references (see Supplementary References below). *: *in vitro* recording data, $^{+}$: *in vivo* recording data. Only baseline firing rates were deduced due to the higher variation in stimulus-evoked activities. Note: references shown are samples but do not reflect the complete list in the literature. These ranges provide a leverage to identify acceptable activity profile deviations for the degenerate neural circuit models and the perturbative effects of drugs (see below).

4.2.6. Simulating the effects of D_2 agonist

DA and 5-HT induced currents can lead to overall excitatory or inhibitory effects, depending on receptor subtype(s) and the targeted neurons. In particular, DA enhances VTA GABAergic neuronal activity via D_2 receptors and depolarizes the membrane of 5-HT neurons (Haj-Dahmane, 2001; Aman et al., 2007; Ludlow et al., 2009; Courtney et al., 2012; Ford, 2014). DA also regulates the activity of other DA neurons via D_2 auto-inhibitory receptors (Adell and Artigas, 2004). To study how D_2 receptor mediated drugs can affect DRN-VTA architecture differently, different D_2 agonist dosage levels were simultaneously simulated by multiplying the connection weights (see Fig. 4.1) of D_2

receptor mediated currents by a factor ‘X’ of 10, 40, 70 and 100 times. Then for each dosage, we separately observed the deviation in activity profiles for each neural population with respect to the allowed range. Again, we considered the maximal percentage changes due to the drug as significant if the percentage changes in at least one population activity profile were more than the inclusion criterion defined for each population.

4.2.7. Computational simulations, numerical scheme and modelling procedures

Simulations were performed using MATLAB with forward Euler numerical integration method on the dynamical (ordinary differential) equations (see above). A simulation time step of 1 ms was used and smaller time steps did not affect the results. MATLAB were used for analyses of network stability and sensitivity.

For each potential degenerate model circuit architecture investigated, either Type I or II 5-HT neuronal population were considered in the circuit (Cohen et al., 2015). The possibility of excitatory and inhibitory projections from 5-HT to DRN Glu/GABA and DA neurons, and from DA to GABA neurons in the VTA were also considered. To allow tractability in the search for the many possible connectivity structures, the models’ connections were largely based on experimental evidences. For example, connections between VTA GABAergic and DRN Glu neurons were not considered as, to date, there is little experimental support. We also focused only on learned reward (with reward-predicting cue followed by reward outcome) and unexpected punishment conditions, simulated using a combination of tonic and/or phasic afferent inputs. Note that we did not consider other conditions and network learning effects (e.g. (Hu, 2016; Zhou et al., 2018)) as the main aim was to demonstrate the plausibility of DRN-VTA circuit degeneracy and stability. This was done through the investigation of various DRN-VTA circuit architectures with network activity profiles that closely resembled that in Fig. 1.3b. Note also that all activity profiles in Fig. 1.3b were based on experimental studies except VTA Glu neural

activity, which we deduced to be similar to that of DA neuronal behaviour in reward task (McDevitt et al., 2014a) and assumed to be non-responsive in punishment task.

The modelling procedure first begins with a parsimonious model (Fig. 4.2, and model k in Fig. 4.5). Some model parameters were constrained by information from experiments (see references in Sections 4.2.2 and 4.2.3). The connection weights (Table 4.1) and afferent inputs (Section 4.2.4) were adjusted by trial-and-error method to mimic the neuronal activity profiles, including tonic (Table 4.2) and phasic activities (Fig. 2.3b and Fig. 4.3), as observed in separate experimental studies (cited in Section 4.1). In particular, the range of values for the connection weights are determined such that the activity profiles conform to experimental observations (see above). For each model architecture, different 5-HT neuronal types (Type-I or Type-II) and connectivity signs (mimicking effective excitatory or inhibitory effects) are investigated. The model's complexity is then increased by adding more connections, and the above process is repeated.

The maximal percentage of deviations of the activity outcomes of each neuronal population activity compared to the activities of the corresponding neuronal population of the template is computed, 1000 ms before cue onset and 1000 ms after outcome onset (Fig. 4.4). The maximal percentage of deviations are checked if they lie within the allowable ranges (see above), as per the experimental results (Section 4.2.3). Only those models are considered as valid (Table 4.2). Thus, in all, 84 different models are investigated.

4.3. Results

4.3.1. A DRN-VTA model can reconcile many signalling patterns

A parsimonious, sparsely connected DRN-VTA model architecture was developed and the strength of the afferent inputs and the internal connection weights of the network were

adjusted such that the network activity profiles attained qualitatively similar profiles to that illustrated in Fig. 2.3.1b. The resultant network configuration (Fig. 4.2) was our most sparsely connected DRN-VTA circuit model. All other subsequent architecture considered would henceforth be derived from this basic architecture.

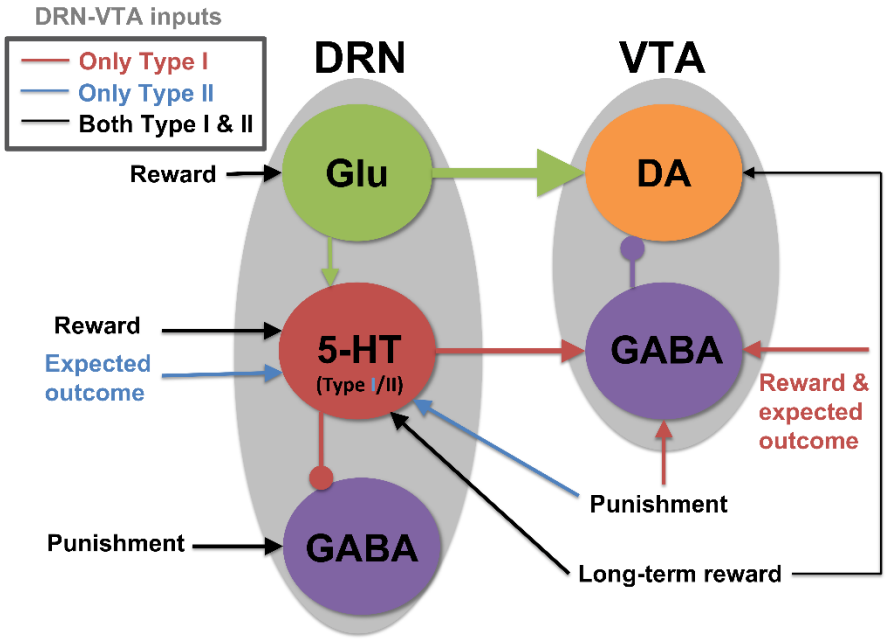

Figure 4.2. A sparsely connected DRN-VTA circuit model. Grey: brain region. Coloured circle: neuronal population. Legend: network's afferent inputs. Model architecture implicitly encompasses either Type I or II 5-HT neurons with two different inputs for reward/punishment task (bright red arrows if Type I; blue arrows if Type II; black arrows denote common inputs for reward/punishment task for both Types). Circuit connections: triangular-end arrows (excitatory); circle-end arrows (inhibitory). Thicker arrows: stronger connection weights. Constant long-term reward inputs simultaneously to 5-HT and DA neurons to alter baseline activities. Sustained activity for expectation of reward outcome implemented with tonic input between cue and reward outcome. All other inputs are brief, at cue or reward/punishment outcome, producing phasic excitations/inhibitions. Note: Self-inhibitory (self-excitatory) connections within GABAergic (Glu) neurons, and autoreceptor inhibitions within 5-HT or DA neurons were implemented (see Fig. 4.1) but not shown here. This is the most sparsely connected model architecture considered in this work.

This minimal network architecture readily recapitulated many of the neuronal signalling changes in the DRN and VTA in separate experimental studies, both for reward (Fig. 4.3,

black dashed) and punishment (Fig. 4.3, orange bold) tasks. Moreover, only modifications to afferent inputs to DRN 5-HT and VTA GABA neurons were required to replicate the signalling of Type I or II 5-HT neurons (Figs. 4.3a and b, respectively), while maintaining the same internal connectivity structure. For example, a lack of sustained reward-based activity of Type I 5-HT activity (Fig. 4.3b, 2nd row, black dashed) required additional external input to sustain VTA GABAergic neural activity (Fig. 4.2; Fig. 4.3a, bottom row, black dashed). It should be noted that this was based on the assumption that the activity profiles for these non-5-HT neurons were qualitatively similar, regardless of the 5-HT neuronal types (Fig. 4.2).

For the punishment task with Type I 5-HT neurons, brief excitatory inputs to GABAergic neurons in the DRN and VTA led to their punishment-based phasic activation (Fig. 4.2; Fig. 4.3a, 3rd and 5th rows, orange) (Li et al., 2016; Tan et al., 2012). To replicate the activity profiles for a circuit with Type II 5-HT neurons, brief excitatory inputs to the DRN GABAergic and 5-HT neurons were implemented instead, leading to punishment-based phasic activation for both (Cohen and Uchida, 2012; Li et al., 2016; Tan et al., 2012) (Fig. 2; Fig. 3b, 2nd and 3rd rows, orange). With both Types I and II 5-HT neurons, there was also phasic inhibition of VTA DA activity via VTA GABAergic neurons (Fig. 3, 1st row, orange), in line with the findings from previous studies (Schultz et al., 1997; Cohen et al., 2012; Tan et al., 2012; Watabe-Uchida et al., 2017). It should be noted that with Type II 5-HT neurons, the phasic activation of VTA GABAergic neurons was not as potent due to the filtering by the slow excitatory connection from 5-HT to VTA GABA neurons. Alternatively, a phasic input might instead be sent to VTA GABAergic neurons, leading to a more potent activation of the latter.

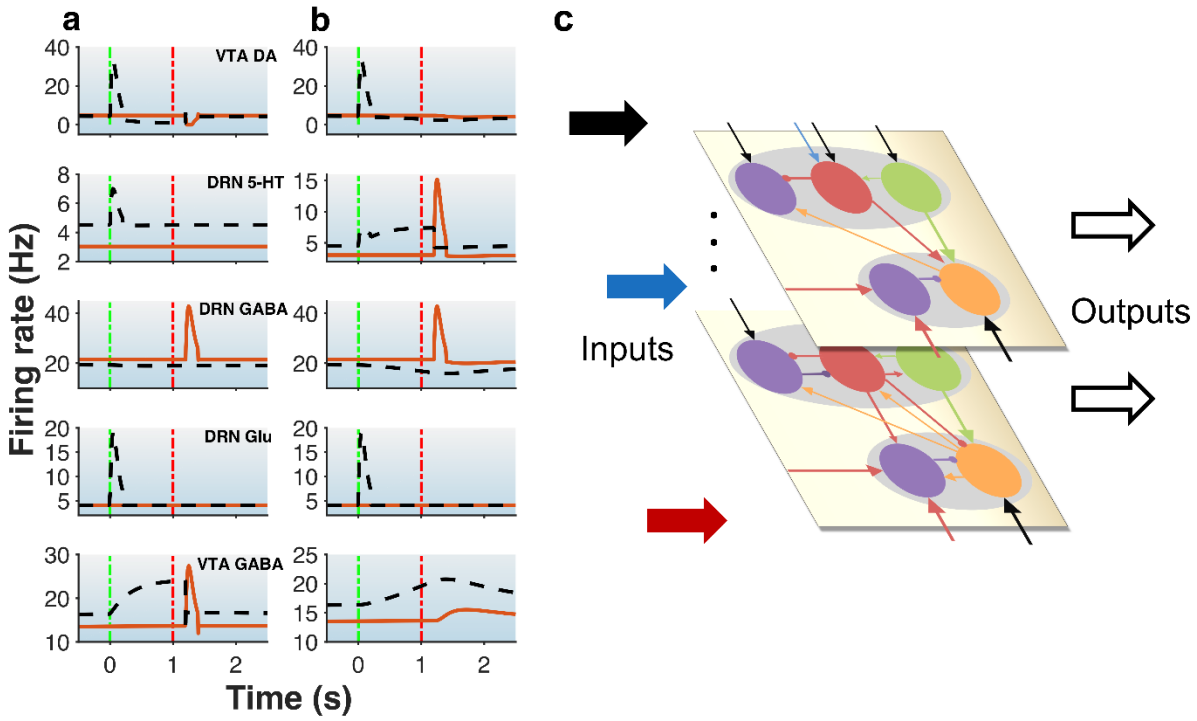

Figure 4.3. DRN-VTA model replicates signalling patterns and suggests multiple parallel circuits. a-b, Model with reward (black dashed lines) and punishment (orange bold lines) tasks with 5-HT neurons that are of Type I **(a)** or Type II **(b)**. Time label from cue onset. Green (red) vertical dashed-dotted lines: cue (outcome) onset time (as in Fig. 2.3b). Top-to-bottom: VTA DA, DRN 5-HT, DRN GABAergic, DRN Glu, and VTA GABAergic neural populations. **c,** Coloured circle: neuronal population. Colour of arrows as in Fig. 4.1. Hypothesis for multiple different DRN-VTA circuits operating in parallel, which may consist of different clusters of neuronal sub-populations and different set of afferent inputs. Vertical dots denote the potential of having more than two distinctive circuits.

For the reward task, to replicate a sustained Type II 5-HT neuronal reward signalling between cue onset and reward outcome (Fig. 4.3b, 2nd row, black dashed) (Cohen et al., 2015; Liu et al., 2014; Li et al., 2016), tonic excitatory input to DRN Type II 5-HT was implemented. The resulting sustained 5-HT activity led to a gradual suppression of DRN GABAergic activity (Fig. 4.3b, 3rd row, black dashed) (Li et al., 2016; Liu et al., 2014b) but also a gradual rise in VTA GABAergic activity regardless of reward outcome (Figure 3b, last row, black dashed) (Cohen and Uchida, 2012; Eshel et al., 2015). The effects on these two GABAergic populations were respectively due to 5-HT's inhibitory connection to DRN GABAergic neurons and excitatory connection to VTA GABAergic neurons. With

regards to the latter, evidence of such excitatory influence via 5-HT_{2C} receptors was reported (Valencia-Torres et al., 2017). Further, it should be noted that in this particular model, it could also lead to a slight suppression of tonic DA activity (Fig. 4.3b, top row, black dashed).

To understand across-trial reward versus punishment effects in the model, a higher constant excitatory input into both DRN 5-HT and VTA DA neurons was implemented under reward compared to punishment conditions (Fig. 4.2, long black arrows). This particular model required differential inputs to 5-HT and DA neurons such that the overall tonic 5-HT neural activity was higher for reward than punishment trials, while DA neural activity remained unchanged (Fig. 4.2, black dashed vs orange bold lines in top two rows), again consistent with experimental observation (Cohen et al., 2015). In the model, although both 5-HT and DA neurons directly received constant across-trial reward-based excitatory inputs, the indirect inhibitory pathway from 5-HT neurons through VTA GABA neurons onto VTA DA neurons nullified the overall effects on DA neurons (Figs. 4.2 and 4.3). In other words, increased firing of 5-HT neurons could be activating VTA GABAergic neurons to a level sufficient to inhibit VTA DA neurons and thereby cancelling out the net long-term reward signals (Fig. 4.2).

It was noticed in this model (and subsequent models) that the excitatory connection from DRN Glu to VTA DA neurons was particularly strong, providing a possible major pathway from the DRN to the VTA (Fig. 4.2). This, together with no (or weak) 5-HT-to-DA connection, was consistent with (McDevitt et al., 2014a). A brief excitatory input to the DRN Glu neuronal population led to its reward-sensitive phasic activation (Fig. 4.3, 4^{th} row, black dashed). This model suggested that the observed peak activity of Type-I 5-HT neurons at cue onset observed experimentally might possibly be due to this phasic local DRN Glu activity, provided the projection from DRN Glu to 5-HT neurons is sufficiently potent. Here, it should also be noted that for the reward task, phasic inputs to the DRN, but not VTA, was implemented. In particular, DRN Glu phasic activity led to the phasic activation of VTA DA neurons. Alternatively, a direct phasic excitatory input to the VTA DA neurons could have been implemented instead. In any case, the phasic activation of DA activity was consistent with the reported DA neuronal response to a fully learned

reward-predicting cue (Cohen and Uchida, 2012; Schultz et al., 1997; Watabe-Uchida et al., 2017).

Under these conditions, with both Types I and II 5-HT neurons, the baseline DRN and VTA GABAergic activities in the reward task were slightly different than those in the punishment task (Fig. 4.3, 3rd and 5th rows, black dashed vs orange bold), which have yet to be observed in experiments. The model's inability to recapitulate all experimental findings with a single neural circuit architecture might perhaps suggest that there are more complex features in the system, such as further division of neuronal subgroups. This also holds for other model architectures investigated (see below, Fig. 4.5). For example, a sub-population of DRN GABAergic neurons might be directly connected to 5-HT neurons (as in Fig. 4.3c, bottom layer), while another DRN GABAergic neuronal sub-population might not be connected such that across-trial reward signal inputs are distributed differently than that of Fig. 4.3c (top layer). Moreover, high chemical and functional diversity amongst DRN 5-HT neurons is now well recognised (Okaty et al., 2019). Hence, it might be possible that there could exist multiple neural circuits with different circuit architectures operating in parallel, as illustrated in Fig. 4.3c.

Taken together, the above have shown that, under reward and punishment conditions, many of the observed signalling patterns in different DRN and VTA neuronal types could readily be reconciled within a single sparsely connected DRN-VTA circuit model. However, not all the signalling patterns could be captured, suggesting that multiple different neuronal sub-populations and circuits may be operating in parallel within the DRN-VTA system. The next sub-section shall investigate whether various different DRN-VTA neural circuits could produce the same output, i.e. be degenerate.

4.3.2. Multiple degenerate DRN-VTA circuits

To search for degenerate DRN-VTA models, various combinations of connections within and between the DRN and VTA were implemented, and where necessary, adjusted any afferent inputs. The network activity profile illustrated in Figs. 4.3a and b was used as an output "target" to check whether other different circuits could replicate a similar activity profile. Given the variability of neuronal firing rates reported in the literature, to be

considered a degenerate neural circuit, an inclusion criterion that permitted maximal deviations of the firing activities of the DRN 5-HT, DRN GABA, DRN Glu, VTA DA, and VTA GABA neural populations was set to be less than 10%, 17%, 10%, 10% and 17%, respectively, from those illustrated in Fig. 4.3, respectively (see Table 4.2, and Fig. 4.4). This was quantified within a 3 s time duration, from 1 s before cue onset to 1 s after outcome onset, encompassing both baseline and stimulus-evoked activities. Within the inclusion criteria, any neural circuit architecture which could not replicate the activity profiles shown in Fig. 4.3 was discarded.

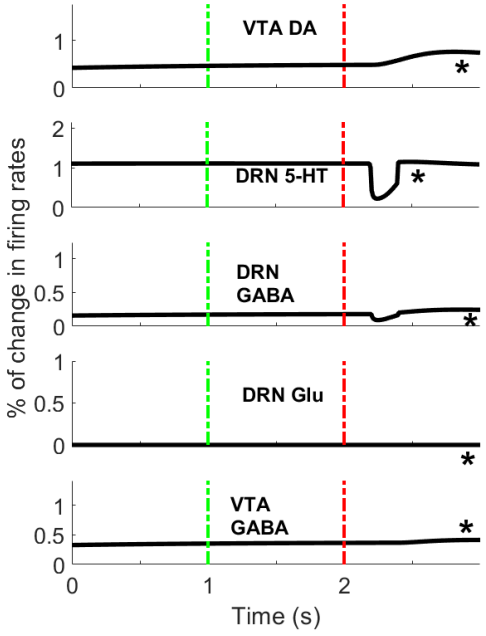

Figure 4.4. Sample of mean percentage changes in neural population firing rates (from activity profile template) of a specific network model under a certain condition. Mean percentage of deviations from the template outputs of a specific model architecture ('I'; see Fig. 4.5) and excitatory 5-HT-to-DA connection, with Type-I 5-HT neurons under reward task. The maximum of mean percentage deviation within this time period for each neural population is denoted with an asterisk. Green (Red) vertical dashed line: Cue (Outcome) onset time.

Various neural circuits were created by systematic addition and modification of connections of our sparsely connected DRN-VTA circuit (now presented as Fig. 4.5k), until a highly connectivity model structure was reached (Fig. 4.5a) yet which was constrained by experimental findings (see above). Each of the circuits was simulated and

evaluated in both reward and punishment tasks using both Type I and II 5-HT neurons, as done above. Both excitatory and inhibitory connections from DRN 5-HT to DRN Glu/GABA and VTA DA neurons were explored. Thus, based on these combinations, we obtained a total of 84 different neural circuit model architectures (including the one in Fig. 4.3 and its variants, as Fig. 4.5k) that fitted our definition of degeneracy (with respect to Fig. 4.3). The high-level model architectures were illustrated in Fig. 4.5 (see also Tables 4.1 and 4.3, and Chapter 5).

Model architecture (Fig. 4)				Type-I 5-HT neurons		Type-II 5-HT neurons	
				Punishment	Reward	Punishment	Reward
				Model #			
a	DA→GABA-VTA (−) 5HT→GABA-DRN (−)	5HT→DA (−)	5HT→Glu (−)	1	2	3	4
			5HT→Glu (+)	5	6	7	8
		5HT→DA (+)	5HT→Glu (−)	9	10	11	12
			5HT→Glu (+)	13	14	15	16
	DA→GABA-VTA (+) 5HT→GABA-DRN (+)	5HT→DA (−)	5HT→Glu (−)	17	18	19	20
			5HT→Glu (+)	21	22	23	24
		5HT→DA (+)	5HT→Glu (−)	25	26	27	28
			5HT→Glu (+)	29	30	31	32
b	5HT→Glu (−)			33	34	35	36
	5HT→Glu (+)			37	38	39	40
c	-			41	42	43	44
d	-			45	46	47	48
e	-			49	50	51	52
f	-			53	54	55	56
g	-			57	58	59	60
h	-			61	62	63	64
i	-			65	66	67	68
j	-			69	70	71	72
k	-			73	74	75	76
l	5HT→DA (−)			77	78	79	80
	5HT→DA (+)			81	82	83	84

Table 4.3. Degenerate DRN-VTA model #'s and architectures based on specific connectivity and 5-HT neuronal types and reward/punishment task. The model architectures and #'s (right side of table) discussed in Figs. 4.5 (and Chapter 5) are dependent on specific connectivity type (left side of table), 5-HT neuronal type and punishment/reward task (right side of table). Arrows denote connections. Sub-divisions or branching of the connectivity types from the model architectures are also indicated. + / − : effectively positive or negative connection.

Some boxes are not filled due to those connections being absent in those models (e.g. model k has no 5-HT→Glu and 5-HT→DA connections; see Fig. 4.5).

For instance, model architecture 'a' in Fig. 4.5a (see Fig. 4.1 for detailed architecture) actually consisted of 32 distinctive models with different 5-HT neuron types and connectivity signs (see Table 4.3). Interestingly, the model parameters remained the same with either excitatory or inhibitory connections (Fig. 4.2, diamond connections; Table 4.1). Fig. 4.4 shows an example of the percentage change in firing rates (from activity profile template) with model architecture 'l' and an excitatory 5-HT-to-DA connection, using Type-I 5-HT neurons under the reward task.

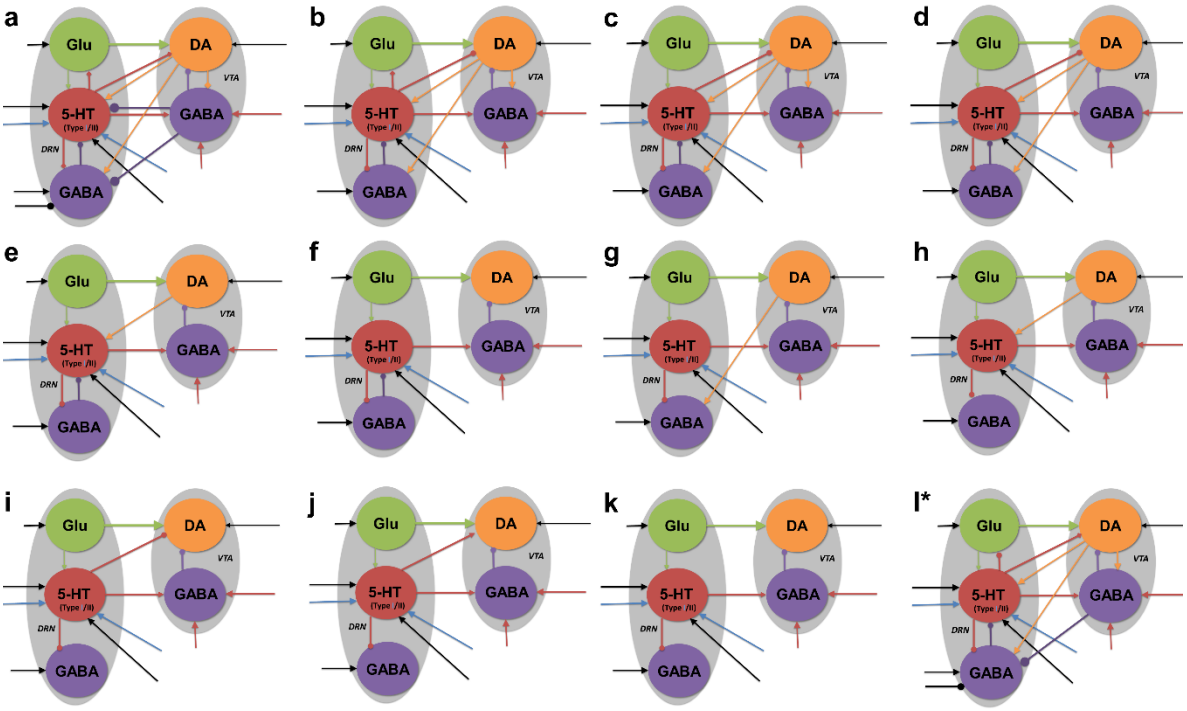

Figure 4.5. Neural circuit model architectures with similar network activity profiles. Grey: local brain region (VTA/DRN). Coloured circle: neuronal population. Arrow colours as in Fig. 4.1. The activity profiles (not shown) were similar to that in Figs. 4.3 a and b, confining within set ranges of values (see text). **a-k,** Architectures of decreasing connectivity, with Fig. 4.3 in **(l)**. **l,** with an asterisk denotes the only model with fast 5-HT to VTA DA connection, simulating fast 5-HT_3 or Glu receptor mediated connection or their combination (co-transmission). **a, l,** Additional inhibitory input to DRN GABA neurons in reward task. All labels, connections and nomenclature

have the same meaning as that in Fig. 4.2, except that, for simplicity, the relative connection weights (thickness) are not shown, and the diamond-end arrows denote connections which are either excitatory or inhibitory, with both explored. Self-connectivity not shown (see Fig. 4.1 for a detailed version of Fig. 4.5a). Note: Each architecture consists of several distinctive model types (with a total of 84 types) with different 5-HT neuronal or excitatory/inhibitory connectivity types (see Tables 4.1 and 4.3, and Chapter 5).

In contrast to the sparsely connected model shown in Fig. 4.2, the highly connected model of Fig. 4.5a had connectivity within the DRN that was consistent with our previous DRN model (Jalewa et al., 2014). For this model to replicate the activity profiles shown in Figs. 1.3b and 4.3, it was found that a direct connection from 5-HT neurons to DA neurons had to be relatively weak or not required, consistent with (McDevitt et al., 2014a). However, experiments have shown the existence of potential direct modulation (Di Giovanni et al., 2009) and more recently, a direct influence of 5-HT on VTA DA neurons mediated by the fast excitatory ionotropic 5-HT_3 receptor was reported (Wang et al., 2019), and is discussed below. Further, a substantial number of other connections in the DRN-VTA model were identified to be redundant or relatively weak, at least in the context of the conditions investigated. These connections included inputs from DRN Glu neurons to any GABA neurons, DRN 5-HT neurons to DRN Glu neurons, DRN 5-HT to DRN GABA neurons and vice versa, VTA DA neurons to DRN Glu neurons, VTA GABA neurons to DRN Glu neurons, VTA DA neurons to VTA GABA neurons, and VTA GABA neurons to 5-HT neurons (Supplementary Table 2). The relatively weak VTA DA-to-GABA connection was consistent with studies so far that showed either a weak or non-existent effect of D_2 receptor activation on VTA GABA neurons (Morales and Margolis, 2017).

With these degenerate models, the effects of specific DRN-VTA connectivity in which there are mixed findings in the literature could now be investigated, and specifically the connectivity within the DRN or VTA, or connectivity between the DRN and VTA. For instance, previous studies had suggested that the influence of 5-HT on DRN GABA neurons could be either excitatory or inhibitory (Hernández-Vázquez et al., 2019). In the case when this connection was inhibitory, it was found that it harboured several degenerate circuits (Figs. 4.5b to 4.5l). On the other hand, when this connection was

excitatory (Fig. 4.5a), under punishment conditions, no modification was required to either the afferent inputs or internal connection strengths. This was the case for networks with both Types I and Type II 5-HT neurons. However, for the reward task, DRN GABAergic neurons was found to generally require an additional inhibitory input to fit the required decreasing activity profile (Figs. 4.5a and 4.5l).

With regards to the connection from DRN 5-HT to DRN Glu neurons, when it was inhibitory, the range of allowed values was more restricted (0-0.1 a.u.) than when excitatory (0-1 a.u.) (Table 4.2), but this applied only to model architecture 'b' (Fig. 4.5b) – model architecture 'a' showed no difference. Interestingly, upon removal of this connection, be it excitatory or inhibitory, the feedback excitatory connection from DRN Glu to 5-HT neurons had to be weakened by ~16% (Fig. 4.5c). With additional removal of the connection from VTA DA to VTA GABA neurons, we found that the strength of the DRN 5-HT to DRN GABA inhibitory connection increased by ~150% (Fig. 4.5d).

As there are also mixed findings regarding the influence of 5-HT on VTA DA neurons (De Deurwaerdère and Di Giovanni, 2017) we explored both excitatory and inhibitory effects. When this connection was inhibitory, we found several degenerate models (Figs. 4a-d, 4i and 4l). Unlike all other models, model 'l' took into account the fast connection from 5-HT to VTA DA neurons, mimicking either 5-HT_3 receptor mediated transmission or 5-HT-glutamate co-transmission (Wang et al., 2019). Moreover, in both reward and punishment tasks, the 5-HT-to-DA connection strength in model 'l' was the same as that in model 'a'. Further, unlike other models, those models with architectures 'a' and 'l' had to include the inhibitory connection from VTA GABA to DRN GABA neurons, as observed in (Li et al., 2019). For models with architectures 'i' and 'j', the 5-HT-to-DA connection strength was twice that of other models with such connections, including 'a' and 'l'. Models 'i' and 'j' also did not have VTA DA to DRN 5-HT, VTA DA to DRN GABA, and DRN GABA to 5-HT connections.

4.3.3. D2 mediated drugs can distinguish some degenerate DRN-VTA circuits

Given the large number of degenerate and stable DRN-VTA circuits that were possible, how can one distinguish among at least some of them? To address this, the circuit responses to simulated D_2 receptor agonists were investigated. This approach was selected due to the extensive D_2 receptor mediated connectivity within the degenerate DRN-VTA circuits (Fig. 4.5). In particular, these connections involved those from VTA DA neurons to DRN 5-HT, DRN GABA and VTA GABA neurons, and also self-inhibition (D_2 autoreceptor-mediated) of DA neurons. To mimic the effects in the model of D_2 receptor agonist drugs, we gradually increased the strengths of connections mediated by D_2 receptors (Fig. 4.1, orange connections emanating from DA neurons) by some factor (X) and observed the neural activity changes.

As the strengths of these specific sets of connection were increased, subsets of the degenerate models gradually behave differently from the activity profile template of Figs. 4.3a and b (Figs. 4.6a and b), allowing the distinguishing between these model groups. Fig. 4.6c showed an example of such differences. However, such evaluation under punishment condition (Fig. 4.6a) was slightly more limited than reward condition (Fig. 4.6b) in terms of distinguishing the degenerate circuits.

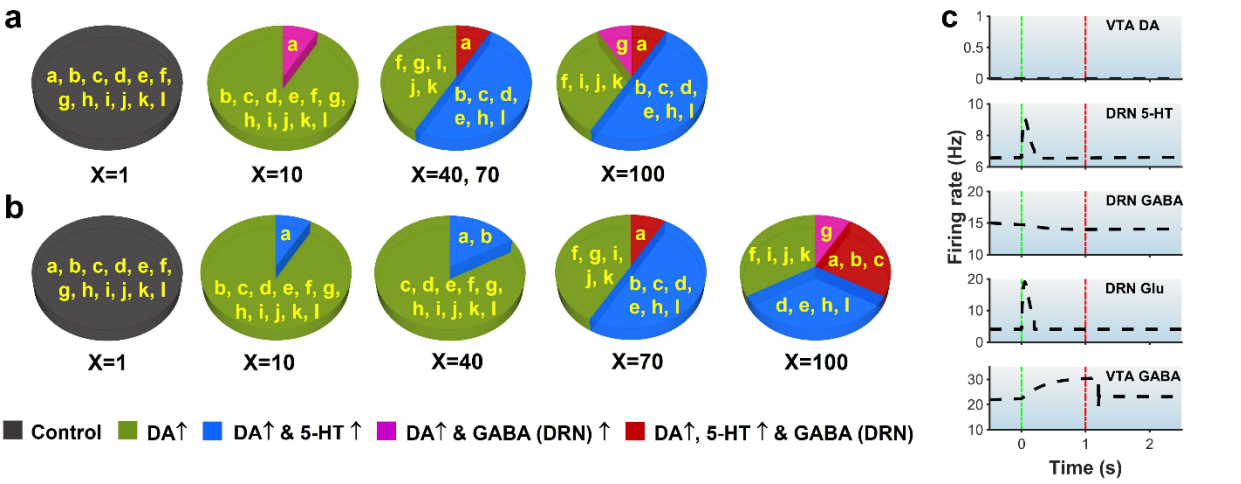

Figure 4.6. D_2 receptor agonist can distinguish subsets of DRN-VTA neural circuits. a-b, Drug administered in punishment **(a)** and reward **(b)** task with efficacy factor X increments of 1, 2, 10, 40, 70 and 100 times. Letters in yellow label model circuit architectures as in Fig. 4.5. (See Tables 4.4-4.7 for details.). The colours represent a particular group of the models behaving in the similar manner to the D_2 receptor agonist. **c,** High D_2 receptor agonist substantially changed

DA and 5-HT activities with model architecture 'e' and Type-I 5-HT neurons in reward task (black dashed lines). D_2 agonist dosage was enhanced by 100 times (compared with Fig. 4.3). Time label from cue onset. Green (Red) vertical dashed line: Cue (Outcome) onset time.

When the strengths of connections mediated by D_2 receptors were increased by a factor of 10, the activity of DA neurons in all the degenerate neural circuits was increased under both reward and punishment conditions (Figs. 4.6a and b, with factor X = 10; Table 4.4).

Arc	Connection type			With Type-I 5-HT neurons									
				Punishment					Reward				
a				VTA DA *	DRN 5-HT *	DRN GABA *	VTA GABA *	VTA Glu *	VTA DA *	DRN 5-HT *	DRN GABA *	VTA GABA *	VTA Glu *
	DA→ VTA GABA (−)	5HT→ DA (−)	5HT→ Glu (−)	64.43	4.56	7.36	0.34	0.50	64.01	13.85	5.82	3.68	0.72
			5HT→ Glu (+)	66.19	4.91	7.35	0.38	0.50	63.46	2.37	5.86	0.46	0.66
	5-HT→ VTA GABA (−)	5HT→ DA (+)	5HT→ Glu (−)	67.34	4.47	7.35	0.34	0.50	64.88	2.13	5.85	0.40	0.66
			5HT→ Glu (+)	66.19	4.91	7.35	0.38	0.50	61.98	1.55	6.05	1.24	0.64
	DA→ VTA GABA (+)	5HT→ DA (−)	5HT→ Glu (−)	64.91	4.18	17.41	0.94	0.50	64.50	13.81	6.56	4.27	0.72
			5HT→ Glu (+)	66.66	4.53	17.41	0.97	0.50	63.95	2.29	6.54	1.04	0.66
	5-HT→ VTA GABA (+)	5HT→ DA (+)	5HT→ Glu (−)	67.82	4.10	17.40	0.93	0.50	65.37	2.05	6.53	0.98	0.66
			5HT→ Glu (+)	66.66	4.53	17.41	0.97	0.50	62.47	1.59	6.38	0.66	0.64
b	5HT→Glu (−)			66.73	6.05	8.47	1.02	0.50	64.09	4.23	11.30	1.16	0.67
	5HT→Glu (+)			60.91	3.31	8.59	0.38	4.95	56.91	2.67	11.46	0.45	6.54
c	-			66.66	2.22	8.58	0.27	0.00	64.02	1.70	11.45	0.30	0.00
d	-			66.81	4.67	1.01	0.44	0.00	64.27	3.31	1.05	0.55	0.00
e	-			64.99	2.45	0.04	0.12	0.00	62.02	1.90	0.04	0.12	0.00
f	-			64.63	2.27	0.17	0.45	0.00	61.55	1.52	0.22	0.52	0.00
g	-			65.00	0.00	2.35	0.00	0.00	61.99	0.00	2.59	0.00	0.00
h	-			65.37	4.69	0.16	0.44	0.00	62.47	3.33	0.24	0.55	0.00
i	-			62.15	0.00	0.00	0.00	0.00	58.45	0.00	0.00	0.00	0.00
j	-			67.86	0.00	0.00	0.00	0.00	65.54	0.00	0.00	0.00	0.00
k	-			65.00	0.00	0.00	0.00	0.00	61.99	0.00	0.00	0.00	0.00
l	5HT→DA (−)			67.33	2.12	7.44	1.13	0.49	65.22	1.76	5.23	1.67	0.65
	5HT→DA (+)			65.50	2.17	7.45	1.14	0.49	62.69	1.81	5.22	1.67	0.65

Table 4.4. Simulated D2 agonist changes in neural population firing rates with D2 receptor-mediated connection strengths changed by a factor of 10 (X=10). *: Percentage changes in neural population activities. Values in red: Percentage changes beyond the allowed ranges. Arc: Architecture type. Only models with Type-I 5-HT neurons shown; results with Type-II 5-HT neurons are similar. Nomenclatures the same as in Table 4.3.

For the punishment task, VTA DA neuronal activity increased the DRN GABAergic neuronal activities, particularly when the connections from VTA DA to VTA GABA neurons or from DRN 5-HT to DRN GABAergic neurons were excitatory. For the reward task, VTA DA neuronal activity increased the DRN 5-HT neural activity in models with inhibitory DRN 5-HT-to-DA and 5-HT-to-Glu neuronal connections irrespective of the connections from VTA DA to VTA GABAergic neurons (see model with architecture 'a'; Figs. 4.6a and b, blue and magenta regions with X = 10; Table 4.4).

For the punishment task, increasing simulated D_2 agonist further (40 times higher) additionally increased the activity of the DRN 5-HT neurons in ~58% of the models with architectures 'a', 'b', 'c', 'd', 'e', 'h' and 'l' (Fig. 4.6a, blue and red regions with X = 40; Table 4.5). Additionally, models with architecture 'a' also showed increased VTA DA and GABA neuron activity. This led to increased DRN GABA neuron activity, particularly when connections from DRN 5-HT to DRN GABAergic neurons or DA to VTA GABAergic neurons were excitatory. In comparison, in the reward task, the same level of D_2 receptor activation increased the activity of DRN 5-HT neurons in models with architecture 'a'. However, for models with architecture 'b', this occurred only when the DRN 5-HT-to-Glu neuronal connections were inhibitory (Fig. 4.6b, blue region; Table 4.5).

Arc	With Type-I 5-HT neurons										
a	Connection type			Punishment					Reward				
				VTA DA *	DRN 5-HT *	DRN GABA *	VTA GABA *	VTA Glu *	VTA DA *	DRN 5-HT *	DRN GABA *	VTA GABA *	VTA Glu *
	DA→ VTA GABA (–)	5HT→ DA (–)	5HT→ Glu (–)	100.00	24.32	9.58	1.56	0.53	100.00	27.04	10.98	5.35	0.76
			5HT→ Glu (+)	100.00	24.74	9.57	1.61	0.53	100.00	15.17	11.02	2.03	0.70
	5-HT→ VTA GABA (–)	5HT→ DA (+)	5HT→ Glu (–)	100.00	24.31	9.58	1.56	0.53	100.00	14.80	11.02	1.97	0.70
			5HT→ Glu (+)	100.00	24.74	9.57	1.61	0.53	100.00	20.25	11.21	1.37	0.69
	DA→ VTA GABA (+)	5HT→ DA (–)	5HT→ Glu (–)	100.00	23.64	20.18	3.47	0.53	100.00	26.95	11.76	7.14	0.75
			5HT→ Glu (+)	100.00	24.06	20.19	3.52	0.53	100.00	14.87	11.74	3.79	0.70
	5-HT→ VTA GABA (+)	5HT→ DA (+)	5HT→ Glu (–)	100.00	23.64	20.18	3.47	0.53	100.00	14.49	11.74	3.73	0.70
			5HT→ Glu (+)	100.00	24.06	20.19	3.52	0.53	100.00	20.10	11.56	3.16	0.69
b	5HT→Glu (–)			100.00	16.08	10.85	2.63	0.52	100.00	10.88	13.71	2.85	0.68
	5HT→Glu (+)			100.00	13.30	10.95	1.96	5.09	100.00	9.28	13.84	2.12	6.72

c	-	100.00	12.26	10.97	1.86	0.00	100.00	8.36	13.86	1.97	0.00
d	-	100.00	14.76	3.18	1.37	0.00	100.00	10.00	3.18	1.63	0.00
e	-	100.00	12.52	0.33	0.90	0.00	100.00	8.58	0.47	1.10	0.00
f	-	100.00	2.27	0.17	0.45	0.00	100.00	1.52	0.22	0.52	0.00
g	-	100.00	0.00	7.39	0.00	0.00	100.00	0.00	7.77	0.00	0.00
h	-	100.00	14.76	0.51	1.37	0.00	100.00	10.00	0.70	1.63	0.00
i	-	100.00	0.00	0.00	0.00	0.00	100.00	0.00	0.00	0.00	0.00
j	-	100.00	0.00	0.00	0.00	0.00	100.00	0.00	0.00	0.00	0.00
k	-	100.00	0.00	0.00	0.00	0.00	100.00	0.00	0.00	0.00	0.00
l	**5HT→DA (–)**	100.00	12.16	9.82	2.06	0.51	100.00	8.43	3.71	2.66	0.67
	5HT→DA (+)	100.00	12.18	9.83	2.06	0.51	100.00	8.45	3.69	2.67	0.67

Table 4.5. Simulated D2 agonist changes in neural population firing rates with D2 receptor-mediated connection strengths changed by a factor of 40 (X=40). *: Percentage changes in neural population activities. Values in red: Percentage changes beyond the allowed ranges. Arc: Architecture type. Only models with Type-I 5-HT neurons shown; results with Type-II 5-HT neurons are similar. Nomenclatures the same as in Table 4.3.

Interestingly, for the punishment task, the above behaviour remained stable as the level of D_2 receptor activation increased by a factor of 70 (Figs. 4.6a, blue and red regions for X=40 and 70; Table 4.6), suggesting some form of saturation effects might have occurred. For the reward task, the results were different; an additional cluster of models could be identified, with models 'a' and 'b' being split into different clusters (Fig. 4.6b, blue and red regions for X=70; Table 4.6). In particular, models with architecture 'a' did not follow the same cluster as that with lower levels of D_2 receptor activation, and exhibited increased DRN GABAergic neuronal activities. On the other hand, the models with architecture 'b' exhibited increased activities of DRN 5-HT and VTA DA neurons without changes in the activity of DRN GABA neurons.

Arc	Connection type			With Type-I 5-HT neurons									
				Punishment					Reward				
a				VTA DA *	DRN 5-HT *	DRN GABA *	VTA GABA *	VTA Glu *	VTA DA *	DRN 5-HT *	DRN GABA *	VTA GABA *	VTA Glu *
	DA→ VTA GABA (−)	5HT→ DA (−)	5HT→ Glu (−)	100.00	45.26	11.93	2.90	0.56	100.00	41.15	16.50	7.03	0.79
			5HT→ Glu (+)	100.00	45.70	11.92	2.94	0.56	100.00	29.12	16.54	3.65	0.74
	5-HT→ VTA GABA (−)	5HT→ DA (+)	5HT→ Glu (−)	100.00	45.26	11.93	2.90	0.56	100.00	28.73	16.54	3.58	0.74
			5HT→ Glu (+)	100.00	45.70	11.92	2.94	0.56	100.00	41.39	16.73	4.13	0.75
	DA→ VTA GABA (+)	5HT→ DA (−)	5HT→ Glu (−)	100.00	44.26	23.12	6.20	0.56	100.00	41.01	17.31	10.10	0.79
			5HT→ Glu (+)	100.00	44.70	23.13	6.25	0.56	100.00	28.61	17.30	6.66	0.74
	5-HT→ VTA GABA (+)	5HT→ DA (+)	5HT→ Glu (−)	100.00	44.26	23.12	6.20	0.56	100.00	28.21	17.29	6.60	0.74
			5HT→ Glu (+)	100.00	44.70	23.13	6.25	0.56	100.00	41.13	17.10	7.18	0.74
b	5HT→Glu (−)			100.00	26.68	13.37	4.32	0.53	100.00	17.99	16.29	4.61	0.70
	5HT→Glu (+)			100.00	23.94	13.48	3.64	5.23	100.00	16.42	16.42	3.86	6.90
c	-			100.00	22.87	13.49	3.53	0.00	100.00	15.48	16.45	3.71	0.00
d	-			100.00	25.43	5.49	2.34	0.00	100.00	17.16	5.47	2.75	0.00
e	-			100.00	23.20	0.69	1.86	0.00	100.00	15.74	0.95	2.21	0.00
f	-			100.00	2.27	0.17	0.45	0.00	100.00	1.52	0.22	0.52	0.00
g	-			100.00	0.00	12.72	0.00	0.00	100.00	0.00	13.31	0.00	0.00
h	-			100.00	25.43	0.87	2.34	0.00	100.00	17.16	1.18	2.75	0.00
i	-			100.00	0.00	0.00	0.00	0.00	100.00	0.00	0.00	0.00	0.00
j	-			100.00	0.00	0.00	0.00	0.00	100.00	0.00	0.00	0.00	0.00
k	-			100.00	0.00	0.00	0.00	0.00	100.00	0.00	0.00	0.00	0.00
l	5HT→DA (−)			100.00	22.78	12.34	3.13	0.52	100.00	15.55	3.89	3.86	0.69
	5HT→DA (+)			100.00	22.79	12.34	3.13	0.52	100.00	15.56	3.90	3.87	0.69

Table 4.6. Simulated D2 agonist changes in neural population firing rates with D2 receptor-mediated connection strengths changed by a factor of 70 (X=70). *: Percentage changes in neural population activities. Values in red: Percentage changes beyond the allowed ranges. Arc: Architecture type. Only models with Type-I 5-HT neurons shown; results with Type-II 5-HT neurons are similar. Nomenclatures the same as in Table 4.3.

For the punishment task, when the level of D_2 receptor activation was increased by a factor of 100, an increase in DRN GABA and VTA DA neuronal activity was observed in

models with architecture 'g' (Fig. 4.6a, magenta regions with X = 100; Table 4.7). This was not surprising as DRN GABA neurons received an excitatory input from VTA DA neurons (Fig. 4.5). In comparison, for the reward task, an increase in D_2 receptor activation by a factor of 100 substantially affected GABA, 5-HT and DA neuronal activities in models with architectures 'a', 'b' and 'c' (Figs. 4.6b, red regions with X = 100; Table 4.7). Fig. 4.6c shows an example of substantial changes of DA and 5-HT neuronal activity for a model with architecture 'e' using Type I 5-HT neurons in the reward task. Specifically, DA activity was almost totally suppressed while 5-HT activity was increased by about 23% (Table 4.6). These were beyond the acceptable ranges defined (see above).

Arc	With Type-I 5-HT neurons											
a	Connection type			Punishment					Reward				
				VTA DA *	DRN 5-HT *	DRN GABA *	VTA GABA *	VTA Glu *	VTA DA *	DRN 5-HT *	DRN GABA *	VTA GABA *	VTA Glu *
	DA→ VTA GABA (–)	5HT→ DA (–)	5HT→ Glu (–)	100.00	66.19	14.26	4.36	0.60	100.00	55.31	22.04	8.72	0.83
			5HT→ Glu (+)	100.00	66.66	14.25	4.42	0.60	100.00	43.10	22.08	5.31	0.78
	5-HT→ VTA GABA (–)	5HT→ DA (+)	5HT→ Glu (–)	100.00	66.19	14.26	4.36	0.60	100.00	42.69	22.08	5.25	0.77
			5HT→ Glu (+)	100.00	66.66	14.25	4.42	0.60	100.00	62.58	22.27	6.96	0.80
	DA→ VTA GABA (+)	5HT→ DA (–)	5HT→ Glu (–)	100.00	64.87	26.08	9.06	0.59	100.00	55.12	22.89	13.08	0.83
			5HT→ Glu (+)	100.00	65.34	26.09	9.12	0.59	100.00	42.38	22.87	9.59	0.77
	5-HT→ VTA GABA (+)	5HT→ DA (+)	5HT→ Glu (–)	100.00	64.87	26.08	9.06	0.59	100.00	41.97	22.87	9.52	0.77
			5HT→ Glu (+)	100.00	65.34	26.09	9.12	0.59	100.00	62.21	22.67	11.29	0.80
b	5HT→Glu (–)			100.00	37.30	15.90	6.05	0.55	100.00	25.13	18.88	6.39	0.72
	5HT→Glu (+)			100.00	34.60	16.00	5.35	5.38	100.00	23.59	19.01	5.64	7.09
c	-			100.00	33.50	16.02	5.24	0.00	100.00	22.62	19.04	5.49	0.00
d	-			100.00	36.11	7.78	3.36	0.00	100.00	24.33	7.77	3.88	0.00
e	-			100.00	33.90	1.07	2.86	0.00	100.00	22.92	1.43	3.34	0.00
f	-			100.00	2.27	0.17	0.45	0.00	100.00	1.52	0.22	0.52	0.00
g	-			100.00	0.00	18.07	0.00	0.00	100.00	0.00	18.87	0.00	0.00
h	-			100.00	36.12	1.25	3.36	0.00	100.00	24.33	1.67	3.88	0.00
i	-			100.00	0.00	0.00	0.00	0.00	100.00	0.00	0.00	0.00	0.00
j	-			100.00	0.00	0.00	0.00	0.00	100.00	0.00	0.00	0.00	0.00
k	-			100.00	0.00	0.00	0.00	0.00	100.00	0.00	0.00	0.00	0.00

I	**5HT→DA (–)**	100.00	33.41	14.85	4.23	0.54	100.00	22.68	6.51	5.09	0.71
	5HT→DA (+)	100.00	33.42	14.85	4.24	0.54	100.00	22.70	6.52	5.10	0.71

Table 4.7. Simulated D2 agonist changes in neural population firing rates with D2 receptor-mediated connection strengths changed by a factor of 100 (X=100). *: Percentage changes in neural population activities. Values in red: Percentage changes beyond the allowed ranges. Arc: Architecture type. Only models with Type-I 5-HT neurons shown; results with Type-II 5-HT neurons are similar. Nomenclatures the same as in Table 4.3.

Interestingly, the overall effects of D_2 receptor activation remained regardless of whether the circuits encompassed Type I or Type II 5-HT neurons. Thus, the modelling predicted that a gradual increment of the level of D_2 receptor activation (such as through administration of D_2 agonist drugs) could lead to differential suppressions and/or enhancements of firing rate activities that could be used to distinguish subsets of the degenerate DRN-VTA circuits.

4.4. Discussion

In this work, the question of whether neural circuits that utilised neuromodulators can themselves be degenerate was addressed by computationally modelling DRN-VTA circuits, which had been known to share structural and functional structural and functional bidirectional relationship among their constituent neuron types. Moreover, these circuits are involved in the regulation of key cognitive, emotional and behavioural processes, and implicated in many common and disabling neuropsychiatric conditions. To begin, a biologically-based, mean-field computational model of the DRN-VTA circuit with several neuronal types was developed and tested under classic conditions of reward and punishment. The modelling was partially constrained by known connectivity within and between the DRN and VTA regions, and their inputs from multiple other brain regions, including mixed combinations of inputs (Beier et al., 2015; Ogawa et al., 2014; Ogawa and Watabe-Uchida, 2018; Dorocic et al., 2014; Tian et al., 2016; Watabe-Uchida et al., 2017, 2012). We found that a parsimonious, sparsely connected version of the DRN-VTA model could reconcile many of the diverse phasic and tonic neural signalling events

reported in the DRN and VTA in (unexpected) punishment and (learned) reward tasks observed across separate experimental studies (Fig. 4.2). This model was evaluated using Type I and Type II 5-HT neurons in the DRN as defined electrophysiologically in a previous study (Cohen et al., 2015). In the case of Type II 5-HT neurons under the reward task, the model predicted that sustained 5-HT neuron activity between cue and reward outcome (Cohen et al., 2015) would lead to the gradual inhibition of DRN GABA neuron activity and enhancement of VTA GABA neuron activity, as previously observed experimentally (Cohen and Uchida, 2012; Li et al., 2016). The sparsely connected model could also reproduce experimental observations (Cohen et al., 2015). of an increase in baseline firing of Type I 5-HT neurons across several trials in the rewarding task, without similar effects on VTA DA neurons, or in the punishment task. This model suggested that slow, across-trial reward-based excitatory inputs could potentially be directly targeted to both DRN 5-HT and VTA DA neurons, and that inhibitory 5-HT to GABA to DA connectivity cancelled out the effects of the direct input to VTA DA neurons, rendering only long timescale changes on baseline activity of DRN 5-HT neurons. Such a cancellation effect is reminiscent of parallel excitatory and inhibitory pathways operating in conditioning tasks (e.g. Zhou et al. (2018)).

Despite the strong predictive validity of the model, it was not able to fully capture some of the activity profiles with Type I 5-HT neurons, namely, the differential baseline activities of VTA GABA neurons and DRN GABA neurons between reward and punishment conditions. Perhaps the DRN-VTA circuit model might not be sufficiently complex to capture all the signalling effects reported in experimental studies, even though we observed similar results with more complex model architectures. Thus, further additional neuronal populations and DRN-VTA circuits could be operating in parallel. Such parallel circuits could be validated experimentally in the future, for example, using gene-targeting of specific DRN and VTA neuron subtypes and projections. Indeed, there is increasing evidences that DRN 5-HT neurons are more chemically diverse than previously expected, and that there is a high level of functional diversity in output pathways of the DRN and VTA (Dorocic et al., 2014; Ogawa et al., 2014; Weissbourd et al., 2014; Beier et al., 2015; Liu et al., 2015; Tian et al., 2016; Fernandez et al., 2017; Morales and Margolis, 2017;

Watabe-Uchida et al., 2017, 2012; Ogawa and Watabe-Uchida, 2018; Ren et al., 2018; Zhou et al., 2018;Okaty et al., 2019;)

To demonstrate degeneracy in the DRN-VTA system, several variants of the DRN-VTA circuit model were shown to readily recapitulate the same neural signalling profiles, even with occasional slight changes made to their afferent inputs. Finally, we simulated increased D_2 receptor activation by increasing the connection strengths emanating from the VTA DA neurons. D_2 receptor agonist was targeted due to its extensive influence in the DRN-VTA circuit. This allowed us to distinguish some of the degenerate DRN-VTA neural circuits by identifying substantial deviations in specific neural population activities in conditioning tasks. Interestingly, more degenerate neural circuits could be identified in rewarding than in punishment tasks. Thus, D_2 receptor agonist, and perhaps more generally certain neuro-transmitter based drugs, can modify the activities of some of the apparently degenerate DRN-VTA circuits and distinguish some of these circuits due to their structural differences. Together, this computational modelling and analytical work supported the existence of degeneracy and stability in the DRN-VTA circuits, and subsets of these degenerate circuits could be distinguished through pharmacological means.

From a more general perspective, our computational modelling and analytical framework could be applied to the study of degeneracy of neural circuits involving the interactions of other neuromodulators such as norepinephrine/noradrenaline (e.g. Jalewa et al., 2014; Joshi et al., 2017). It should also be noted that in the development of the models, we had resorted to a minimalist approach by focusing only on sufficiently simple neural circuit architectures that could replicate closely to the experimentally observed data. Future modelling work may investigate the relative relevance of these connections with respect to larger circuits involving cortical and subcortical brain regions across multiple scales, especially during adaptive learning (e.g. Wang and Wong-Lin, 2013; Zhou et al., 2018).

Overall, through computational modelling, our study suggests the plausibility of degenerate neural circuits that encompass serotonin and dopamine neuromodulators.

Chapter 5
Stability of degenerate DRN-VTA circuits

This contributing chapter uses dynamical systems theory to demonstrate the stability of the identified degenerate DRN-VTA neural circuits in Chapter 4. Parts of this review are archived in a pre-print manuscript.

5.1. Introduction

In Chapter 4, degenerate DRN-VTA neural circuit models were modelled, demonstrating the plausibility of generate neural circuits of neuromodulators. Here, the local dynamical stability of these degenerate circuit models will be mathematically determined. Specifically, for each degenerate circuit model, local stability analysis will be used to find the stability of a system of dynamical equations that describe DRN-VTA circuit dynamics. The local stability of the network can be determined by first determining the steady states (also called fixed points) and then identifying whether each of these fixed points, if they exists, are stable (Strogatz, 2018).

5.2. Steady states (fixed points) for each DRN-VTA model

The computational models to be investigated were based on our previous mean-field, neural population based modelling framework for neuromodulator circuits (Joshi et al., 2017), in which the averaged concentration releases of neuromodulators ([5-HT] and [DA]) were monotonic functions of the averaged firing rate of (5-HT and DA) neuronal populations via some neuromodulator induced slow currents.

Rewriting Eqns. (4.11)-(4.16) in Chapter 4, and inserting the explicit model parameter values to these coupled dynamical equations for the DRN-VTA system, they became:

$$500\,\frac{dI_{auto,5-HT}}{dt} = -I_{auto,5-HT} + \frac{80}{1+e^{-10([5-HT]-0.1)}} \tag{5.1}$$

$$150\,\frac{dI_{auto,DA}}{dt} = -I_{auto,DA} + \frac{80}{1+e^{-10([DA]-0.1)}} \tag{5.2}$$

$$1200\,\frac{dI_{DA,5-HT}}{dt} = -I_{DA,5-HT} + \frac{0.03}{1+e^{-20([5-HT]-0.1)}} \tag{5.3}$$

$$1000\,\frac{dI_{5-HT,DA}}{dt} = -I_{5-HT,DA} + \frac{0.03}{1+e^{-20([DA]-0.3)}} \tag{5.4}$$

$$\frac{d[5-HT]}{dt} = \frac{0.08F_{5-HT}}{1000} - \frac{0.0013[5-HT]}{0.17+[5-HT]} \tag{5.5}$$

$$\frac{d[DA]}{dt} = \frac{0.1F_{DA}}{1000} - \frac{0.004[DA]}{0.15+[DA]} \tag{5.6}$$

Substituting Eqns. (4.6)-(4.10) into Eqns. (4.1)-(4.5), and inserting the explicit model parameters, it led to the following 5 input-output or current-frequency equations:

$$F_{5-HT} = g_{5-HT}[-I_{auto,5-HT} + W_{5d}\,I_{5-HT,DA} + J_{55e}\,I_{5-HT,Glu} - J_{55i}\,I_{5-HT,GABA-DRN} - J_{5i}\,I_{5-HT,GABA-VTA} + 99.87 + I_{5-\mathrm{HT,ext}}]_+ \tag{5.7}$$

$$F_{DA} = g_{DA}[-I_{auto,DA} \pm W_{d5}\,I_{DA,5-HT} + J_{d5e}\,I_{DA,Glu} - J_{di}\,I_{DA,VTA-GABA} + 210 + I_{DA,ext}]_+ \tag{5.8}$$

$$F_{Glu} = g_{Glu}[J_{self,Glu}\,F_{Glu} \pm W_{5e5}\,I_{Glu,5-HT} + 100 + I_{Glu,ext}]_+ \tag{5.9}$$

$$F_{GABA-DRN} = g_{GABA-DRN}[-J_{self,GABA-DRN}\,F_{GABA-DRN} \pm W_{5i5}\,I_{GABA-DRN,5-HT} + W_{5id}\,I_{GABA-DRN,DA} - W_{5ii}\,I_{GABA-DRN,GABA-VTA} + 450 + I_{GABA-DRN,ext}]_+ \tag{5.10}$$

$$F_{GABA-VTA} = g_{GABA-VTA}[-J_{self,GABA-VTA}\,F_{GABA-VTA} + W_{i5}\,I_{GABA-VTA,5-HT} \pm W_{id}\,I_{GABA-VTA,DA} + 200 + I_{GABA-VTA,ext}]_+ \tag{5.11}$$

Each network's steady state (or equilibrium/fixed point) can be obtained by setting the rate of change for all the above dynamical equations (Eqns. (5.1)-(5.6)) to zero, i.e.

$\frac{dI_{auto,5-HT}}{dt} = \frac{dI_{auto,DA}}{dt} = \frac{dI_{DA,5-HT}}{dt} = \frac{dI_{5-HT,DA}}{dt} = \frac{d[5-HT]}{dt} = \frac{d[DA]}{dt} = 0$, and then solving them algebraically. The solution of these equations will give the steady-state value for each model. Specifically, the currents (dynamical variables) from Eqns. (5.1)-(5.6) (e.g. $I_{auto,5-HT} = \frac{80}{1+e^{-10([5-HT]-0.1)}}$) were substituted into Eqns. (5.7)-(5.11). Note that the different model architectures (Fig. 4.5 and Table 4.3) can be determined from the specific sets of values of W's and J's, and occasionally specific biased currents (see Table 4.1). Henceforth, only the generic solution is provided. The steady state values for the model as described above can be re-written as under using Eqns 5.1-5.6,

$$I_{auto,5-HT} = \frac{80}{1+x} \tag{5.12}$$

$$I_{auto,DA} = \frac{80}{1+y} \tag{5.13}$$

$$I_{DA,5-HT} = \frac{0.03}{1+x^2} \tag{5.14}$$

$$I_{5-HT,DA} = \frac{0.03}{1+ay^2} \tag{5.15}$$

$$F_{DA} = \frac{40[DA]}{0.15+[DA]} \tag{5.16}$$

$$F_{5-HT} = \frac{16.25[5HT]}{0.17+[5HT]} \tag{5.17}$$

where $x = e^{-10([5-HT]-0.1)}$,$y = e^{-10([DA]-0.1)}$ and with $a = e^4$.

Hence, at the steady state, considering all-to-all connectivity (the most general case), and using the explicit parameter values and equations (5.12-5.17) the afferent input currents from Eqns. (4.6)-(4.10) can be written as

$$I_{DA} = -J_{self,DA}\frac{80}{1+y} \pm W_{d5}\frac{0.03}{1+x^2} + J_{d5e}F_{Glu} - J_{di}F_{GABA-VTA} - J_{d5i}F_{GABA-DRN} + 210 + I_{DA,ext} \tag{5.18}$$

$$I_{5-HT} = -J_{self,5-HT}\frac{80}{1+x} + W_{5d}\ \frac{0.03}{1+ay^2} + J_{55e}F_{Glu} - J_{55i}F_{GABA-DRN} - J_{5i}\ F_{GABA-VTA} + 99.87 + I_{5-HT,ext} \quad (5.19)$$

$$I_{Glu} = J_{self,Glu}\ F_{Glu} \pm W_{5e5}\ \frac{0.03}{1+x^2} - W_{5edi}F_{GABA-VTA} + W_{5e2}\frac{0.03}{1+ay^2} + 100\ + I_{Glu,ext} \quad (5.20)$$

$$I_{GABA-DRN} = -J_{self,GABA-DRN}\ F_{GABA-DRN} \pm\ W_{5i5}\ \frac{0.03}{1+x^2} + W_{5id}\ \frac{0.03}{1+ay^2} +\ W_{5ie} * F_{Glu} - W_{5ii}\ I_{GABA-DRN,GABA-VTA} + 450 +\ I_{GABA-DRN,ext} \quad (5.21)$$

$$I_{GABA-VTA} = -J_{self,GABA-VTA}\ F_{GABA-VTA} + W_{i5}\ \frac{0.03}{1+x^2} \pm W_{id}\ \frac{0.03}{1+ay^2} +\ 200 + I_{GABA-VTA,ext} \quad (5.22)$$

Now, using only the linear parts of the above threshold-linear functions (which were validated post-hoc), the firing rates in Eqns. (5.7)-(5.11) can be written, after some algebraic manipulations, as

$$F_{DA} = g_{DA}\left(-J_{self,DA}\frac{80}{1+y} \pm W_{d5}\frac{0.03}{1+x^2} + J_{d5e}F_{Glu} - J_{di}F_{GABA-VTA} -\ J_{d5i}F_{GABA-DRN} + 210 + I_{DA,ext}\right) \quad (5.23)$$

$$F_{5-HT} = g_{5-HT}\left(-J_{self,5-HT}\frac{80}{1+x} + W_{5d}\ \frac{0.03}{1+ay^2} + J_{55e}F_{Glu} - J_{55i}F_{GABA-DRN} - J_{5i}\ F_{GABA-VTA} + 99.87 + I_{5-HT,ext}\right) \quad (5.24)$$

$$F_{Glu} = g_{Glu}\left(J_{self,Glu}\ F_{Glu} \pm W_{5e5}\ \frac{0.03}{1+x^2} - W_{5edi}F_{GABA-VTA} + W_{5e2}\frac{0.03}{1+ay^2} + 100\ + I_{Glu,ext}\right) \quad (5.25)$$

$$F_{GABA-DRN} = g_{GABA-DRN}\left(-J_{self,GABA-DRN}\ F_{GABA-DRN} \pm\ W_{5i5}\ \frac{0.03}{1+x^2} + W_{5id}\ \frac{0.03}{1+ay^2} + W_{5ie}\ F_{Glu}\ -\ W_{5ii}F_{GABA-VTA} + 450 +\ I_{GABA-DRN,ext}\right) \quad (5.26)$$

$$F_{GABA-VTA} = g_{GABA-VTA}\left(-J_{self,GABA-VTA}\,F_{GABA-VTA} + W_{i5}\,\frac{0.03}{1+x^2} \pm W_{id}\,\frac{0.03}{1+ay^2} + 200 + I_{GABA-VTA,ext}\right) \quad (5.27)$$

These 5 left-hand-side of these equations represent the 5 different types of neurons in each DRN-VTA model. The right-hand-side of the above equations have 5 terms of synaptic currents, implying all-to-all connectivity.

Next, considering non-DA and non-5-HT neurons, and rearranging Eqn. (5.27) we obtain

$$F_{GABA-VTA} = \frac{g_{GABA-VTA}}{(1+g_{GABA-VTA}J_{self,GABA-VTA})}\left(\frac{0.03w_{i5}}{(1+x^2)} \pm \frac{0.03w_{id}}{(1+ay^2)} + 200 + I_{GABA-VTA,ext}\right) \quad (5.28)$$

Substituting Eqn. (5.28) into Eqn. (5.25), we obtain

$$F_{Glu} = g_{Glu}\left(J_{self,Glu}\,F_{Glu} \pm W_{5e5}\,\frac{0.03}{1+x^2} - W_{5edi}\left(\frac{g_{GABA-VTA}}{(1+g_{GABA-VTA}J_{self,GABA-VTA})}\left(\frac{0.03w_{i5}}{(1+x^2)} \pm \frac{0.03w_{id}}{(1+ay^2)} + 200 + I_{GABA-VTA,ext}\right)\right) + W_{5e2}\,\frac{0.03}{1+ay^2} + 100 + I_{Glu,ext}\right) \quad (5.29)$$

Rearranging Eqn. (5.29), we obtain

$$F_{Glu} = \frac{g_{Glu}}{(1-g_{Glu}J_{self,Glu})}\left(\left(\pm W_{5e5} - \frac{W_{5edi}g_{GABA-VTA}W_{i5}}{(1+g_{GABA-VTA}J_{self,GABA-VTA})}\right)\frac{0.03}{1+x^2} + \left(W_{5e2} \pm \frac{-W_{5edi}g_{GABA-VTA}w_{id}}{(1+g_{GABA-VTA}J_{self,GABA-VTA})}\right)\frac{0.03}{(1+ay^2)} - \frac{W_{5edi}g_{GABA-VTA}(200+I_{GABA-VTA,ext})}{(1+g_{GABA-VTA}J_{self,GABA-VTA})} + 100 + I_{Glu,ext}\right) \quad (5.30)$$

Substituting Eqn. (5.30) in Eqn. (5.26) results in

$$F_{GABA-DRN} = g_{GABA-DRN}(-J_{self,GABA-DRN}\,F_{GABA-DRN} \pm W_{5i5}\,\frac{0.03}{1+x^2} + W_{5id}\,\frac{0.03}{1+ay^2} + W_{5ie}\left(\frac{g_{Glu}}{(1-g_{Glu}J_{self,Glu})}\left(\left(\pm W_{5e5} - \frac{W_{5edi}g_{GABA-VTA}W_{i5}}{(1+g_{GABA-VTA}J_{self,GABA-VTA})}\right)\frac{0.03}{1+x^2} + \left(W_{5e2} \pm$$

$$\frac{-W_{5edi}g_{GABA-VTA}w_{id}}{(1+g_{GABA-VTA}J_{self,GABA-VTA})}\Big)\frac{0.03}{(1+ay^2)} - \frac{W_{5edi}g_{GABA-VTA}(200+I_{GABA-VTA,ext})}{(1+g_{GABA-VTA}J_{self,GABA-VTA})} + 100 + I_{Glu,ext}\Big)\Big) -$$

$$W_{5ii}\, I_{GABA-DRN,GABA-VTA} + 450 + \; I_{GABA-DRN,ext}) \tag{5.31}$$

and with some rearrangement, $F_{GABA-DRN} = \frac{g_{GABA-DRN}}{(1+g_{GABA-DRN}J_{self,GABA-DRN})}\Big(\Big(-w_{5i5} \pm$

$$\frac{g_{Glu}w_{5ie}w_{5e5}}{(1-g_{Glu}J_{self,Glu})} - \frac{g_{Glu}w_{5ie}}{(1-g_{Glu}J_{self,Glu})}\frac{w_{5edi}g_{GABA-VTA}w_{i5}}{(1+g_{GABA-VTA}J_{self,GABA-VTA})}\Big)\frac{0.03}{1+x^2} + \Big(w_{id} + \frac{g_{Glu}w_{5ie}W_{5e2}}{(1-g_{Glu}J_{self,Glu})} \pm$$

$$\frac{g_{Glu}w_{5ie}W_{5e2}}{(1-g_{Glu}J_{self,Glu})}\frac{w_{5edi}g_{GABA-VTA}w_{id}}{(1+g_{GABA-VTA}J_{self,GABA-VTA})}\Big)\frac{0.03}{1+ay^2} -$$

$$\frac{g_{Glu}\,W_{5ie}}{(1-g_{Glu}J_{self,Glu})}\frac{w_{5edi}g_{GABA-VTA}(200+I_{GABA-VTA,ext})}{(1+g_{GABA-VTA}J_{self,GABA-VTA})} + \frac{g_{Glu}\,W_{5ie}(100+I_{Glu,ext})}{(1-g_{Glu}J_{self,Glu})} + \; I_{GABA-DRN,ext} +$$

$$450\Big) \tag{5.32}$$

Then Eqns. (5.28), (5.30), and (5.32) can be expressed in matrix form as

$$\begin{pmatrix} F_{Glu} \\ F_{GABA-VTA} \\ F_{GABA-DRN} \end{pmatrix}$$

$$= \begin{pmatrix} 1-g_{Glu}J_{self,Glu} & g_{Glu}w_{5edi} & 0 \\ 0 & 1+g_{GABA-VTA}\,J_{self,GABA-VTA} & 0 \\ 0 & g_{GABA-DRN}\,W_{5ii} & 1+g_{GABA-DRN}\,J_{self,GABA-DRN} \end{pmatrix}^{-1}$$

$$\begin{pmatrix} \frac{\pm W_{5e5}0.03g_{Glu}}{1+x^2} + \frac{0.03W_{5e2}g_{Glu}}{1+ay^2} + g_{Glu}(100+I_{Glu,ext}) \\ \frac{0.03\,W_{i5}g_{GABA-VTA}}{1+x^2} + \frac{0.03\,W_{id}g_{GABA-VTA}}{1+ay^2} + g_{GABA-VTA}(200+\; I_{GABA-VTA}) \\ \frac{\pm 0.03W_{5i5}g_{GABA-DRN}}{1+x^2} + \frac{0.03\,W_{5id}g_{GABA-DRN}}{1+ay^2} + g_{GABA-DRN}(450+\; I_{GABA-DRN}) \end{pmatrix} \tag{5.33}$$

Using the parameter values as per the connections in the model W_{5edi}=0, $W_{5e2} = 0$, as there is no connections from VTA GABA and VTA DA to DRN Glu, further $x = e^{-10([5HT]-0.1)}$,$y = e^{-10([DA]-0.1)}$, Eqn. (5.33) can be simplified to

$$\begin{pmatrix} F_{Glu} \\ F_{GABA-VTA} \\ F_{GABA-DRN} \end{pmatrix}$$

$$= \begin{pmatrix} 1 - g_{Glu} J_{self-Glu} & 0 & 0 \\ 0 & 1 + g_{GABA-VTA} J_{self,GABA-VTA} & 0 \\ 0 & g_{GABA-DRN} W_{5ii} & 1 + g_{GABA-DRN} J_{self,GABA-DRN} \end{pmatrix}^{-1}$$

$$\begin{pmatrix} \frac{\pm 0.03\, W_{5e5} g_{Glu}}{1+e^{-20([5-HT]-0.1)}} + \frac{0}{1+e^{-16([DA]-0.1)}} + g_{Glu}(100 + I_{Glu,ext}) \\ \frac{0.03\, W_{i5} g_{GABA-VTA}}{1+e^{-20([5-HT]-0.1)}} \pm \frac{0.03\, W_{id} g_{GABA-VTA}}{1+ae^{-20([DA]-0.1)}} + g_{GABA-VTA}(200 + I_{GABA-VTA}) \\ \frac{\pm 0.03 W_{5i5} g_{GABA-DRN}}{1+e^{-20([5-HT]-0.1)}} + \frac{0.03\, W_{5id} g_{GABA-DRN}}{1+ae^{-20([DA]-0.1)}} + g_{GABA-DRN}(450 + I_{GABA-DRN}) \end{pmatrix} \quad (5.34)$$

By substituting Eqns. (5.28), (5.30), and (5.32) into Eqn. (5.23), the latter becomes

$$F_{DA} = g_{DA}(-J_{self,DA}\frac{80}{1+y} \pm W_{d5}\frac{0.03}{1+x^2} + J_{d5e}\left(\frac{g_{Glu}}{(1-g_{Glu}J_{self,Glu})}\left(\left(\pm W_{5e5} - \frac{W_{5edi} g_{GABA-VTA} W_{i5}}{(1+g_{GABA-VTA}J_{self,GABA-VTA})}\right)\frac{0.03}{1+x^2} + \left(W_{5e2} \pm \frac{-W_{5edi} g_{GABA-VTA} w_{id}}{(1+g_{GABA-VTA}J_{self,GABA-VTA})}\right)\frac{0.03}{(1+ay^2)} - \frac{W_{5edi} g_{GABA-VTA}(200+I_{GABA-VTA,ext})}{(1+g_{GABA-VTA}J_{self,GABA-VTA})} + 100 + I_{Glu,ext}\right)\right) - J_{di}(\frac{g_{GABA-VTA}}{(1+g_{GABA-VTA}J_{self,GABA-VTA})}\left(\frac{0.03 w_{i5}}{(1+x^2)} \pm \frac{0.03 w_{id}}{(1+ay^2)} + 200 + I_{GABA-VTA,ext}\right) - J_{d5i}\left(\frac{g_{GABA-DRN}}{(1+g_{GABA-DRN}J_{self,GABA-DRN})}\left(\left(-w_{5i5} \pm \frac{g_{Glu} w_{5ie} w_{5e5}}{(1-g_{Glu}J_{self,Glu})} - \frac{g_{Glu} w_{5ie}}{(1-g_{Glu}J_{self,Glu})}\frac{w_{5edi} g_{GABA-VTA} w_{i5}}{(1+g_{GABA-VTA}J_{self,GABA-VTA})}\right)\frac{0.03}{1+x^2} + \left(w_{id} + \frac{g_{Glu} w_{5ie} W_{5e2}}{(1-g_{Glu}J_{self,Glu})} \pm \frac{g_{Glu} w_{5ie} W_{5e2}}{(1-g_{Glu}J_{self,Glu})}\frac{w_{5edi} g_{GABA-VTA} w_{id}}{(1+g_{GABA-VTA}J_{self,GABA-VTA})}\right)\frac{0.03}{1+ay^2} - \frac{g_{Glu}\, W_{5ie}}{(1-g_{Glu}J_{self,Glu})}\frac{w_{5edi} g_{GABA-VTA}(200+I_{GABA-VTA,ext})}{(1+g_{GABA-VTA}J_{self,GABA-VTA})} + \frac{g_{Glu}\, W_{5ie}(100+I_{Glu,ext})}{(1-g_{Glu}J_{self,Glu})} + I_{GABA-DRN,ext} + 450\right)\right) + 210 + I_{DA,ext}) \quad (5.35)$$

Again, by substituting Eqns. (5.28), (5.30), and (5.32) into Eqn. (5.24), the latter becomes

$$F_{5HT} = g_{5-HT}\left(-J_{self,5-HT}\frac{80}{1+x} + W_{5d}\ \frac{0.03}{1+ay^2} + J_{55e}\left(\frac{g_{Glu}}{(1-g_{Glu}J_{self,Glu})}\left(\left(\pm W_{5e5} - \frac{W_{5edi}g_{GABA-VTA}W_{i5}}{(1+g_{GABA-VTA}J_{self,GABA-VTA})}\right)\frac{0.03}{1+x^2} + \left(W_{5e2} \pm \frac{-W_{5edi}g_{GABA-VTA}w_{id}}{(1+g_{GABA-VTA}J_{self,GABA-VTA})}\right)\frac{0.03}{(1+ay^2)} - \frac{W_{5edi}g_{GABA-VTA}(200+I_{GABA-VTA,ext})}{(1+g_{GABA-VTA}J_{self,GABA-VTA})} + 100 + I_{Glu,ext}\right)\right) - J_{55i}\left(\frac{g_{GABA-DRN}}{(1+g_{GABA-DRN}J_{self,GABA-DRN})}\left(\left(-w_{5i5} \pm \frac{g_{Glu}w_{5ie}w_{5e5}}{(1-g_{Glu}J_{self,Glu})} - \frac{g_{Glu}w_{5ie}}{(1-g_{Glu}J_{self,Glu})}\frac{w_{5edi}g_{GABA-VTA}w_{i5}}{(1+g_{GABA-VTA}J_{self,GABA-VTA})}\right)\frac{0.03}{1+x^2} + \left(w_{id} + \frac{g_{Glu}w_{5ie}W_{5e2}}{(1-g_{Glu}J_{self,Glu})} \pm \frac{g_{Glu}w_{5ie}W_{5e2}}{(1-g_{Glu}J_{self,Glu})}\frac{w_{5edi}g_{GABA-VTA}w_{id}}{(1+g_{GABA-VTA}J_{self,GABA-VTA})}\right)\frac{0.03}{1+ay^2} - \frac{g_{Glu}\,W_{5ie}}{(1-g_{Glu}J_{self,Glu})}\frac{w_{5edi}g_{GABA-VTA}(200+I_{GABA-VTA,ext})}{(1+g_{GABA-VTA}J_{self,GABA-VTA})} + \frac{g_{Glu}\,W_{5ie}(100+I_{Glu,ext})}{(1-g_{Glu}J_{self,Glu})} + \ I_{GABA-DRN,ext} + 450\right)\right) - J_{5i}\left(\frac{g_{GABA-VTA}}{(1+g_{GABA-VTA}J_{self,GABA-VTA})}\left(\frac{0.03w_{i5}}{(1+x^2)} \pm \frac{0.03w_{id}}{(1+ay^2)} + 200 + I_{GABA-VTA,ext}\right)\right) + 99.87 + I_{5-HT,ext}\right) \quad (5.36)$$

Using Eqn. (5.34), we can rewrite Eqns. (5.35) and (5.36) in matrix form as

$$\begin{pmatrix}F_{5HT}\\F_{DA}\end{pmatrix} = \begin{pmatrix}g_{5-HT}\left(\frac{-80J_{self,5-HT}}{1+x} + \frac{0.03W_{5d}}{1+ay^2} + 99.87 + I_{5-HT,ext}\right)\\ -g_{DA}\left(\frac{\pm 0.03W_{d5}}{1+x^2} + \frac{80\,J_{self,DA}}{1+y} - 210 - I_{DA,ext}\right)\end{pmatrix} + \begin{pmatrix}g_{5-HT} & 0\\0 & g_{DA}\end{pmatrix}\begin{pmatrix}J_{55e} & -J_{5i} & -J_{55i}\\J_{d5e} & -J_{di} & -J_{d5i}\end{pmatrix}\begin{pmatrix}F_{Glu}\\F_{GABA-VTA}\\F_{GABA-DRN}\end{pmatrix} \quad (5.37)$$

Using the parameter value $J_{d5i} = 0$, $x = e^{-10([5HT]-0.1)}$, $y = e^{-10([DA]-0.1)}$ and Eqn. (5.34), then Eqn. (5.37) can be rewritten as

$$\begin{pmatrix} F_{5HT} \\ F_{DA} \end{pmatrix} = \begin{pmatrix} g_{5-HT}\left(\frac{-80J_{self,5-HT}}{1+e^{-10([5HT]-0.1)}} + \frac{0.03W_{5d}}{1+ae^{-20([DA]-0.1)}} + 99.87 + I_{5-HT,ext}\right) \\ -g_{DA}\left(\frac{\pm 0.03W_{d5}}{1+e^{-20([5HT]-0.1)}} + \frac{80J_{self,DA}}{1+e^{-10([DA]-0.1)}} - 210 - I_{DA,ext}\right) \end{pmatrix} + \begin{pmatrix} g_{5-HT} & 0 \\ 0 & g_{DA} \end{pmatrix}\begin{pmatrix} J_{55e} & -J_{5i} & -J_{55i} \\ J_{d5e} & -J_{di} & 0 \end{pmatrix}$$

$$\begin{pmatrix} 1-g_{Glu}J_{self-Glu} & 0 & 0 \\ 0 & 1+g_{GABA-VTA}J_{self,GABA-VTA} & 0 \\ 0 & g_{GABA-DRN}W_{5ii} & 1+g_{GABA-DRN}J_{self,GABA-DRN} \end{pmatrix}^{-1}$$

$$\begin{pmatrix} \frac{\pm 0.03\,W_{5e5}g_{Glu}}{1+e^{-20([5-HT]-0.1)}} + \frac{0}{1+e^{-16([DA]-0.1)}} + g_{Glu}(100 + I_{Glu,ext}) \\ \frac{0.03\,W_{i5}g_{GABA-VTA}}{1+e^{-20([5-HT]-0.1)}} \pm \frac{0.03\,W_{id}g_{GABA-VTA}}{1+ae^{-20([DA]-0.1)}} + g_{GABA-VTA}(200 + I_{GABA-VTA,ext}) \\ \frac{\pm 0.03W_{5i5}g_{GABA-DRN}}{1+e^{-20([5-HT]-0.1)}} + \frac{0.03\,W_{5id}g_{GABA-DRN}}{1+ae^{-20([DA]-0.1)}} + g_{GABA-DRN}(450 + I_{GABA-DRN,ext}) \end{pmatrix} \quad (5.38)$$

Suppose we define some constant matrix,

$$A = \begin{pmatrix} a_{11} & a_{12} & a_{13} \\ a_{21} & a_{22} & a_{23} \end{pmatrix} = \begin{pmatrix} g_{5-HT} & 0 \\ 0 & g_{DA} \end{pmatrix}\begin{pmatrix} J_{55e} & -J_{5i} & -J_{55i} \\ J_{d5e} & -J_{di} & 0 \end{pmatrix}$$

$$\begin{pmatrix} 1-g_{Glu}J_{self-Glu} & 0 & 0 \\ 0 & 1+g_{GABA-VTA}J_{self,GABA-VTA} & 0 \\ 0 & g_{GABA-DRN}W_{5ii} & 1+g_{GABA-DRN}J_{self,GABA-DRN} \end{pmatrix}^{-1}$$

Then, from Eqn, (5.38), we can obtain the firing rates of 5-HT and DA in terms of only [5-HT] and [DA], i.e.

$$F_{5HT} = g_{5-HT}\left(\frac{-80J_{self,5-HT}}{1+e^{-10([5HT]-0.1)}} + \frac{0.03W_{5d}}{1+ae^{-20([DA]-0.1)}} + 99.87 + I_{5-HT,ext}\right) + a_{11}\left(\frac{\pm 0.03\,W_{5e5}g_{Glu}}{1+e^{-20([5-HT]-0.1)}} + \frac{0}{1+e^{-16([DA]-0.1)}} + g_{Glu}(100 + I_{Glu,ext})\right) + a_{12}\left(\frac{0.03\,W_{i5}g_{GABA-VTA}}{1+e^{-20([5-HT]-0.1)}} \pm \frac{0.03\,W_{id}g_{GABA-VTA}}{1+ae^{-20([DA]-0.1)}} + g_{GABA-VTA}(200 + I_{GABA-VTA,ext})\right) + a_{13}\left(\frac{\pm 0.03W_{5i5}g_{GABA-DRN}}{1+e^{-20([5-HT]-0.1)}} + \frac{0.03\,W_{5id}g_{GABA-DRN}}{1+ae^{-20([DA]-0.1)}} + g_{GABA-DRN}(450 + I_{GABA-DRN,ext})\right) \quad (5.39)$$

$$F_{DA} = -g_{DA}\left(\frac{\pm 0.03 W_{d5}}{1+e^{-20([5HT]-0.1)}} + \frac{80 J_{self,DA}}{1+e^{-10([DA]-0.1)}} - 210 - I_{DA,ext}\right) + a_{21}\left(\frac{\pm 0.03\, W_{5e5} g_{Glu}}{1+e^{-20([5-HT]-0.1)}} + \frac{0}{1+e^{-16([DA]-0.1)}} + g_{Glu}\left(100 + I_{Glu,ext}\right)\right) + a_{22}\left(\frac{0.03\, W_{i5} g_{GABA-VTA}}{1+e^{-20([5-HT]-0.1)}} \pm \frac{0.03\, W_{id} g_{GABA-VTA}}{1+ae^{-20([DA]-0.1)}} + g_{GABA-VTA}\left(200 + I_{GABA-VTA,ext}\right)\right) + a_{23}\left(\frac{\pm 0.03 W_{5i5} g_{GABA-DRN}}{1+e^{-20([5-HT]-0.1)}} + \frac{0.03\, W_{5id} g_{GABA-DRN}}{1+ae^{-20([DA]-0.1)}} + g_{GABA-DRN}\left(450 + I_{GABA-DRN,ext}\right)\right) \quad (5.40)$$

However, in Eqns. (5.16) and (5.17), $F_{DA} = \frac{40[DA]}{0.15+[DA]}$ and $F_{5HT} = \frac{16.25[5-HT]}{0.17+[5-HT]}$, at the steady state. Hence, substituting these values into the above Eqns. (5.39) and (5.40), we can solve for the values of [DA] and [5-HT] at the steady state as follows:

$$\frac{40[DA]}{0.15+[DA]} = -g_{DA}\left(\frac{\pm 0.03 W_{d5}}{1+e^{-20([5HT]-0.1)}} + \frac{80 J_{self,DA}}{1+e^{-10([DA]-0.1)}} - 210 - I_{DA,ext}\right) + a_{21}\left(\frac{\pm 0.03\, W_{5e5} g_{Glu}}{1+e^{-20([5-HT]-0.1)}} + \frac{0}{1+e^{-16([DA]-0.1)}} + g_{Glu}\left(100 + I_{Glu,ext}\right)\right) + a_{22}\left(\frac{0.03\, W_{i5} g_{GABA-VTA}}{1+e^{-20([5-HT]-0.1)}} + \frac{0.03\, W_{id} g_{GABA-VTA}}{1+ae^{-20([DA]-0.1)}} + g_{GABA-VTA}\left(200 + I_{GABA-VTA,ext}\right)\right) + a_{23}\left(\frac{\pm 0.03 W_{5i5} g_{GABA-DRN}}{1+e^{-20([5-HT]-0.1)}} + \frac{0.03\, W_{5id} g_{GABA-DRN}}{1+ae^{-20([DA]-0.1)}} + g_{GABA-DRN}\left(450 + I_{GABA-DRN,ext}\right)\right) \quad (5.41)$$

$$\frac{16.25[5-HT]}{0.17+[5-HT]} = g_{5-HT}\left(\frac{-80}{1+e^{-10([5HT]-0.1)}} + \frac{0.03 W_{5d}}{1+ae^{-20([DA]-0.1)}} + 99.87 + I_{5-HT,ext}\right) + a_{11}\left(\frac{\pm 0.03\, W_{5e5} g_{Glu}}{1+e^{-20([5-HT]-0.1)}} + \frac{0}{1+e^{-16([DA]-0.1)}} + g_{Glu}\left(100 + I_{Glu,ext}\right)\right) + a_{12}\left(\frac{0.03\, W_{i5} g_{GABA-VTA}}{1+e^{-20([5-HT]-0.1)}} + \frac{0.03\, W_{id} g_{GABA-VTA}}{1+ae^{-20([DA]-0.1)}} + g_{GABA-VTA}\left(200 + I_{GABA-VTA,ext}\right)\right) + a_{13}\left(\frac{\pm 0.03 W_{5i5} g_{GABA-DRN}}{1+e^{-20([5-HT]-0.1)}} + \frac{0.03\, W_{5id} g_{GABA-DRN}}{1+ae^{-20([DA]-0.1)}} + g_{GABA-DRN}\left(450 + I_{GABA-DRN,ext}\right)\right) \quad (5.42)$$

In particular, from Eqns. (5.41) and (5.42), we can find the solutions for [DA] and [5-HT] at the steady state, as all the parameters in these equations have fixed values at the fixed point. Then using these [DA] and [5-HT] values, we can find the population firing rates of 5-HT and DA neurons at the steady state from Eqns. (5.16) and (5.17), respectively. We can also solve for the values of the other dynamical variables (Eqns. (5.12)-(5.15)). Using

Eqns. (5.25)-(5.27), the population firing rates at steady state for the 3 other non-DA/non-5-HT neurons can also be obtained.

5.3. Stability analysis of the DRN-VTA models

After determining the solutions at steady state, we can next check whether the DRN-VTA model is stable at steady state. To enable this, we can compute the 6-by-6 Jacobian matrix $M_{Jacobian}$ for the 6 dynamical equations (Eqns. (5.1)-(5.6)), which can be computed by applying the partial derivatives on the right-hand-side of these equations (Strogatz, 2018):

$$M_{Jacobian} = \begin{pmatrix} -1/500 & 0 & 0 & 0 & \frac{80}{500}\frac{10e^{-10([5-HT]-0.1)}}{(1+e^{-10([5-HT]-0.1)})^2} & 0 \\ 0 & -1/150 & 0 & 0 & 0 & \frac{80}{150}\frac{10e^{-10([DA]-0.1)}}{(1+e^{-10([DA]-0.1)})^2} \\ 0 & 0 & -1/1200 & 0 & \frac{0.03}{1200}\frac{20e^{-20([5-HT]-0.1)}}{(1+e^{-20([5-HT]-0.1)})^2} & 0 \\ 0 & 0 & 0 & -1/1000 & 0 & \frac{0.03}{1000}\frac{20e^{-20([DA]-0.3)}}{(1+e^{-20([DA]-0.3)})^2} \\ \frac{0.008}{1000}g_{5-HT} & 0 & 0 & \frac{0.08}{1000}g_{5-HT} & 0 & 0 \\ 0 & \frac{0.1}{1000}g_{DA} & -\frac{0.1}{1000}g_{DA} & 0 & \frac{-0.0013}{0.17+[5-HT]}+\frac{0.0013[5-HT]}{(0.17+[5-HT])^2} & -\frac{0.004}{0.15+[DA]}+\frac{0.004[DA]}{(0.15+[DA])^2} \end{pmatrix} \quad (5.43)$$

The eigenvalues of this Jacobian matrix were computed for each steady state for each model type under each simulated condition (e.g. reward/punishment task). If the real parts of all the eigenvalues of the Jacobian matrix were negative at a given steady state, then the model was considered to be dynamically and locally stable at that steady state (Strogatz, 2018).

The network model's stability analysis is performed at each steady state, for each model type, conditioning task and 5-HT neuronal type. By incorporating the tonic and phasic (maximal) input currents into the Jacobian matrix (Eqn. (5.43)), via Eqns. (5.34) and (5.38), the full set of eigenvalues can be obtained using the MATLAB package *eig()*. Note that for phasic activity mode, a constant input current value is used based on the maximal current amplitude for each set of conditions.

5.4. Degenerate DRN-VTA circuit models are dynamically stable

Fig. 5.1a plotted the complete set of the real part of the eigenvalues for model #1 with architecture 'a' (Fig. 4.5a). This model has inhibitory connections from VTA DA to VTA GABA neurons and from DRN 5-HT to VTA DA/Glu neurons, using Type I 5-HT neurons and under punishment conditions (Table 4.3). It was observed that the eigenvalues with a phasic input (blue) were generally larger (magnitude wise) than those with tonic input (red). This was more pronounced for the eigenvalues with the largest magnitude (maximal eigenvalues) (Fig. 4.5a, asterisk). Moreover, all the eigenvalues were negative, indicating a dynamically stable network model even in the presence of additional phasic stimulus input. The non-maximal eigenvalues were similar to those of the other models (not shown).

We repeated the analysis for all 84 models, under both phasic and tonic input conditions. This analysis is presented in Fig. 5.1b only for the maximal eigenvalues (red circles and blue crosses). Note that for each model, different 5-HT neuron, connectivity types (excitatory/inhibitory), and tasks, were evaluated (e.g. model 'a' had 32 different types) (Supplementary Tables 4.1 and 4.3). In general, with phasic activities (blue crosses), the models were more stable than with tonic activities (red circles). However, during phasic activations, there were 18 models with rather small (close to zero) eigenvalues (magnitude wise), albeit still negative. This was not observed for tonic activations, where the (most negative) eigenvalues were found to hover within a small range of values (-0.017 to -0.016), except models with architecture 'l' (~ -0.03). In fact, the latter models, which were the only ones with a fast 5-HT-to-DA connection (Fig. 5.1b, models #77-84), were the most stable under both phasic and tonic conditions. The other non-maximal eigenvalues remain similar to those of the other models (not shown). Further, there was no difference identified between the excitatory (models #77-80) and inhibitory (models #81-84) connections. Moreover, most of their eigenvalues in phasic condition were more negative than their tonic counterparts.

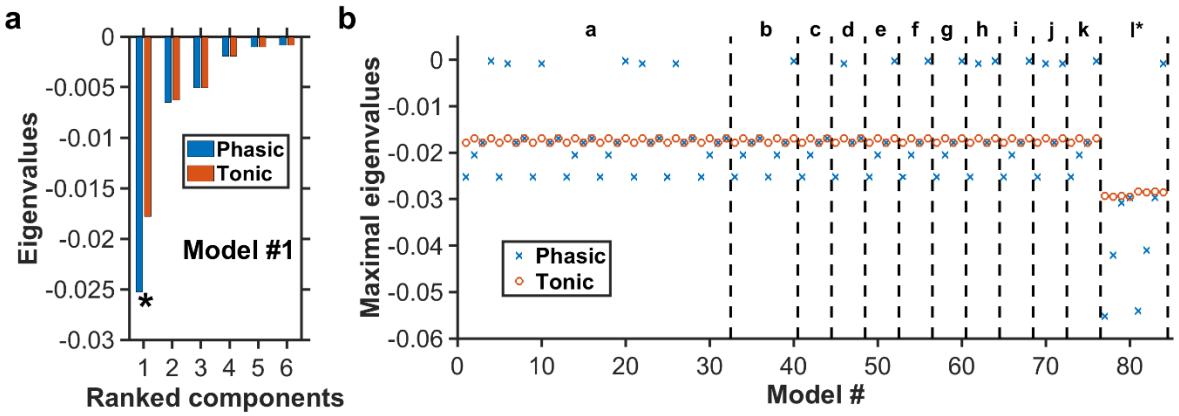

Figure 5.1. Negative real eigenvalues at steady states of degenerate models. a, Complete set of the real part of the eigenvalues for Model #1 (Tables 4.1 and 4.3) with architecture 'a' illustrated in Fig. 4.5. Horizontal axis: Components from PCA ranked from the largest to the smallest eigenvalues (magnitude wise). Blue (red): More negative eigenvalues with phasic (blue) than tonic (red) input. Asterisk: Leading/Maximal eigenvalue (largest magnitude) for each input condition. **b,** For each of the 84 models, only the real part of the eigenvalue with the largest magnitude is plotted under phasic (blue cross) and tonic (red circle) input condition. Model category a to l* refer to the different architectures in Fig. 4.5, in which each has their own distinctive model types (e.g. different 5-HT neuronal or excitatory/inhibitory connectivity types). Eigenvalues for all model types have negative real parts, indicating dynamically stable. For most models, the eigenvalues are generally more negative during phasic than tonic activities.

5.5. Discussion

After identifying the degenerate models in the previous Chapter (Fig. 4.5, and Tables 4.1 and 4.3), we used dynamical systems theory to determine whether they are dynamically stable, i.e. (local) perturbation from their steady states will eventually lead them back to their initial steady states (see Methods). Namely, the stability of each neural circuit could be determined by first finding the possible steady state(s) (i.e. fixed point(s)). This was achieved by setting all the dynamical (differential) equations to zero and finding the algebraic solutions for the dynamical variables. Then the eigenvalues of the system's Jacobian matrix at the steady states were computed. For a neural circuit to be dynamically stable, the real part of all the eigenvalues associated with the steady state has to be

negative. This was exactly what we found for all the degenerate neural circuits. Hence, all the 84 models, were found to be stable.

In Chapter 4, when compared to the sparsely connected model, more highly connected and degenerate versions of the DRN-VTA model predicted a relatively weaker direct DRN 5-HT-VTA DA neuron connectivity than that of DRN Glu-VTA DA neurons (McKevitt et al., 2014). However, previous studies had demonstrated a direct influence of DRN 5-HT on VTA DA neuron activity as well as reward (e.g. De Deurwaerdère and Di Giovanni (2017)). More recent work has shown that DRN 5-HT terminals in the VTA co-release glutamate and 5-HT, eliciting fast excitation (via ionotropic receptors) onto VTA DA neurons and increased DA release in the nucleus accumbens to facilitate reward (Wang et al., 2019). Hence, in Chapter 4, we developed a model of this fast 5-HT-to-DA connection and found such system to be plausible in terms of capturing the stereotypical reward and punishment signalling (Fig. 4.5l). Interestingly, in this Chapter, we also found that this model configuration was dynamically more stable than all other architectures (Fig. 5.1b)

Chapter 6
Dynamic relationship between neural population activities in corticoraphe system

This contributing chapter provides the processing and analyses of new, simultaneously recorded electrophysiological data in anaesthesised rodents based on multi-unit recordings in the DRN, and ECoG activities across multiple sites. In particular, the analyses aim to uncover the dynamic relationships between neuronal units within the DRN and that between the DRN neuronal units with cortical activities. Parts of the review are published in a conference paper.

6.1. Introduction

As discussed in Chapter 2, the DRN receives several inputs from various parts of the brain (Dorocic et al., 2014; Ranade and Mainen, 2009) including from the prefrontal cortex (PFC) (Fig. 1.2) (Celada et al., 2013, 2001; Challis and Berton, 2015; Hajós et al., 1998; Heidbreder and Groenewegen, 2003). There are evidences that indicate the prefrontal cortico-raphe projection could be mediated by glutamatergic synapses (Challis and Berton, 2015; Geddes et al., 2016). Further, high frequency stimulation of pyramidal neurons in the PFC is shown to inhibit 5-HT activities in the DRN (Celada et al., 2001; Shaw, 1981). More precise state-of-the-art optogenetic stimulation of the PFC has shown potent effects on the DRN activity and behaviour (Geddes et al., 2016; Warden et al., 2012), which may have implications in brain disorders, especially the dysfunctions in mood regulation and stress processing (Geddes et al., 2016; Srejic et al., 2016; Warden et al., 2012), as also reflected in abnormal neural activity oscillatory patterns (Basar and Guntekin, 2008). Reciprocally, 5-HT-producing neurons from the DRN are known to innervate the cortex, providing dense projection to the frontal cortex (Celada et al., 2013), including the modulating of both the frequency and amplitude of cortical slow-wave

oscillations in the prefrontal cortex (PFC) (Celada et al., 2013, 2008; Gartside et al., 2000; Totah et al., 2018). The work in (Schweimer et al., 2011) reveals that most DRN 5-HT neurons, including those with clock-like and bursting firing activities, are found to have significant coherence with cortical oscillations. Hence, there is a tight relationship of reciprocal interactions between the cortex, particularly the PFC, and the DRN. However, so far, none of the previous studies have recorded multiple DRN neurons simultaneously with ECoG activities, and hence how DRN neuronal units interactions and with ECoG remain unclear.

To address these, simultaneous (extracellular) recordings of the DRN neuronal population firing activity in conjunction with the monitoring of ECoGs across multiple cortical regions have been performed in a collaborator's lab. Here, based on the collected data, spike correlations and pairwise coherence between DRN neuronal firing activities, and between the DRN neuronal activities and the ECoGs were computed. Anaesthetized animals were used as the data was more stable to analyse. Overall, at least for the samples investigated, the coherence analyses found that, within the frequency domain and in anaesthetized rodents, most slow firing DRN neurons with regular and irregular firing (putative 5-HT neurons) have a stronger relationship with slow (3.5 – 3.8 Hz) cortical oscillatory dynamics, especially the frontal cortices. Further, the DRN neurons are found to be sparsely correlated with each other.

6.2 Methods

6.2.1 Experiment procedures

Anaesthesia on the mice was induced with isoflurane and maintained with urethane. A local anaesthetic was applied to the scalp and pinna. Additional doses of urethane were administered throughout the recording period to maintain a constant level of anaesthetic depth. Animals were placed onto a homoeothermic heating blanket and fastened to a stereotaxic frame.

The skull was exposed and steel EEG screws were inserted over the left frontal cortex (recording channel and cerebellum (reference channel). Extracellular signals, recorded in an alternate current configuration, were amplified (x100) and band pass filtered (300-500Hz). EEG signals were amplified (x2000) and band pass filtered (0.3-150 Hz. -3dB limits). All signals underwent mains noise filtering (Humbug 50/60Hz Noise Eliminator) before analogue to digital conversion.

Single units were recorded by lowering the electrode to the region of the DRN (approximately 1400-2200 μm ventral to the brain surface). The electrode was then slowly advanced (approximately 0.5 μm/s) until spikes were detected. At this point, the electrode was halted and the spiking neuron(s) was recorded for a period of 2 to 5 minutes. A total of 30 mice were used. All procedures complied with the Animal (Scientific Procedures) Act of 1986 and were performed in accordance with the ethical guidelines of the University of Oxford.

The open-source Open Ephys tool (Siegle et al., 2017) was used to record the electrocorticograms (ECoGs) in two urethane-anaesthetised SERT-CRE mice. Simultaneously, extracellular electrophysiological recordings were done using 32 channels using a silicon probe (Cambridge NeuroTech, 32 channels) stereotaxically implanted into the DRN (-4mm posterior to brema). The recordings were done continuously for 1 hour for each session with sampling rate, Fs = 30 KHz.

ECoG electrodes (3 channels) were placed bilaterally over the frontal cortex and right occipital cortex to record brain state (frontal channels: +1 mm anterior and +- 1.5mm lateral to bregma; occipital channel: -2.5mm posterior and + 1.5mm lateral to bregma). The left and right frontal (LF and RF) cortices were selected based on previous studies showing their interactions with the DRN, while the (right) occipital (RO) cortex was selected based on previous study showing 5-HT influence in this brain region (Jonsson et al., 1984) Further, the frontal cortex is well-known for high-level cognitive control (Funahashi, 2017) while the occipital cortex is more for sensory (visual) processing (Nazari et al., 2010) very different functional roles.

6.2.2. Data pre-processing

Raw neuronal spiking data acquired from the 32 channels were filtered and single units were identified automatically using Kilosort (Pachitariu et al., 2016) and verified by manual clustering using the software package Phy (Rossant et al., 2016). Spike trains were further analysed to reveal spike waveform characteristics, firing rate and firing regularity.

The spiking activities over time, or spike trains, of DRN neurons were labelled and grouped based on their corresponding subtypes, namely, slow regular, slow irregular, fast regular, fast irregular. Instantaneous firing rates (IFR) of the DRN neurons were derived from the corresponding neuronal spike trains using non overlapping time bins of 5 ms, using the Elephant toolbox in Python 3.0 (Yegenoglu et al., 2015).

The 3 ECoG signals were band limited to 25 Hz using a 5th order Butterworth high pass filter, because we were interested in low-frequency oscillations and the signals were then concatenated for analysis. No further filtration or average referencing methods were used, which would impart spurious results based on the nature of our dataset (low-density recording, and sensors were not close to each other).

Power spectral analysis of the ECoG signals showed that most of the signal powers were concentrated at the lower frequency components. This was consistent with the nature of our experimental data – the use of anaesthetized mice having brain waves in the delta band of frequency (Schweimer et al., 2011; Steriade et al., 2000). Hence, we focused on the lower frequencies of 0.5 to 4 Hz in our analysis.

To assess the relationship between simultaneously recorded neuronal activities between two brain regions (cortex and DRN) we perform coherence analysis (Bowyer, 2016; Schweimer et al., 2011). We also computed the coherence between each DRN neurons to find whether the DRN neurons were correlated with each other. We then used statistical analysis to find the significance of our measures. These are described in detail below.

6.2.3. Data analysis

The correlation analysis is performed to see the interactions between the spike trains in DRN. Using Pearson's correlation coefficient, it is found that the interactions between the IFRs of the spiking activities in DRN are sparse (see chapter 3 for the equations and details) This result is further backed the coherence analysis.

Coherence analysis, which is performed in frequency space by applying Fourier Transform, is a well-known method to compute the frequency dependent relationship (correlation) between two signals (Rosenberg et al., 1989) (see Chapter 3). This method will be used to find the interactions within the raphe, cortex and between them. This was performed within the 0.5-4 Hz frequency band based on previous evidences, and the use of anaesthetized mice. Note that for DRN unit activities, coherence analysis is performed only on their IFRs (as continuous variables), derived from the spike trains of the DRN. Similarly, coherence analysis was performed to find the interactions between the ECoG signals of the three cortical regions, namely left frontal, right frontal and right occipital cortex. Finally, analysis of coherence is performed between each IFR and each of the 3 ECoG activities.

6.2.4. Statistical analysis

In order to test whether the interaction between the neurons as depicted by the coherence analyses are statistically significant, we calculated the threshold above which coherence level is considered to be statistically significant with $p<0.01$. To do this, suppose that T_1, T_2, ….T_n are test numbers and P_1, P_2,… P_n are the corresponding p-values, then the test corresponding to the maximum p-value is calculated as T_{max}.

While comparing two signals, such as between IFR and ECoG, and to find the coherence estimates inferred from simultaneous trials, we first computed the distribution of T_{max}. This gives the original statistics of the coherence indices (Nichols and Hayasaka, 2003). Hence, the data recorded simultaneously (ECoG and IFR) is divided into 'n' epochs. There are 37 IFRs and 3 ECoG signals for mouse 1. Similarly, mouse 2, 3 and 4 have 29,

25, 36 IFRs respectively, with every mouse having 3 ECoG signals. The coherence values between one IFR signal and an ECoG signal of a particular mouse, are calculated for every epoch. The maximum value of these coherences in all the epochs is computed, which constitutes towards the T_{max}. This is repeated for every pair of IFRs and ECoGs to calculate the corresponding T_{max}. The tests in our data are basically the coherence values between one IFR and an ECoG signals of a particular mouse.

After that, the T_{max} for the surrogate data was computed in a similar manner by deriving the surrogate data from the original data. This was done by keeping one signal, e.g. the IFR to be the same as the original while permuting the other signal (e.g. ECoG) randomly. The procedure was repeated for all the three combinations of the ECoG signals and the corresponding T_{max} values were calculated. The absolute value of these T_{max} was then found. This process was repeated for 1000 Monte Carlo resampling. The 99% percentile value of these T_{max}'s was taken as the threshold, which corresponds to p-value equals 0.01. The tests (i.e. the coherences between different IFR and ECoG signals) having $p<0.01$, were considered to be significant. Thus, we find the significant coherence or interaction between the IFRs and the ECoG signals of a particular mouse. This process is repeated for all the mice.

6.3. Results

It should be noted that the results presented in this work are based on transgenic, sert-cre type mice and not wild type mice. As discussed earlier, the DRN consists of electrophysiologically distinct subgroups of neurons. Specifically, in the neural recordings, and as discussed in Chapter 3 (section 3.2.1), using the criteria of firing rate of 5 Hz and CV of 0.7 led to the identification of 4 different subgroups of DRN neurons, namely: (i) fast and irregular spiking; (ii) slow and regular spiking; (iii) slow and irregular spiking; and (iv) fast and regular spiking. These categories will be used in the below analyses.

6.3.1. Weak spike correlation within the DRN

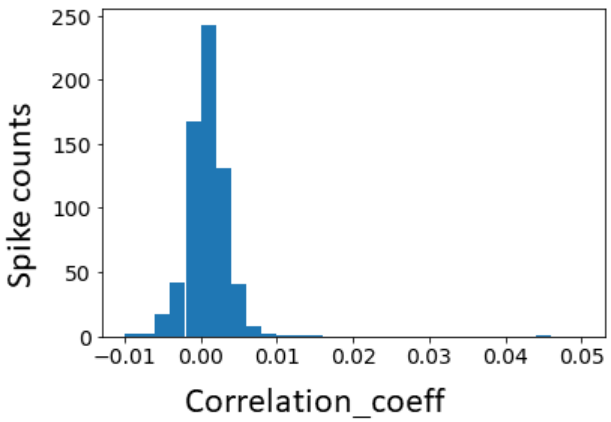

Figure 6.1. Pearson's Correlation Coefficient of spike trains in DRN. Most of the spikes are found to have the correlation coefficient less than 0.01 within the DRN for mouse 1.

The correlation between spike trains in DRN was computed across all neuronal pairs within each animal, and found to be sparse. This was based on very low maximum magnitude of correlation coefficient of 0.045 (Fig. 6.1). In fact, most of the pairs of spike trains had correlation coefficients below 0.01. This showed that the neurons in the DRN were sparsely correlated. Due to a general lack of significant results, the analysis was shifted to frequency based analysis using coherence.

6.3.2. Weak and sparse coherence within the DRN or cortex

To understand whether the simultaneously recorded DRN neurons are functionally linked to each other in the frequency domain, COH was computed between the IFRs of every pair of DRN neurons within the same recording session. The coherence matrix was found to be relatively sparse (Fig. 6.2A), with only a few relatively stronger interactions between slow-regular firing DRN neurons (Fig. 6.2A, between orange and yellow). Hence, the DRN neuronal connectivity overall seemed to be potentially sparse, perhaps indicating very weak interactions among the DRN neurons.

By repeating the analysis for different mice (in different sessions), similar patterns were observed (Fig. 6.2B-6.2D). As in the results from the previous mouse data, the DRN

neurons were found to be sparsely and weakly interacting with each other, with their very weak coherence magnitudes, and that the neuronal pairs with stronger interactions mainly consisted of slow-regular DRN firing neurons. A key difference with the previous data was that there were now more slow-regular firing DRN neurons with stronger relationships between each other (cf. Figs. 6.2A and 6.2B-6.2D).

Next, for completeness, the coherences between the ECoGs were analysed. The frequency spectral for any two ECoGs for each mouse was presented in Fig. 6.3. One could see some strong correlations across the frequencies, especially robustly around ~3.7 Hz. In order to visualize which channels of the ECoG signals were highly correlated, coherence values between the ECoG signals were presented in heatmap in Fig. 6.4. We could see that for all the mice, there were overall strong interactions between the ECoGs.

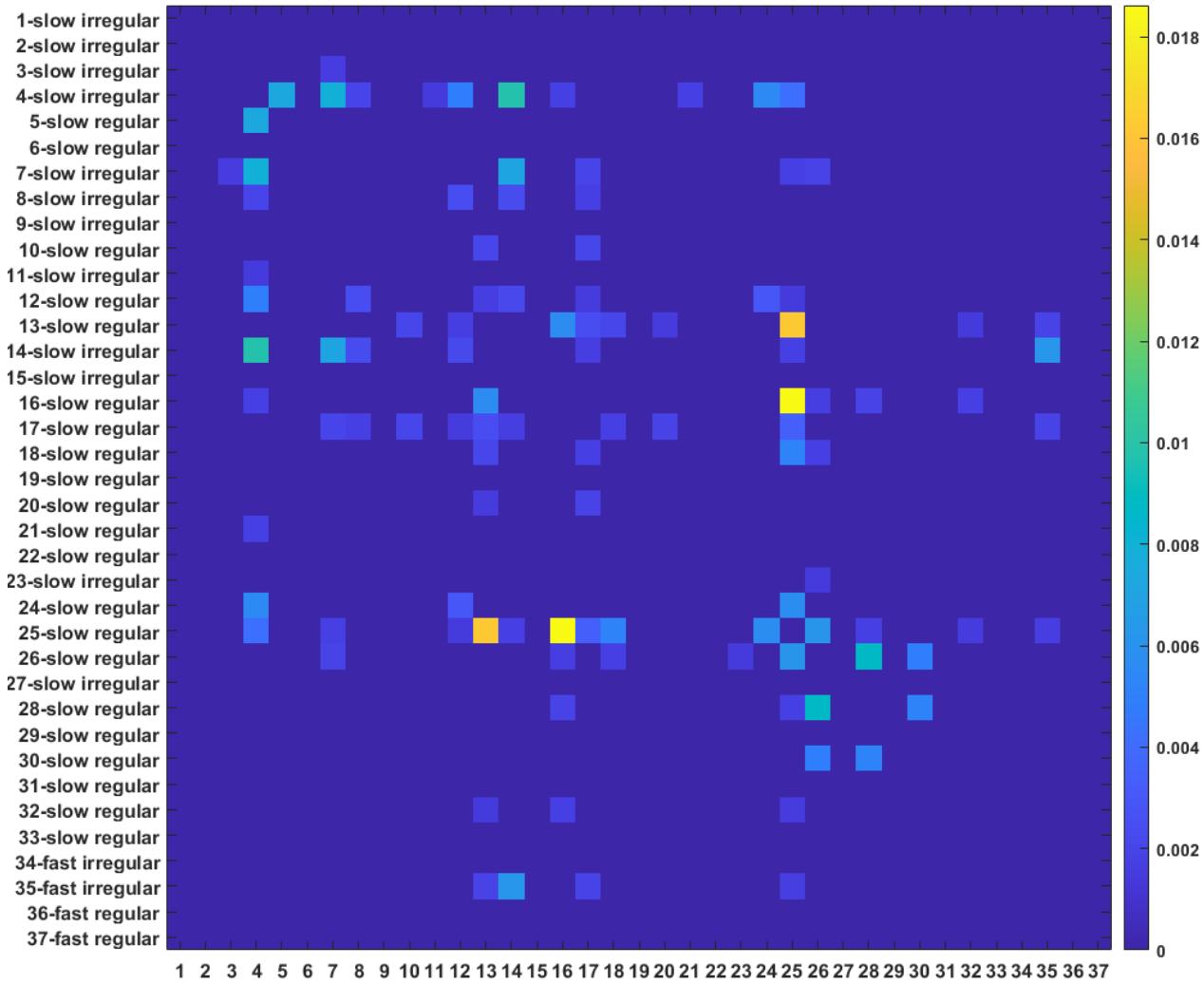

Figure 6.2A. Sparse and very weak interactions among 37 simultaneously recorded DRN neurons based on magnitude of coherence for mouse 1. Colour bar: COH level. Most pair of DRN neurons have very low coherence magnitudes (less than 0.018), indicating weak interactions. Threshold for significant coherence (0.02) is determined by maximum statistic.

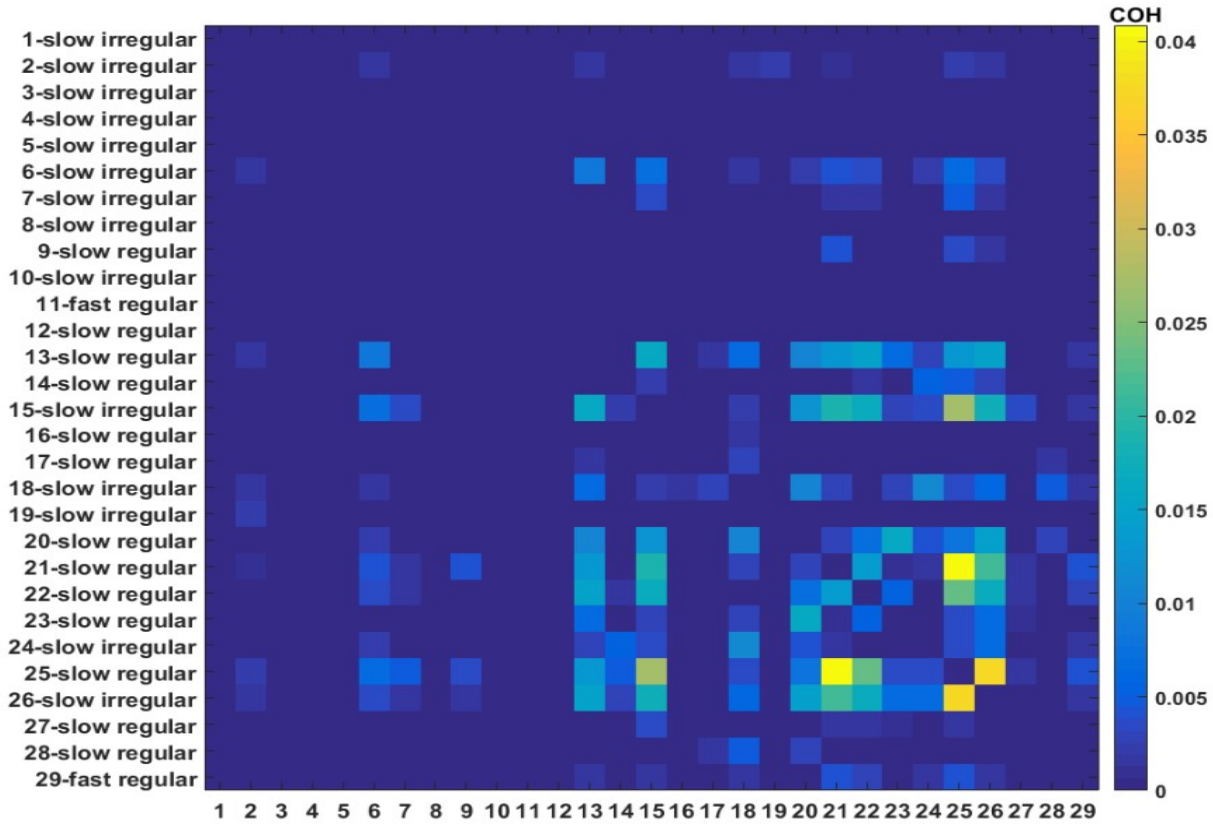

Figure 6.2B. Sparse and very weak interactions among 29 simultaneously recorded DRN neurons based on magnitude of coherence for mouse 2. Labels as in Fig. 6.2A.

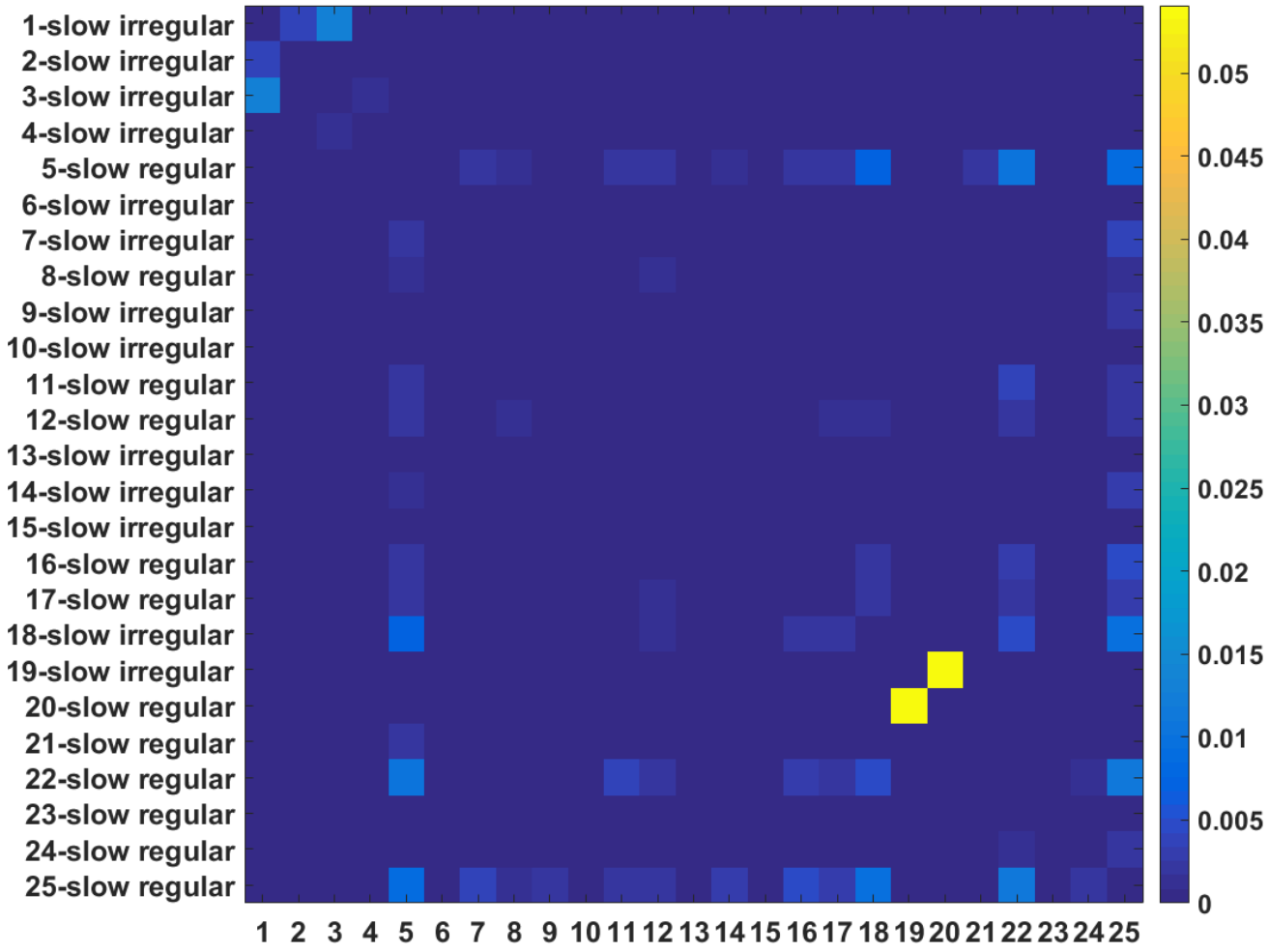

Figure 6.2C. Sparse and very weak interactions among 25 simultaneously recorded DRN neurons based on magnitude of coherence four mouse 3. Labels as in Fig. 6.2A.

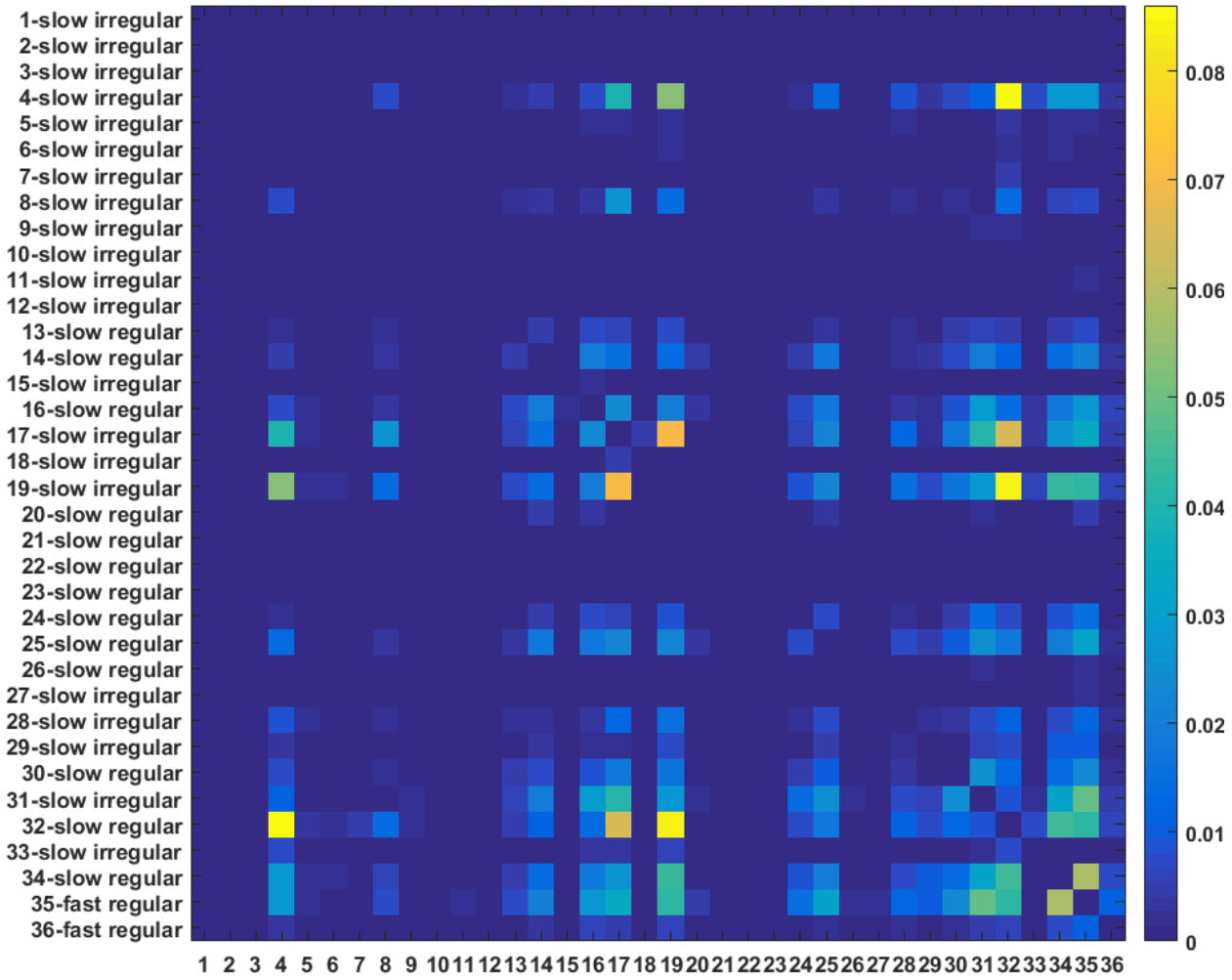

Figure 6.2D. Sparse and very weak interactions among 36 simultaneously recorded DRN neurons based on magnitude of coherence for mouse 4. Labels as in Fig. 6.2A.

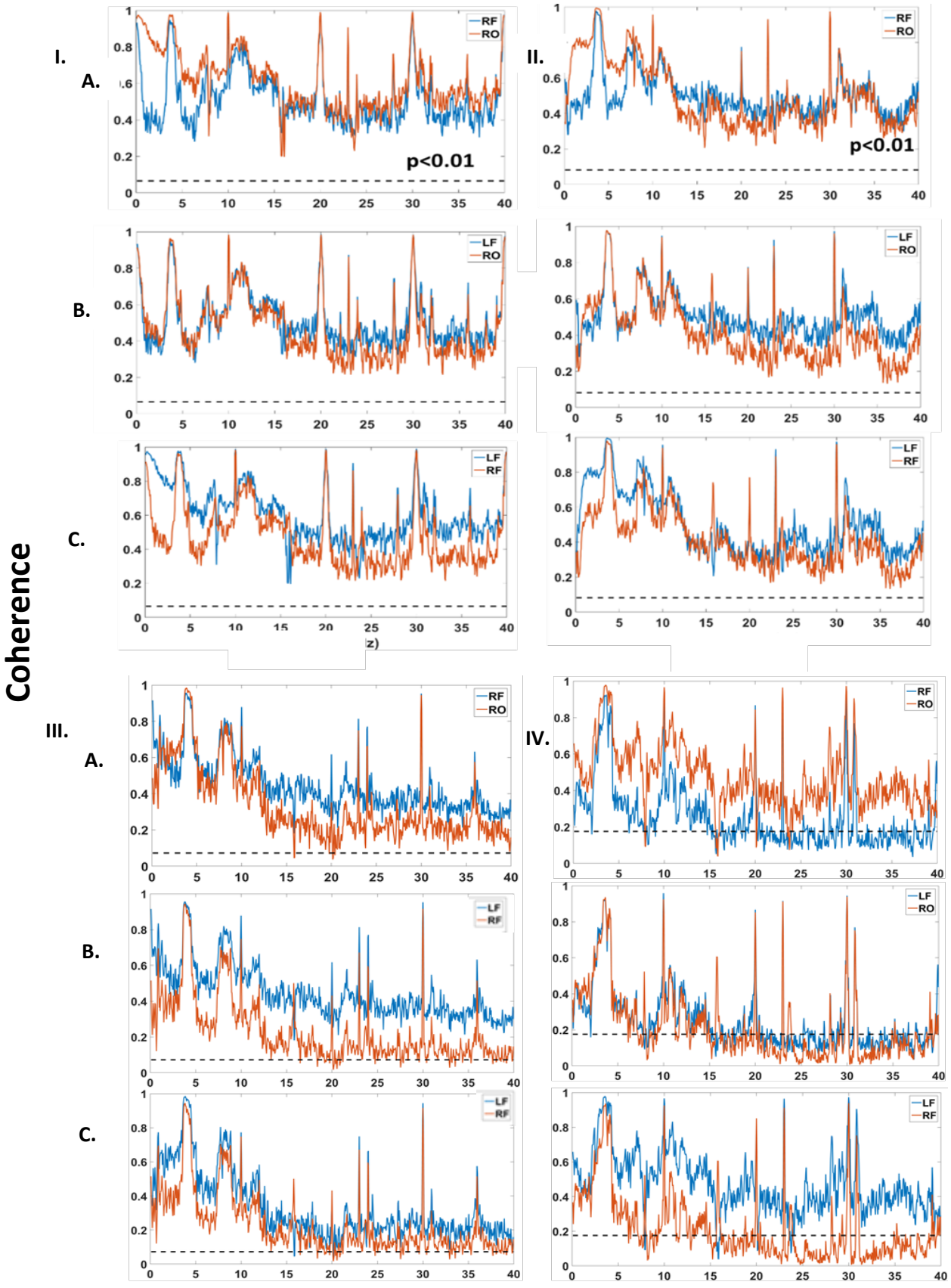
I.
A.
RF
RO
p<0.01
II.
RF
RO
p<0.01
B.
LF
RO
LF
RO
C.
LF
RF
LF
RF
III.
A.
RF
RO
IV.
RF
RO
B.
LF
RF
LF
RO
C.
LF
RF
LF
RF
Coherence
Frequency (Hz)

Figure 6.3. Frequency spectral of the ECoG activities. Threshold for significant coherence (0.065) is determined by maximum statistic. I.-IV. Results for four different mice. A. Coherences of RF and RO with LF. B. Coherences of RF with LF and RO. C. Coherences of RO with LF and RF. LF, RF, RO denote left frontal, right frontal, right occipital cortex, respectively.

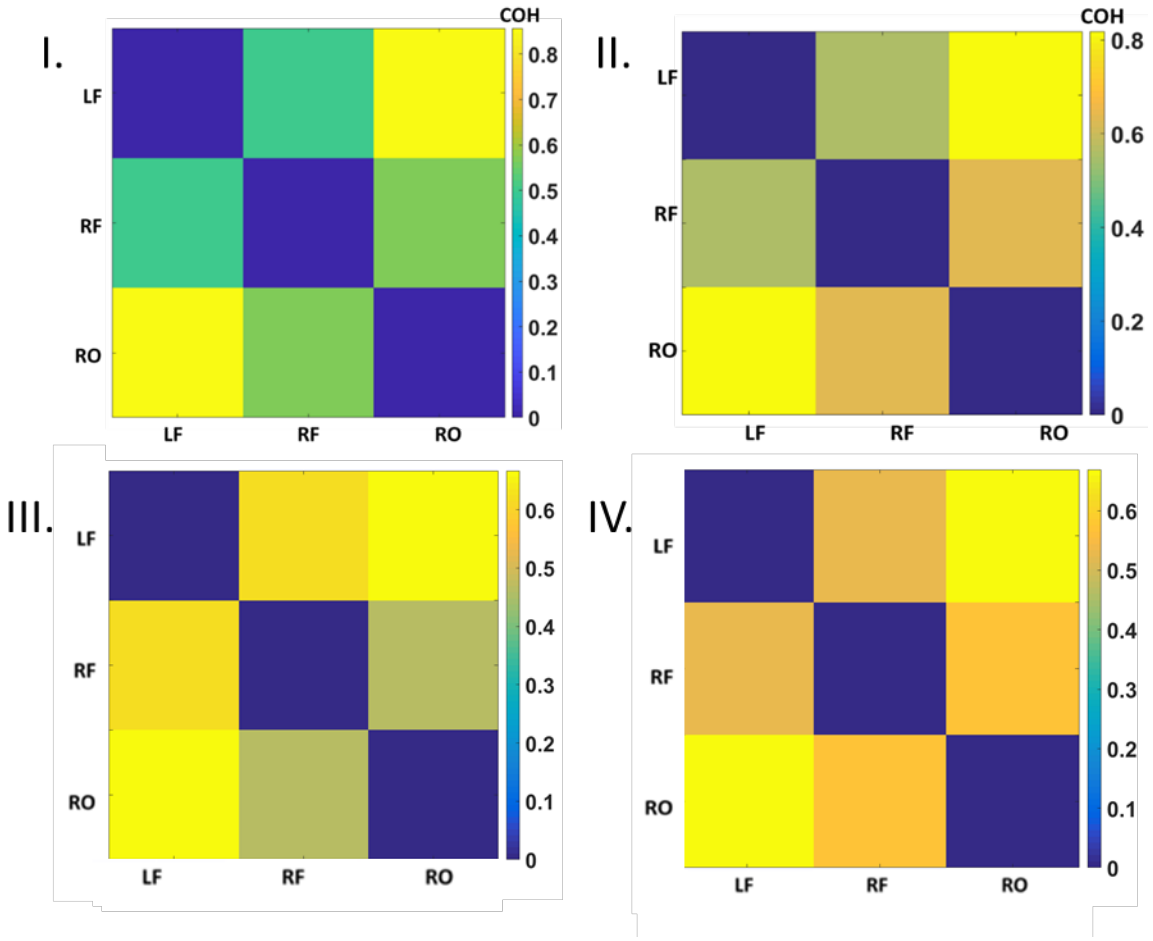

Figure 6.4. Very strong and significant interactions among the simultaneously recorded ECoG activities. LF: left frontal; RF; right frontal; and R: right occipital cortical region recorded. I., II., III., IV. represent the results for 4 different mice. Auto-coherence (coherence with the signals from the same electrodes) are patched with blue colours (indicating highest interactions), irrespective of the coherences indicated in the colour bar.

6.3.3. Significant coherence between slow-irregular and slow-regular firing DRN neurons and right frontal cortex

After identifying the coherences within either the DRN or cortical activities, we shall now discuss about the coherences between the DRN and cortical activities. Fig. 6.5 showed the coherence analysis within the frequency band of 0.5-4 Hz for four mice in separate recording sessions, breaking down into the individual neurons labelled by their electrophysiological (spiking) characteristics and the 3 ECoG channels. Panels I, II, III, IV were for four recording sessions. Coherence magnitudes were plotted against the frequencies to find the frequency at which the signals were more correlated. Note that in the first session (I), there were 37 recorded units in the DRN while in the second session (II) there were 29 units, in the third session (III) there were 36 units and in the fourth session (IV) there were 25 recorded units. We could easily observe that the slow and regular, and slow and irregular DRN neurons were the majority of neurons in the session. In general, one could observe that the right frontal cortex generally exhibited the highest coherence with the DRN neurons.

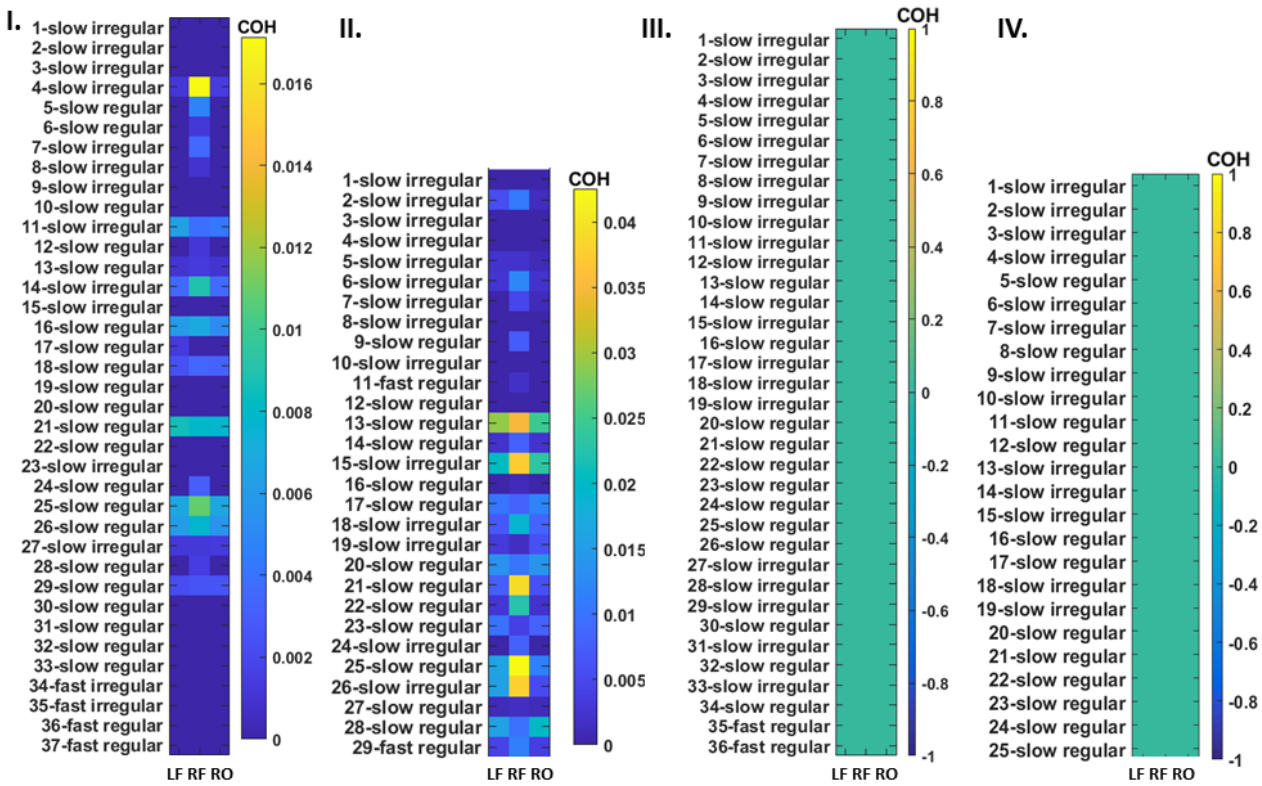

Figure 6.5. Interaction between DRN neuronal firing activities and 3 cortical regions. I, II , III, IV are for the four different mice (and recording sessions). Significant interactions, measured by the magnitude of coherence (COH), between different subgroups of DRN neurons (vertical axis) and ECoG signals (horizontal axis). Colour bar: COH level. LF (RF): ECoG from left (right) frontal cortices; RO: ECoG from right occipital cortex. DRN neuronal subgroups based on slow regular, slow irregular, fast regular, and fast irregular firing characteristics. Coherence is analysed for frequency range between 0.5 to 4 Hz.

For a more detailed evaluation of the coherences, Fig. 6.6 was plotted, for the same recording sessions, the coherences across a continuous range of oscillation frequencies, up till 5 Hz. Panels I, II, III, IV were for four recording sessions. This was shown for all the 37 and 29 recorded neurons and their coherences with the left frontal cortex (LF) (Fig. 6.6A), right frontal cortex (RF) (Fig. 6.6B) and right occipital (RO) cortex (Fig. 6.6C). The coherences between ECoG activities and DRN neuronal firing rates were found to generally have statistically significant peaks at around 0.5-1 Hz and 3.5-3.8 Hz (Fig. 6.6, above black dashed lines). This observation was also consistent with a previous work using extracellular single-cell recording (Schweimer et al., 2011). In some recordings,

especially in session II, slow-irregular (red) and fast-regular (blue) neurons seemed to have very weak but significant coherence with the ECoG signals, especially the right frontal ECoG signals, at a much lower frequency of ~0.17 Hz (Fig. 6.6, blue).

Dominance of the coherences fluctuates across neurons and cortical regions. For the second mouse (and session), the double frequency peaks for the high coherences were not as apparent, but more prominently peaking around 0.5-1.5 Hz. A key difference of this mouse/session compared with the previous mouse/session was that there were now more slow-regular firing DRN neurons with stronger relationships between each other (magnitude wise), and also with the right frontal ECoG signals.

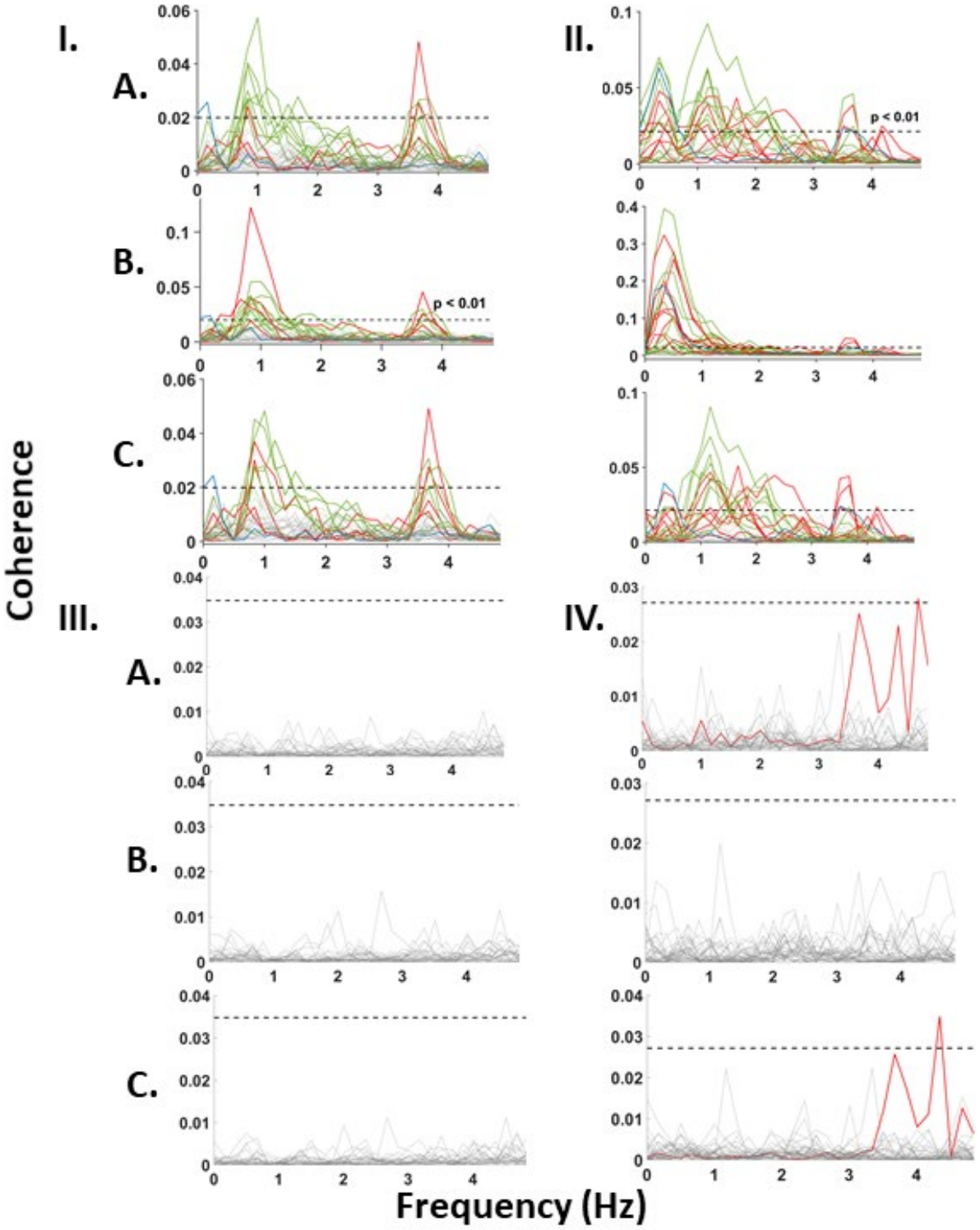

Figure 6.6. Double frequency peaks for significant COH between the DRN neurons and cortical ECoGs. I, II, III, IV are for four different mice (and recording sessions). Threshold for significant coherence (0.02) is determined by maximum statistic. Statistically significant thresholds ($p < 0.01$): black dashed lines. A-C. Interactions between DRN neurons and ECoG

signals in LF (A), RF (B) and RO (C). Only statistically significant traces are coloured. Colours of the lines distinguishes the interactions of ECoG signals with different DRN neurons

6.4. Discussion

Previous studies have indicated a relationship between the frontal cortex, particularly the PFC, and the DRN neurons (Celada et al., 2001; Puig et al., 2005). However, most of these studies had investigated using either single-neuron recordings (Gartside et al., 2000) or single ECoG channel (Schweimer et al., 2011). Hence, it is not clear how the diverse DRN neuronal population work together to coordinate, and communicate with cortical rhythms, and the relative contributions of the electrophysiologically distinct DRN neuronal types. In this work, first, the technical feasibility of experimentally recording simultaneous DRN neurons and multiple cortical regions (ECoGs) in four anaesthesised mice were successfully tested. Coherence analytical methods were also successfully applied to reveal the relationship between DRN neurons, and between DRN and ECoGs.

It was found that that only a small proportion of the recorded DRN neurons were found to be correlated, and if so, weakly with each other. This was demonstrated in both spike correlations and coherence analysis of neuronal firing rates. This finding was reminiscent of a recent work which indicated low correlation between pairs of neurons in the locus coeruleus brain region which consisted of another type of monoaminergic neurons, the norepinephrine/noradrenergic neurons (Totah et al., 2018). In contrast, the 3 ECoG signals strongly interacted with each other (with maximum coherence magnitude of 0.99).

Using coherence analysis, the DRN neuronal firing activities of simultaneously recorded DRN neurons were shown to be linked to the slow neural oscillations in the cortex as reflected in the ECoG signals. In particular, the slow-regular and slow-irregular firing DRN neurons were shown to be coupled more strongly with ECoG signals, especially in the right frontal cortex. Corticoraphe interactions seemed to operate at a low frequency band of 0.5-1 Hz, which was consistent with a previous work (Schweimer et al., 2011). In addition, this new work also revealed another peak at a slightly higher frequency band of 3.5-3.8 Hz. Based on previous studies (Allers and Sharp, 2003; Mihály Hajós et al., 2007;

Mlinar et al., 2016), 5-HT neurons in the DRN typically exhibit slow regular or irregular firing characteristics and so the identified slow-firing DRN neurons could potentially be 5-HT neurons.

In summary, our work has demonstrated technical feasibility, both experimentally and analytical, to understand the dynamic relationship between neurons and neuronal populations in the corticoraphe system. This work was presented in 31st Irish Signals and Systems Conference (ISSC), Letterkenny, Ireland, 2020 (Behera et al., 2020).

Chapter 7
Summary, general discussion and future directions

This chapter summarises the research in this thesis and provides future directions for further work.

In Chapter 2, a concise review of the neurobiology and functions of serotonergic system was provided. Serotonin (5-HT), being an endogenous neurochemical is responsible for modulating various physiological and behavioural processes (Müller and Jacobs, 2009; Müller and Cunningham, 2020). The major area in which 5-HT is located in the brain, is the midbrain raphe nuclei, especially the dorsal raphe nucleus DRN and midbrain raphe nucleus MRN. There is extensive projection from the DRN to the cortex, regulating various cognitive functions, and also to neuromodulator systems, regulating emotion and learning (Müller and Jacobs, 2009; Müller and Cunningham, 2020). Thus, this thesis is focused on investigating 5-HT in the DRN.

5-HT from the DRN is known to strongly innervate the prefrontal cortex (PFC), which is known to be linked to executive functions such as working memory (Celada et al., 2013, 2008; Gartside et al., 2000; Totah et al., 2018). Although previous studies had successfully shown evidence of a tight reciprocal relationships between the PFC and the DRN, most typically involved singe-cell recordings and/or coarse-grained neuroimaging activity (Gartside et al., 2000; Schweimer et al., 2011). Thus, it was unclear how the population of DRN neuronal activity relates, as a group, with different cortical activities. This knowledge gap was filled by this thesis work (Chapter 6).

In Chapter 2, there was also the mentioning of the complexity of the 5-HT system. In particular, 5-HT system consists of several receptor subtypes (Sharp and Barnes, 2020), which in turn can modulate targeted neuronal firing and synaptic changes and controlling neural information flow. Moreover, there is heterogeneity in the electrophysiological properties of DRN neurons, although the consensus so far is that the DRN neurons have

slow firing rates, wide action potentials and slow after-spike hyperpolarization and recovery in its neuronal membrane potential (Aghajanian and Vandermaelen, 1982; Li et al., 2001; Allers and Sharp, 2003; Marinelli, 2004; Kocsis, et al., 2006). In Chapter 2, it was also discussed that the use of multi-electrode arrays for electrophysiological recording was not very prominent in 5-HT/raphe research, which was taken into account in this thesis work (Chapter 6).

Based on several neurochemical, electrophysiological, optogenetic, tracing and pharmacological studies, 5-HT is found to interact with other neurotransmitters and co-modulates cognition and behaviour. Particularly, there is evidence of direct and indirect interactions between the 5-HT neurons in the DRN and dopaminergic (DA) neurons in the ventral tegmental area (VTA) (Di Giovanni et al., 2009; Boureau and Dayan, 2011; De Deurwaerdère and Di Giovanni, 2017). For many years, DA neurons have been shown to signal reward prediction error to guide reinforcement learning (Schultz et al., 1997; Cohen et al., 2012; Watabe-Uchida et al., 2017). On the other hand, DRN 5-HT neuronal signalling is relatively more complex. For example, certain type of 5-HT neurons, named Type-I 5-HT neurons, respond to reward but not punishment whereas, a different type, Type-II 5-HT neurons, signal both expected reward and punishment (Cohen et al., 2015).

Further, adding to the complexity, the non-5-HT/DA neurons local to the DRN and VTA also exhibit complex signalling in reward/punishment tasks. For example, the response of GABAergic neurons to reward and punishment in the DRN and VTA are opposite, to certain extent (Cohen and Uchida, 2012; Tan et al., 2012; Liu et al., 2014; Li et al., 2016;). Thus, the overall signalling pattern within DRN-VTA system in response to reward and punishment is complex, diverse, heterogeneous, distributed and mixed. It is also unclear whether the DRN-VTA neural circuits, or more generally, neural circuits that encompass neuromodulators, can be degenerate and stable.

In this thesis work, several of the findings from separate experimental studies were reconciled in a single neural circuit model encompassing DRN and VTA (Chapter 4). Further, in Chapters 4 and 5, it was shown through computational modelling, that there can be degeneracy in DRN-VTA neural circuits, which were dynamically stable. These

degenerate and stable DRN-VTA circuit models were then shown, through computational simulations, to be identifiable through pharmacological means.

In Chapter 3, a focussed review of the methodologies adopted for neural computational modelling and the analysis of electrophysiological data of the 5-HT system is presented. In particular, in terms of computational modelling, to allow better scalability and computational simulation efficiency, biologically based mean-field models have been developed (e.g., Joshi et al., 2017). Such modelling techniques bridge from more biophysical spiking neuronal network models to abstract population firing-rate models. In the context of neuromodulation, sufficiently realistic population-based neural network modelling approach that takes into account the nonlinear input-output functions modulated by 5-HT, and the release-and-reuptake dynamics of the neuromodulator (including 5-HT) based on voltammetry measurements have been developed (Joshi et al., 2017). Importantly, the modelling framework developed by Joshi et al. (2017) that describes the interactions among several sources of neuromodulators is adopted in modelling the DRN-VTA system in this thesis. However, there is no mean-field neural circuit model that has investigated the direct and indirect interactions between 5-HT neurons in the DRN and DA neurons in the VTA especially during reward- or punishment-based conditioning tasks. This was covered in the computational modelling Chapters (4 and 5) of this thesis. Brief pedagogical discussion of dynamical systems theory was also mentioned in Chapter 3. This was used to evaluate the local dynamical stability of neural network models. Such method was used in Chapter 5 to evaluate the stability of the degenerate DRN-VTA circuit models found in Chapter 4.

As discussed above, the thesis analysed new data from simultaneously DRN neuronal spiking activities and electrocorticographic (ECoG) activities (data provided by experimental collaborators) (Behera et al., 2020). Hence, the latter part of Chapter 3 was devoted to discussing the analytical methods to understand such data types. Specifically, signal processing techniques, neuronal spiking characteristics, spike correlation and coherence measures were introduced. In this thesis Pearson's correlation coefficient (Perkel et al., 1967; De La Rocha et al., 2007; Greenberg et al., 2008; Shea-Brown et al., 2008) was used to evaluate the spike relationships among DRN neurons.

However, to identify the relationships across data types, particularly the neuronal instantaneous firing rates (IFR) and ECoG activities, coherence technique was used, which is a spectral analysis method of transforming signals into the frequency spectra which quantify the relative contributions of these components (Rosenberg et al., 1989). Using this approach, the cross-spectral analysis is performed among the IFRs of DRN neurons, ECoG signals of cortical regions, and between IFRs of DRN and ECoG signals. Taken together, Chapter 2 provided the background and scope for the research questions, while Chapter 3 provided the tools to undertake the original research studies.

In Chapter 4, computational mean-field modelling was used to demonstrate the theoretical plausibility of degeneracy in the DRN-VTA neural circuits, at least within the context of reward/punishment-based tasks. In this chapter, the direct and indirect interactions between neural populations producing 5-HT and DA and the models were constrained by data from known electrophysiological, neuropharmacological and voltammetry parameters. Upon simulating a parsimonious, simple DRN-VTA circuit model under reward and punishment conditions, it was found that many, but not all of the experimental findings, could be captured by a single DRN-VTA model. This could be due to simplicity of the model, or it could be that there exists multiple different neural circuit operating in parallel. Further, several distinct model architectures could replicate the same neural circuit activity response profile, hence demonstrating degeneracy. Due to the extensiveness of D_2-receptor connections in the networks, simulations of D_2 antagonist showed that some of these degenerate DRN-VTA networks could be distinguishable especially during reward-based tasks.

In Chapter 5, dynamical systems theory was used to demonstrate the local stability of the identified degenerate DRN-VTA neural circuits as described in Chapter 4. Specifically, for each degenerate circuit model, local stability analysis was used to find the stability of a system of dynamical equations that describe DRN-VTA circuit dynamics. The real parts of all the eigenvalues of the Jacobian matrices were negative at any given steady state even in the presence of additional phasic stimulus input, implying the models were considered to be dynamically and locally stable at that steady state (Strogatz, 2018). It was observed that the eigenvalues with a phasic input were generally larger (magnitude

wise) than those with tonic input. Interestingly, the models with a fast 5-HT-to-DA connection were found to be the most stable under both phasic and tonic conditions.

In Chapter 6, the processing and analyses of new, simultaneously recorded electrophysiological data in anaesthesized rodents based on multi-unit recordings in the DRN, and ECoG activities across multiple sites were presented In this chapter, the experimental details of simultaneous (extracellular) recordings of the DRN neuronal population firing activity in conjunction with the monitoring of ECoGs across multiple cortical regions were presented along with the computational analyses of spike correlations and pairwise coherence between DRN neuronal firing activities, and between the DRN neuronal activities and the ECoGs. Anaesthetized animals were used as the data was more stable to analyse. In the recordings, the left and right frontal (LF and RF) cortices were selected based on previous studies showing their interactions with the DRN, while the (right) occipital (RO) cortex was selected for comparison.

The spiking characteristics of DRN neurons were filtered, analysed to determine measures such as IFR, coefficient of variation (CV), interspike interval (ISI) and subsequently clustered based on their similarities. Similarly, the ECoG signals of the cortex were filtered to low frequency components. Spike correlation of DRN neuronal spike trains were found to be very weak and not pursued further. To assess the frequency-based relationship between simultaneously recorded neuronal activities between two neurons or two brain regions (cortex and DRN), coherence analysis (Bowyer, 2016; Schweimer et al., 2011) was performed. Statistical analysis, using Monte-Carlo re-simulation and T_{max} distribution were performed to find the significance of the coherence measures (Nichols and Hayasaka, 2003). It was found that within the frequency domain, most slow-firing DRN neurons with regular and irregular firing (putative 5-HT neurons) had relatively stronger relationship with slow (3.5 – 3.8 Hz) cortical oscillatory dynamics, especially the frontal cortices.

7.1. Summary of contributions

To summarise, three contributions as an extension to the field of neural circuit modelling and analysis of the serotonergic (5-HT) system were presented in this thesis. These were distributed into the three chapters of the thesis, namely, Chapters 4, 5 and 6.

In the first contribution, through mechanistic neurocomputational modelling it had been shown that neural circuits with neuromodulator-producing neurons can be degenerate, at least under the standard reward/punishment-based tasks. This was addressed by computationally modelling DRN-VTA circuits, which had been known to share structural and functional bidirectional relationship among their constituent neuron types. It was found that a parsimonious, minimally connected DRN-VTA circuit model could reconcile many of the diverse phasic and tonic neural signalling events reported in the DRN and VTA in (unexpected) punishment and (learned) reward tasks observed across separate experimental studies. The model suggested the possibility of more complex architecture such as different neural circuits operating in parallel.

Multiple (at least 84) different DRN-VTA circuit models were also found to capture the same activity response profile as the parsimonious model, thus, indicating degeneracy. There were several testable predictions in this modelling work. For example, the models suggested that slow, across-trial reward-based excitatory inputs could potentially be directly targeted to both DRN 5-HT and VTA DA neurons, and that inhibitory 5-HT GABA to VTA DA could connectivity cancel out the effects of the direct input to VTA DA neurons, rendering only long timescale changes on baseline activity of DRN 5-HT neurons. Further, in this modelling work, using D_2 receptor agonist, some of the degenerate DRN-VTA neural circuits could be distinguished based on the deviations in specific neural population activities, especially in rewarding tasks. Together, this computational modelling and analytical work supported the existence of degeneracy and stability in the DRN-VTA circuits, and a subset of the degenerate circuits could be distinguished through pharmacological means.

In the second contribution, dynamical systems theory was applied to determine whether the degenerate models as identified in Chapter 4 were dynamically and locally stable.

Mathematical derivations for the steady states and the Jacobian matrices were obtained. Then the eigenvalues of the Jacobian matrices for all cases were computed. It was shown that the (84) degenerate neural circuits were dynamically stable as the real parts of the eigenvalues associated with the steady state of the model were negative for every circuit model. Further, a model associated with fast 5-HT-to-DA connection was predicted to be more stable compared to the other degenerate models without this fast connection. Overall, through computational modelling, these two contributions suggest the plausibility of degenerate neural circuits that encompass serotonin and dopamine neuromodulators.

In the third contribution, it was shown how diverse DRN neurons coordinated together, and communicated with cortical rhythms. It was found that the DRN neurons were sparsely correlated with each other, whereas the ECoG signals were strongly correlated with each other. Further, it was shown that the DRN neuronal firing activities of simultaneously recorded DRN neurons were linked to the slow neural oscillations in the cortex as reflected in the ECoG signals. In particular, the slow-regular and slow-irregular firing DRN neurons were shown to be coupled more strongly with ECoG signals, especially in the right frontal cortex. Thus, this contribution had shed light on the heterogeneity and sparsity in terms of neuronal interactions or communications within the DRN, the cortex, and between the DRN and the cortex.

Altogether, the main contributions of this thesis were the theoretical demonstration of degenerate and dynamically stable DRN-VTA neural circuits, and the identification of sparse connectivity among DRN neurons yet significant functional connectivity between slow-firing DRN neurons and the frontal cortices.

These original research contributions have led to a series of publications, preprints and conference presentations/papers (Behera at al, 2017; O'Sullivan et al., 2018; Schweimer et al., 2018; Behera et al. 2018; Behera et al., 2019a; Behera et al., 2019b; Behera et al., 2020; Behera et al. 2020).

7.2. Limitations and future directions

7.2.1. Limitations and future directions in computational modelling:

Although this work was focused more on serotonergic (and dopaminergic) system, from a more general perspective, it would be interesting to apply our computational modelling and analytical framework to the study of degeneracy of neural circuits involving the interactions of other neuromodulators such as norepinephrine/noradrenaline (e.g. (Jalewa et al., 2014; Joshi et al., 2017) and under other behavioural task paradigms. In fact, the mean-field modelling framework (Joshi et al., 2017) is conveniently scalable to multiple brain regions and different neuromodulator types. For example, using the same modelling framework, Deco et al. (2019) have shown using a large-scale neural model to account for how 5-HT_{2A} receptor perturbation can lead to transitions between different brain states. In particular, the model consisted of several local nodes representing local brain regions in a parcellation, based on multimodal human neuroimaging data.

During the development of the neurocomputational models, we had resorted to a minimalist approach by focusing only on sufficiently simple neural circuit architectures that could replicate closely to the experimentally observed data. Future modelling work may investigate the relative relevance of these connections with respect to larger circuits involving cortical and subcortical brain regions across multiple scales, especially during adaptive learning (e.g. Wang and Wong-Lin (2013) and Zhou et al. (2018)). Further, future work should investigate the effects of neural gain modulation instead of modulation of current amplitudes (Deco et al., 2018; Fellous and Linster, 1998).

Among the several degenerate models of DRN-VTA system, a model fast 5-HT-to-DA connection was found to be dynamically more stable than all other architectures. Future modelling work could explore the effects of co-transmission of neurotransmitters on neural circuit degeneracy and functioning. This may require the involvement of more biologically realistic spiking neuronal network models across multiple scales (Canavier et

al., 2016; Cullen and Wong-Lin, 2015; Flower and Wong-lin, 2014; Joshi et al., 2017; Wong-Lin et al., 2012, 2011).

Last but not least, while identifying the degenerate models, lots of efforts were spent on the search for appropriate range of the model parameter values. Future work will investigate the automation of model parameter search (Barak, 2017; Pollock and Jazayeri, 2020; Benuskova and Kasabov, 2010; Espinosa-Ramos et al., 2019).

7.2.2. Limitations and future directions in experiments data analysis:

In the work in Chapter 6, the DRN neurons' types were not precisely labelled, i.e. it was not known whether the slow-firing neurons were actually 5-HT neurons. Future experimental work will confirm this. Future work would also entail more recording sessions and mice, include more minority subgroup (e.g. fast irregular spiking) of neurons, and should identify, using e.g. neuroanatomical tracing methods (Muzerelle et al., 2016), the internal microcircuit structure of the DRN neurons, and how they relate to the cortex, especially the frontal cortex. Also, given that the animals were anaesthetised, future challenge should seek to identify the interactions between DRN and cortex in different brain states in awake or behaving animals (see e.g. Warden et al. (2012)).

In terms of neural circuit degeneracy, the modelling work suggested the possibility of more complex neural circuit architectures, such as different neural circuits operating in parallel. This can perhaps be investigated through unbiased tracing methods. The modelling work also made several testable model predictions (see above). One of these predicted parallel neural pathways from DRN 5-HT neurons to VTA DA neurons that could potentially cancel out afferent across-trial (tonic) input of reward signals. This can be checked using combined optogenetics and tracing methods in brain slices or behaving animals.

Another model prediction was that D_2 receptor antagonist can distinguish certain types of neural circuits. This would perhaps be technically more challenging to validate – most likely a combination of techniques is required. The models' stability analysis had indicated

that DRN-VTA circuit models with fast 5-HT_3 receptor mediated 5-HT-to-DA connections may be more stable than those DRN-VTA circuit models without 5-HT_3 receptors in this pathway. This may perhaps be confirmed using electrical stimulation combined with pharmacological administration.

7.2.3. Limitations and future directions in electrophysiological data analyses

In Chapter 6, the analyses performed on neuronal spiking activities (and the derived firing rates) and ECoG activities were frequency-based techniques. Future work will make use of time-domain techniques to validate the results. Further, multivariate analytical techniques, rather than pairwise techniques, should be explored. Also, different coherence methods should be compared in the analysis of neuronal and neuronal population activities, and their relationships.

References

Adell, A., Artigas, F., 2004. The somatodendritic release of dopamine in the ventral tegmental area and its regulation by afferent transmitter systems. Neurosci. Biobehav. Rev. 28, 415–431. https://doi.org/10.1016/j.neubiorev.2004.05.001

Aghajanian, G.K., Graham, A.W., Sheard, M.H., 1970. Serotonin-containing neurons in brain: depression of firing by monoamine oxidase inhibitors. Science (80-.). 169, 1100–1102.

Aghajanian, G.K., Vandermaelen, C.P., 1982. Intracellular identification of central noradrenergic and serotonergic neurons by a new double labeling procedure. J. Neurosci. 2, 1786–1792.

Aghajanian, G.K., Wang, R.Y., Baraban, J., 1978. Serotonergic and non-serotonergic neurons of the dorsal raphe: reciprocal changes in firing induced by peripheral nerve stimulation. Brain Res. 153, 169–175.

Allers, K.A., Sharp, T., 2003. Neurochemical and anatomical identification of fast- and slow-firing neurones in the rat dorsal raphe nucleus using juxtacellular labelling methods in vivo. Neuroscience 122, 193–204. https://doi.org/https://doi.org/10.1016/S0306-4522(03)00518-9

Aman, T.K., Shen, R.-Y., Haj-Dahmane, S., 2007. D2-like dopamine receptors depolarize dorsal raphe serotonin neurons through the activation of nonselective cationic conductance. J. Pharmacol. Exp. Ther. 320, 376–385. https://doi.org/10.1124/jpet.106.111690

An, J., Yadav, T., Hessburg, J.P., Francis, J.T., 2019. Reward Expectation Modulates Local Field Potentials, Spiking Activity and Spike-Field Coherence in the Primary Motor Cortex. eneuro 6.

Azmitia, E.C., Gannon, P.J., 1986. The primate serotonergic system: a review of human and animal studies and a report on Macaca fascicularis. Adv. Neurol. 43, 407.

Azmitia, E.C., Segal, M., 1978. An autoradiographic analysis of the differential ascending projections of the dorsal and median raphe nuclei in the rat. J. Comp. Neurol. 179, 641–667. https://doi.org/10.1002/cne.901790311

Balasubramani, P.P., Srinivasa Chakravarthy, V., Wong-Lin, K., Wang, D.-H., Cohen, J.Y., Nakamura, K., Moustafa, A.A., 2017. Neural Circuit Models of the Serotonergic System. Comput. Model. Brain Behav., Wiley Online Books. https://doi.org/doi:10.1002/9781119159193.ch28

Barak, O., 2017. Recurrent neural networks as versatile tools of neuroscience research. Curr. Opin. Neurobiol. 46, 1–6. https://doi.org/10.1016/j.conb.2017.06.003

Basar, E., Guntekin, B., 2008. A review of brain oscillations in cognitive disorders and the role of neurotransmitters. Brain Res. 1235, 172–193. https://doi.org/10.1016/j.brainres.2008.06.103

Baxter, M., King, R.G., 1999. Measuring business cycles: approximate band-pass filters for economic time series. Rev. Econ. Stat. 81, 575–593.

Bear, M., Connors, B., Paradiso, M.A., 2020. Neuroscience: Exploring the brain. Jones & Bartlett Learning, LLC.

Behera, C.K., O'Sullivan, R., Sanchez-Bornot, J.M., Joshi, A., Prasad, G., Sharp, T., Wong-Lin, K., 2020. Revealing the Dynamic Relationship Between Neural Population Activities in Corticoraphe System, in: 2020 31st Irish Signals and Systems Conference (ISSC). IEEE, pp. 1–6.

Beier, K.T., Steinberg, E.E., DeLoach, K.E., Xie, S., Miyamichi, K., Schwarz, L., Gao, X.J., Kremer, E.J., Malenka, R.C., Luo, L., 2015. Circuit Architecture of VTA Dopamine Neurons Revealed by Systematic Input-Output Mapping. Cell 162, 622–634. https://doi.org/10.1016/j.cell.2015.07.015

Beliveau, V., Ganz, M., Feng, L., Ozenne, B., Højgaard, L., Fisher, P.M., Svarer, C., Greve, D.N., Knudsen, G.M., 2017. A High-Resolution *In Vivo* Atlas of the Human Brain's Serotonin System. J. Neurosci. 37, 120–128. https://doi.org/10.1523/JNEUROSCI.2830-16.2017

Beliveau, V., Svarer, C., Frokjaer, V.G., Knudsen, G.M., Greve, D.N., Fisher, P.M., 2015. Functional connectivity of the dorsal and median raphe nuclei at rest. Neuroimage 116, 187–195.
Benoit-Marand, M., Borrelli, E., Gonon, F., 2001. Inhibition of dopamine release via presynaptic D2 receptors: time course and functional characteristics in vivo. J. Neurosci. 21, 9134–9141.
Berendsen, H.H., Broekkamp, C.L., 1994. Comparison of stimulus properties of fluoxetine and 5-HT receptor agonists in a conditioned taste aversion procedure. Eur. J. Pharmacol. 253, 83–89.
Bertram, H.N., 1994. Theory of magnetic recording. Cambridge University Press.
Bertram, H.N., Che, X., 1993. General analysis of noise in recorded transitions in thin film recording media. IEEE Trans. Magn. 29, 201–208.
Bi, A., Cui, J., Ma, Y.-P., Olshevskaya, E., Pu, M., Dizhoor, A.M., Pan, Z.-H., 2006. Ectopic expression of a microbial-type rhodopsin restores visual responses in mice with photoreceptor degeneration. Neuron 50, 23–33.
Bornot, J.S., Wong-Lin, K., Ahmad, A.L., Prasad, G., 2018. Envelope of the imaginary coherence can identify EEG/MEG functional connectivity in sensor space, in: MEG UK 2018.
Boureau, Y.L., Dayan, P., 2011. Opponency revisited: Competition and cooperation between dopamine and serotonin. Neuropsychopharmacology 36, 74–97. https://doi.org/10.1038/npp.2010.151
Bowyer, S.M., 2016. Coherence a measure of the brain networks: past and present. Neuropsychiatr. Electrophysiol. 2, 1–12. https://doi.org/10.1186/s40810-015-0015-7
Boyden, E.S., 2005. Zhang F, Bamberg E, Nagel G, Deisseroth K. Millisecond-timescale, Genet. Target. Opt. Control neural Act. Nat Neurosci 8, 1263–1268.
Bromberg-Martin, E.S., Hikosaka, O., Nakamura, K., 2010. Coding of task reward value in the dorsal raphe nucleus. J. Neurosci. 30, 6262–6272.
Bunin, M.A., Prioleau, C., Mailman, R.B., Wightman, R.M., 1998. Release and Uptake Rates of 5-Hydroxytryptamine in the Dorsal Raphe and Substantia Nigra Reticulata of the Rat Brain. J. Neurochem. 70, 1077–1087.
Bunin, M.A., Wightman, R.M., 1998. Quantitative evaluation of 5-hydroxytryptamine (serotonin) neuronal release and uptake: an investigation of extrasynaptic transmission. J. Neurosci. 18, 4854–4860.
Butterworth, S., 1930. On the theory of filter amplifiers. Wirel. Eng. 7, 536–541.
Calizo, L.H., Akanwa, A., Ma, X., Pan, Y., Lemos, J.C., Craige, C., Heemstra, L.A., Beck, S.G., 2011. Raphe serotonin neurons are not homogenous: electrophysiological, morphological and neurochemical evidence. Neuropharmacology 61, 524–543.
Canavier, C.C., Evans, R.C., Oster, A.M., Pissadaki, E.K., Drion, G., Kuznetsov, A.S., Gutkin, B.S., 2016. Implications of cellular models of dopamine neurons for disease. J. Neurophysiol. 116, 2815–2830.
Cano-Colino, M., Almeida, R., Compte, A., 2013. Serotonergic modulation of spatial working memory: predictions from a computational network model. Front. Integr. Neurosci. 7, 71.
Cano-Colino, M., Almeida, R., Gomez-Cabrero, D., Artigas, F., Compte, A., 2014. Serotonin regulates performance nonmonotonically in a spatial working memory network. Cereb. Cortex 24, 2449–2463.
Celada, P., Puig, M.V., Artigas, F., 2013. Serotonin modulation of cortical neurons and networks. Front. Integr. Neurosci. 7, 25. https://doi.org/10.3389/fnint.2013.00025
Celada, P., Puig, M.V., Diaz-Mataix, L., Artigas, F., 2008. The hallucinogen DOI reduces low-frequency oscillations in rat prefrontal cortex: reversal by antipsychotic drugs. Biol. Psychiatry 64, 392–400. https://doi.org/10.1016/j.biopsych.2008.03.013
Celada, P., Puig, M. V, Casanovas, J.M., Guillazo, G., Artigas, F., 2001. Control of dorsal raphe serotonergic neurons by the medial prefrontal cortex: Involvement of serotonin-1A, GABA(A), and glutamate receptors. J Neurosci 21, 9917–9929. https://doi.org/21/24/9917

[pii]
Challis, C., Berton, O., 2015. Top-Down Control of Serotonin Systems by the Prefrontal Cortex: A Path toward Restored Socioemotional Function in Depression. ACS Chem. Neurosci. 6, 1040–1054. https://doi.org/10.1021/acschemneuro.5b00007
Challis, C., Boulden, J., Veerakumar, A., Espallergues, J., Vassoler, F.M., Pierce, R.C., Beck, S.G., Berton, O., 2013. Raphe GABAergic neurons mediate the acquisition of avoidance after social defeat. J. Neurosci. 33, 13978–13988.
Cheer, J.F., Kendall, D.A., Mason, R., Marsden, C.A., 2003. Differential cannabinoid-induced electrophysiological effects in rat ventral tegmentum. Neuropharmacology 44, 633–641.
Cohen, J., Uchida, N., 2012. Neuron-type specific signals for reward and punishment in the ventral tegmental area. Nature 482, 85–88. https://doi.org/10.1038/nature10754.Neuron-type
Cohen, J.Y., Amoroso, M.W., Uchida, N., 2015. Serotonergic neurons signal reward and punishment on multiple timescales. Elife 2015, 1–25. https://doi.org/10.7554/eLife.06346
Cohen, M.R., Kohn, A., 2011. Measuring and interpreting neuronal correlations. Nat. Neurosci. 14, 811.
Courtney, N.A., Mamaligas, A.A., Ford, C.P., 2012. Species Differences in Somatodendritic Dopamine Transmission Determine D2-Autoreceptor-Mediated Inhibition of Ventral Tegmental Area Neuron Firing. J. Neurosci. 32, 13520 LP – 13528.
Crawford, L.K., Craige, C.P., Beck, S.G., 2010. Increased intrinsic excitability of lateral wing serotonin neurons of the dorsal raphe: a mechanism for selective activation in stress circuits. J. Neurophysiol. 103, 2652–2663. https://doi.org/10.1152/jn.01132.2009
Crook, J., Lovick, T., 2016. Urodynamic function during sleep-like brain states in urethane anesthetized rats. Neuroscience 313, 73–82. https://doi.org/10.1016/j.neuroscience.2015.11.027
Cropper, E.C., Dacks, A.M., Weiss, K.R., 2016. Consequences of degeneracy in network function. Curr. Opin. Neurobiol. 41, 62–67. https://doi.org/10.1016/j.conb.2016.07.008
Cullen, M., Wong-Lin, K., 2015. Integrated dopaminergic neuronal model with reduced intracellular processes and inhibitory autoreceptors. IET Syst. Biol. 9, 245–258. https://doi.org/10.1049/iet-syb.2015.0018
Cutts, C.S., Eglen, S.J., 2014. Detecting pairwise correlations in spike trains: an objective comparison of methods and application to the study of retinal waves. J. Neurosci. 34, 14288–14303. https://doi.org/10.1523/JNEUROSCI.2767-14.2014
Dankoski, E.C., Wightman, R.M., 2013. Monitoring serotonin signaling on a subsecond time scale. Front. Integr. Neurosci. 7, 1–13. https://doi.org/10.3389/fnint.2013.00044
Dayan, P., Abbott, L.F., 2001. Theoretical neuroscience: computational and mathematical modeling of neural systems. Computational Neuroscience Series.
Dayan, P., Huys, Q.J.M., 2009. Serotonin in Affective Control. Annu. Rev. Neurosci. 32, 95–126. https://doi.org/10.1146/annurev.neuro.051508.135607
De Deurwaerdère, P., Di Giovanni, G., 2017. Serotonergic modulation of the activity of mesencephalic dopaminergic systems: Therapeutic implications. Prog. Neurobiol. 151, 175–236. https://doi.org/10.1016/j.pneurobio.2016.03.004
De Deurwaerdère, P., Stinus, L., Spampinato, U., 1998. Opposite change of in vivo dopamine release in the rat nucleus accumbens and striatum that follows electrical stimulation of dorsal raphe nucleus: role of 5-HT3 receptors. J. Neurosci. 18, 6528–6538. https://doi.org/10.1523/jneurosci.5723-07.2008
de Jong, J.W., Afjei, S.A., Dorocic, I.P., Peck, J.R., Liu, C., Kim, C.K., Tian, L., Deisseroth, K., Lammel, S., 2019. A neural circuit mechanism for encoding aversive stimuli in the mesolimbic dopamine system. Neuron 101, 133–151.
De La Rocha, J., Doiron, B., Shea-Brown, E., Josić, K., Reyes, A., 2007. Correlation between neural spike trains increases with firing rate. Nature 448, 802–806.

Deco, G., Cruzat, J., Cabral, J., Knudsen, G.M., Carhart-Harris, R.L., Whybrow, P.C., Logothetis, N.K., Kringelbach, M.L., 2018. Whole-Brain Multimodal Neuroimaging Model Using Serotonin Receptor Maps Explains Non-linear Functional Effects of LSD. Curr. Biol. 28, 3065-3074.e6. https://doi.org/10.1016/j.cub.2018.07.083

Deco, G., Cruzat, J., Cabral, J., Tagliazucchi, E., Laufs, H., Logothetis, N.K., Kringelbach, M.L., 2019. Awakening: Predicting external stimulation to force transitions between different brain states. Proc. Natl. Acad. Sci. U. S. A. 116, 18088–18097. https://doi.org/10.1073/pnas.1905534116

Di Giovanni, G., Di Matteo, V., Esposito, E., 2009. Birth, life and death of dopaminergic neurons in the substantia nigra. J. Neural Transm. Suppl.

Dorocic, I.P., Fürth, D., Xuan, Y., Johansson, Y., Pozzi, L., Silberberg, G., Carlén, M., Meletis, K., 2014. A whole-brain atlas of inputs to serotonergic neurons of the dorsal and median raphe nuclei. Neuron 83, 663–678.

Doya, K., 2002. Metalearning and neuromodulation. Neural Networks 15, 495–506. https://doi.org/10.1016/S0893-6080(02)00044-8

Duque, A., Zaborszky, L., 2006. Juxtacellular labeling of individual neurons in vivo: From electrophysiology to synaptology, in: Neuroanatomical Tract-Tracing 3: Molecules, Neurons, and Systems. pp. 197–236. https://doi.org/10.1007/0-387-28942-9_7

Edelman, G.M., Gally, J.A., 2001. Degeneracy and complexity in biological systems. Proc. Natl. Acad. Sci. U. S. A. 98, 13763–13768. https://doi.org/10.1073/pnas.231499798

El Mestikawy, S., Wallén-Mackenzie, Å., Fortin, G.M., Descarries, L., Trudeau, L.-E., 2011. From glutamate co-release to vesicular synergy: vesicular glutamate transporters. Nat. Rev. Neurosci. 12, 204–216.

Eshel, N., Bukwich, M., Rao, V., Hemmelder, V., Tian, J., Uchida, N., 2015. Arithmetic and local circuitry underlying dopamine prediction errors. Nature 525, 243–246. https://doi.org/10.1038/nature14855

Fellous, J.-M., Linster, C., 1998. Computational Models of Neuromodulation. Neural Comput. 10, 771–805. https://doi.org/10.1162/089976698300017476

Fernandez, S.P., Muzerelle, A., Scotto-Lomassese, S., Barik, J., Gruart, A., Delgado-Garciá, J.M., Gaspar, P., 2017. Constitutive and Acquired Serotonin Deficiency Alters Memory and Hippocampal Synaptic Plasticity. Neuropsychopharmacology 42, 512–523. https://doi.org/10.1038/npp.2016.134

Fiorillo, C.D., Tobler, P.N., Schultz, W., 2003. Discrete Coding of Reward Probability and Uncertainty by Dopamine Neurons. Science (80-.). 299, 1898 LP – 1902.

Fischer, A.G., Ullsperger, M., 2017. An update on the role of serotonin and its interplay with dopamine for reward. Front. Hum. Neurosci. 11, 484.

Fitoussi, A., Dellu-Hagedorn, F., De Deurwaerdere, P., 2013. Monoamines tissue content analysis reveals restricted and site-specific correlations in brain regions involved in cognition. Neuroscience 255, 233–245. https://doi.org/10.1016/j.neuroscience.2013.09.059

Floresco, S.B., West, A.R., Ash, B., Moore, H., Grace, A.A., 2003. Afferent modulation of dopamine neuron firing differentially regulates tonic and phasic dopamine transmission. Nat. Neurosci. 6, 968.

Flower, G., Wong-lin, K., 2014. Reduced Computational Models of Serotonin 61, 1054–1061.

Ford, C.P., 2014. The role of D2-autoreceptors in regulating dopamine neuron activity and transmission. Neuroscience 282, 13–22.

Fröhlich, F., 2016. Network neuroscience. Academic Press.

Fu, W., Le Maître, E., Fabre, V., Bernard, J.F., Xu, Z.Q.D., Hökfelt, T., 2010. Chemical neuroanatomy of the dorsal raphe nucleus and adjacent structures of the mouse brain. J. Comp. Neurol. 518, 3464–3494. https://doi.org/10.1002/cne.22407

Funahashi, S., 2017. Working Memory in the Prefrontal Cortex. Brain Sci. 7, 49. https://doi.org/10.3390/brainsci7050049

Gartside, S.E., Hajos-Korcsok, E., Bagdy, E., Harsing, L.G.J., Sharp, T., Hajos, M., 2000. Neurochemical and electrophysiological studies on the functional significance of burst firing in serotonergic neurons. Neuroscience 98, 295–300. https://doi.org/10.1016/s0306-4522(00)00060-9

Geddes, S.D., Assadzada, S., Lemelin, D., Sokolovski, A., Bergeron, R., Haj-Dahmane, S., Béïque, J.C., 2016. Target-specific modulation of the descending prefrontal cortex inputs to the dorsal raphe nucleus by cannabinoids. Proc. Natl. Acad. Sci. U. S. A. 113, 5429–5434. https://doi.org/10.1073/pnas.1522754113

Gerstein, G.L., Clark, W.A., 1964. Simultaneous Studies of Firing Patterns in Several Neurons. Science (80-.). 143, 1325–1327. https://doi.org/10.1126/science.143.3612.1325

Glass, J.D., Grossman, G.H., Farnbauch, L., DiNardo, L., 2003. Midbrain raphe modulation of nonphotic circadian clock resetting and 5-HT release in the mammalian suprachiasmatic nucleus. J. Neurosci. 23, 7451–7460. https://doi.org/citeulike-article-id:12006428

Greenberg, D.S., Houweling, A.R., Kerr, J.N.D., 2008. Population imaging of ongoing neuronal activity in the visual cortex of awake rats. Nat. Neurosci. 11, 749–751.

Guru, A., Post, R.J., Ho, Y.-Y., Warden, M.R., 2015. Making sense of optogenetics. Int. J. Neuropsychopharmacol. 18, pyv079.

Haj-Dahmane, S., 2001. D2-like dopamine receptor activation excites rat dorsal raphe 5-HT neurons in vitro. Eur. J. Neurosci. 14, 125–134.

Hajos, M., Allers, K.A., Jennings, K., Sharp, T., Charette, G., Sik, A., Kocsis, B., 2007. Neurochemical identification of stereotypic burst-firing neurons in the rat dorsal raphe nucleus using juxtacellular labelling methods. Eur. J. Neurosci. 25, 119–126. https://doi.org/10.1111/j.1460-9568.2006.05276.x

Hajós, M., Allers, K.A., Jennings, K., Sharp, T., Charette, G., Sík, A., Kocsis, B., 2007. Neurochemical identification of stereotypic burst-firing neurons in the rat dorsal raphe nucleus using juxtacellular labelling methods. Eur. J. Neurosci. 25, 119–126. https://doi.org/10.1111/j.1460-9568.2006.05276.x

Hajos, M., Gartside, S.E., Villa, A.E.P., Sharp, T., 1995. Evidence for a repetitive (burst) firing pattern in a sub-population of 5-hydroxytryptamine neurons in the dorsal and median raphe nuclei of the rat. Neuroscience 69, 189–197.

Hajós, M., Richards, C.D., Székely, A.D., Sharp, T., 1998. An electrophysiological and neuroanatomical study of the medial prefrontal cortical projection to the midbrain raphe nuclei in the rat. Neuroscience 87, 95–108. https://doi.org/https://doi.org/10.1016/S0306-4522(98)00157-2

Hajós, M., Sharp, T., Newberry, N.R., 1996. Intracellular recordings from burst-firing presumed serotonergic neurones in the rat dorsal raphe nucleus in vivo. Brain Res. 737, 308–312. https://doi.org/10.1016/0006-8993(96)00936-5

Hashemi, P., Dankoski, E.C., Petrovic, J., Keithley, R.B., Wightman, R.M., 2009. Voltammetric Detection of 5-Hydroxytryptamine Release in the Rat Brain. Anal. Chem. 81, 9462–9471. https://doi.org/10.1021/ac9018846

Hashemi, P., Dankoski, E.C., Wood, K.M., Ambrose, R.E., Wightman, R.M., 2011. In vivo electrochemical evidence for simultaneous 5-HT and histamine release in the rat substantia nigra pars reticulata following medial forebrain bundle stimulation. J. Neurochem. 118, 749–759.

Hayashi, K., Nakao, K., Nakamura, K., 2015. Appetitive and aversive information coding in the primate dorsal raphe nucleus. J. Neurosci. 35, 6195–6208.

Haykin, S., 2010. Neural Networks and Learning Machines, 3/E. Pearson Education India.

Heidbreder, C.A., Groenewegen, H.J., 2003. The medial prefrontal cortex in the rat: evidence for a dorso-ventral distinction based upon functional and anatomical characteristics. Neurosci. Biobehav. Rev. 27, 555–579. https://doi.org/10.1016/j.neubiorev.2003.09.003

Hernández-Vázquez, F., Garduño, J., Hernández-López, S., 2019. GABAergic modulation of

serotonergic neurons in the dorsal raphe nucleus. Rev. Neurosci. 30, 289–303.
Hodgkin, A.L., Huxley, A.F., 1990. A quantitative description of membrane current and its application to conduction and excitation in nerve. Bull. Math. Biol. 52, 25–71. https://doi.org/10.1007/BF02459568
Hoyer, D., Clarke, D.E., Fozard, J.R., Hartig, P.R., Martin, G.R., Mylecharane, E.J., Saxena, P.R., Humphrey, P.P., 1994. International Union of Pharmacology Classification of Receptors for 5-Hydroxytryptamine (Serotonin). Pharmacol. Rev. 46, 157–203. https://doi.org/7938165
Hu, H., 2016. Reward and aversion. Annu. Rev. Neurosci. 39, 297–324.
Huang, Y., Zheng, M.-Q., M Gerdes, J., 2010. Development of effective PET and SPECT imaging agents for the serotonin transporter: has a twenty-year journey reached its destination? Curr. Top. Med. Chem. 10, 1499–1526.
Jacobs, B.L., Azmitia, E.C., 1992. Structure and function of the brain serotonin system. Physiol Rev 72, 165–229. https://doi.org/10.1152/physrev.1992.72.1.165
Jalewa, J., Joshi, A., McGinnity, T.M., Prasad, G., Wong-Lin, K., Hölscher, C., 2014. Neural Circuit Interactions between the Dorsal Raphe Nucleus and the Lateral Hypothalamus: An Experimental and Computational Study. PLoS One 9, 1–16. https://doi.org/10.1371/journal.pone.0088003
Jonsson, G., Gorio, A., Hallman, H., Janigro, D., Kojima, H., Zanoni, R., 1984. Effect of GM1 ganglioside on neonatally neurotoxin induced degeneration of serotonin neurons in the rat brain. Dev. Brain Res. 16, 171–180. https://doi.org/https://doi.org/10.1016/0165-3806(84)90023-3
Joshi, A., 2014. Neural Circuit Modelling of the Orexin / Hypocretin System with Implications for Clinical Depression.
Joshi, A., Wang, D.-H., Watterson, S., McClean, P.L., Behera, C.K., Sharp, T., Wong-Lin, K., 2020. Opportunities for multiscale computational modelling of serotonergic drug effects in Alzheimer's disease. Neuropharmacology 108118. https://doi.org/https://doi.org/10.1016/j.neuropharm.2020.108118
Joshi, A., Wong-Lin, K., McGinnity, T.M., Prasad, G., 2011. A mathematical model to explore the interdependence between the serotonin and orexin/hypocretin systems, in: 2011 Annual International Conference of the IEEE Engineering in Medicine and Biology Society. pp. 7270–7273. https://doi.org/10.1109/IEMBS.2011.6091837
Joshi, A., Youssofzadeh, V., Vemana, V., McGinnity, T.M., Prasad, G., Wong-Lin, K., 2017. An integrated modelling framework for neural circuits with multiple neuromodulators. J. R. Soc. Interface 14, 20160902. https://doi.org/10.1098/rsif.2016.0902
Judge, S.J., Gartside, S.E., 2006. Firing of 5-HT neurones in the dorsal and median raphe nucleus in vitro shows differential α1-adrenoceptor and 5-HT1A receptor modulation. Neurochem. Int. 48, 100–107.
Kaczmarek, L.K., Levitan, I.B., 1987. Neuromodulation : the biochemical control of neuronal excitability. Oxford Univ. Press, New York.
Kim, C.K., Adhikari, A., Deisseroth, K., 2017. Integration of optogenetics with complementary methodologies in systems neuroscience. Nat. Rev. Neurosci. 18, 222–235.
Kirby, L.G., Pernar, L., Valentino, R.J., Beck, S.G., 2003. Distinguishing characteristics of serotonin and non-serotonin-containing cells in the dorsal raphe nucleus: Electrophysiological and immunohistochemical studies. Neuroscience 116, 669–683. https://doi.org/10.1016/S0306-4522(02)00584-5
Kocsis, B., Varga, V., Dahan, L., Sik, A., 2006. Serotonergic neuron diversity: Identification of raphe neurons with discharges time-locked to the hippocampal theta rhythm. Proc. Natl. Acad. Sci. U. S. A. 103, 1059–1064. https://doi.org/10.1073/pnas.0508360103
Köhler, C., Steinbusch, H., 1982. Identification of serotonin and non-serotonin-containing neurons of the mid-brain raphe projecting to the entorhinal area and the hippocampal formation. A combined immunohistochemical and fluorescent retrograde tracing study in the rat brain.

Neuroscience 7, 951–975. https://doi.org/10.1016/0306-4522(82)90054-9
Kreiter, A.K., Singer, W., 1996. Stimulus-dependent synchronization of neuronal responses in the visual cortex of the awake macaque monkey. J. Neurosci. 16, 2381–2396.
Kremer, Y., Flakowski, J., Rohner, C., Lüscher, C., 2020. Context-dependent multiplexing by individual VTA dopamine neurons. J. Neurosci. 40, 7489–7509.
Kruger, J., Aiple, F., 1988. Multimicroelectrode investigation of monkey striate cortex: spike train correlations in the infragranular layers. J. Neurophysiol. 60, 798–828.
Lammel, S., Lim, B.K., Malenka, R.C., 2014. Reward and aversion in a heterogeneous midbrain dopamine system. Neuropharmacology 76, 351–359.
Lammel, S., Lim, B.K., Ran, C., Huang, K.W., Betley, M.J., 2013. Input-specific control of reward and aversion in the ventral tegmental area 491, 212–217. https://doi.org/10.1038/nature11527.Input-specific
Lefebvre, B., Yger, P., Marre, O., 2016. Recent progress in multi-electrode spike sorting methods. J. Physiol. Paris 110, 327–335. https://doi.org/10.1016/j.jphysparis.2017.02.005
Leotti, L.A., Iyengar, S.S., Ochsner, K.N., 2010. Born to choose: the origins and value of the need for control. Trends Cogn. Sci. 14, 457–463. https://doi.org/10.1016/j.tics.2010.08.001
Li, W., Doyon, W.M., Dani, J.A., 2012. Quantitative unit classification of ventral tegmental area neurons in vivo. J. Neurophysiol. 107, 2808–2820.
Li, Y.-Q., Li, H., Kaneko, T., Mizuno, N., 2001. Morphological features and electrophysiological properties of serotonergic and non-serotonergic projection neurons in the dorsal raphe nucleus: An intracellular recording and labeling study in rat brain slices. Brain Res. 900, 110–118. https://doi.org/https://doi.org/10.1016/S0006-8993(01)02272-7
Li, Y., Li, C.-Y., Xi, W., Jin, S., Wu, Z.-H., Jiang, P., Dong, P., He, X.-B., Xu, F.-Q., Duan, S., Zhou, Y.-D., Li, X.-M., 2019. Rostral and Caudal Ventral Tegmental Area GABAergic Inputs to Different Dorsal Raphe Neurons Participate in Opioid Dependence. Neuron 101, 748-761.e5. https://doi.org/10.1016/j.neuron.2018.12.012
Li, Y., Zhong, W., Wang, D., Feng, Q., Liu, Z., Zhou, J., Jia, C., Hu, F., Zeng, J., Guo, Q., Fu, L., Luo, M., 2016. Serotonin neurons in the dorsal raphe nucleus encode reward signals. Nat. Commun. 7. https://doi.org/10.1038/ncomms10503
Lima, S.Q., Miesenböck, G., 2005. Remote control of behavior through genetically targeted photostimulation of neurons. Cell 121, 141–152.
Liu, Z., Zhou, J., Li, Y., Hu, F., Lu, Y., Feng, Q., Wang, D., Zeng, J., Bao, J., Kim, J., Mestikawy, S. El, Luo, M., 2015. Dorsal Raphe Neurons Signal Reward through 5-HT and Glutamate 81, 1360–1374. https://doi.org/10.1016/j.neuron.2014.02.010.Dorsal
Liu, Z., Zhou, J., Li, Y., Hu, F., Lu, Y., Ma, M., Feng, Q., Zhang, J. en, Wang, D., Zeng, J., Bao, J., Kim, J.Y., Chen, Z.F., ElMestikawy, S., Luo, M., 2014a. Dorsal raphe neurons signal reward through 5-HT and glutamate. Neuron 81, 1360–1374. https://doi.org/10.1016/j.neuron.2014.02.010
Liu, Z., Zhou, J., Li, Y., Hu, F., Lu, Y., Ma, M., Feng, Q., Zhang, J. en, Wang, D., Zeng, J., Bao, J., Kim, J.Y., Chen, Z.F., ElMestikawy, S., Luo, M., 2014b. Dorsal raphe neurons signal reward through 5-HT and glutamate. Neuron 81, 1360–1374. https://doi.org/10.1016/j.neuron.2014.02.010
Ludlow, K.H., Bradley, K.D., Allison, D.W., Taylor, S.R., Yorgason, J.T., Hansen, D.M., Walton, C.H., Sudweeks, S.N., Steffensen, S.C., 2009. Acute and chronic ethanol modulate dopamine D2-subtype receptor responses in ventral tegmental area GABA neurons. Alcohol. Clin. Exp. Res. 33, 804–811.
Marcinkiewcz, C.A., Mazzone, C.M., D'Agostino, G., Halladay, L.R., Hardaway, J.A., Diberto, J.F., Navarro, M., Burnham, N., Cristiano, C., Dorrier, C.E., Tipton, G.J., Ramakrishnan, C., Kozicz, T., Deisseroth, K., Thiele, T.E., McElligott, Z.A., Holmes, A., Heisler, L.K., Kash, T.L., 2016. Serotonin engages an anxiety and fear-promoting circuit in the extended amygdala. Nature 537, 97–101. https://doi.org/10.1038/nature19318

Marder, E., 2012. Neuromodulation of neuronal circuits: back to the future. Neuron 76, 1–11. https://doi.org/10.1016/j.neuron.2012.09.010
Marder, E., O'Leary, T., Shruti, S., 2014. Neuromodulation of circuits with variable parameters: single neurons and small circuits reveal principles of state-dependent and robust neuromodulation. Annu. Rev. Neurosci. 37, 329–346. https://doi.org/10.1146/annurev-neuro-071013-013958
Marinelli, S., Schnell, S.A., Hack, S.P., Christie, M.J., Wessendorf, M.W., Vaughan, C.W., 2004. Serotonergic and nonserotonergic dorsal raphe neurons are pharmacologically and electrophysiologically heterogeneous. J. Neurophysiol. 92, 3532–3537.
Masson, J., Emerit, M.B., Hamon, M., Darmon, M., 2012. Serotonergic signaling: multiple effectors and pleiotropic effects. Wiley Interdiscip. Rev. Membr. Transp. Signal. 1, 685–713.
Matias, S., Lottem, E., Dugue, G.P., Mainen, Z.F., 2017. Activity patterns of serotonin neurons underlying cognitive flexibility. Elife 6, e20552.
McDevitt, R.A., Tiran-Cappello, A., Shen, H., Balderas, I., Britt, J.P., Marino, R.A.M., Chung, S.L., Richie, C.T., Harvey, B.K., Bonci, A., 2014a. Serotonergic versus non-serotonergic dorsal raphe projection neurons: differential participation in reward circuitry. Cell Rep. 8, 1857–1869. https://doi.org/10.1016/j.celrep.2014.08.037
McDevitt, R.A., Tiran-Cappello, A., Shen, H., Balderas, I., Britt, J.P., Marino, R.A.M., Chung, S.L., Richie, C.T., Harvey, B.K., Bonci, A., 2014b. Serotonergic versus non-serotonergic dorsal raphe projection neurons: differential participation in reward circuitry. Cell Rep. 8, 1857–1869. https://doi.org/10.1016/j.jacc.2007.01.076.White
Michalski, A., Gerstein, G.L., Czarkowska, J., Tarnecki, R., 1983. Interactions between cat striate cortex neurons. Exp. Brain Res. 51, 97–107.
Michelsen, K.A., Schmitz, C., Steinbusch, H.W.M., 2007. The dorsal raphe nucleus-From silver stainings to a role in depression. Brain Res. Rev. 55, 329–342. https://doi.org/10.1016/j.brainresrev.2007.01.002
Mihaela Macri, B., Jacquin, T.D., Flonta, M.-L., 2006. Electrophysiological Properties of Dorsal Raphe Nucleus Neurons in 5-Htt +/+ and 5-Htt –/– Mice. Rom. J. Biophys 16, 111–124.
Mitra, P.P., Pesaran, B., 1999. Analysis of dynamic brain imaging data. Biophys. J. 76, 691–708.
Mlinar, B., Montalbano, A., Piszczek, L., Gross, C., Corradetti, R., 2016. Firing Properties of Genetically Identified Dorsal Raphe Serotonergic Neurons in Brain Slices. Front. Cell. Neurosci. 10, 195. https://doi.org/10.3389/fncel.2016.00195
Monti, J.M., 2010. The role of dorsal raphe nucleus serotonergic and non-serotonergic neurons, and of their receptors, in regulating waking and rapid eye movement (REM) sleep. Sleep Med. Rev. 14, 319–327. https://doi.org/10.1016/j.smrv.2009.10.003
Morales, M., Margolis, E.B., 2017. Ventral tegmental area: cellular heterogeneity, connectivity and behaviour. Nat. Rev. Neurosci. 18, 73.
Moran, R.J., Kishida, K.T., Lohrenz, T., Saez, I., Laxton, A.W., Witcher, M.R., Tatter, S.B., Ellis, T.L., Phillips, P.E.M., Dayan, P., 2018. The protective action encoding of serotonin transients in the human brain. Neuropsychopharmacology 43, 1425–1435.
Müller, Christian P., B.L.J., 2010. Handbook Of Behavioral Neuroscience, Handbook of Behavioral Neuroscience. https://doi.org/10.1016/S1569-7339(08)00237-3
Muller, C.P., Cunningham, K.A., 2020. Handbook of the behavioral neurobiology of serotonin. Academic Press.
Muller, C.P., Jacobs, B., 2009. Handbook of the Behavioral Neurobiology of Serotonin, Handbook of Behavioral Neuroscience.
Muzerelle, A., Scotto-Lomassese, S., Bernard, J.F., Soiza-Reilly, M., Gaspar, P., 2016. Conditional anterograde tracing reveals distinct targeting of individual serotonin cell groups (B5-B9) to the forebrain and brainstem. Brain Struct. Funct. 221, 535–561. https://doi.org/10.1007/s00429-014-0924-4
Nazari, M.A., Berquin, P., Missonnier, P., Aarabi, A., Debatisse, D., De Broca, A., Wallois, F.,

2010. Visual sensory processing deficit in the occipital region in children with attention-deficit/hyperactivity disorder as revealed by event-related potentials during cued continuous performance test. Neurophysiol. Clin. Neurophysiol. 40, 137–149. https://doi.org/https://doi.org/10.1016/j.neucli.2010.03.001

Nichols, T., Hayasaka, S., 2003. Controlling the familywise error rate in functional neuroimaging: a comparative review. Stat. Methods Med. Res. 12, 419–446. https://doi.org/10.1191/0962280203sm341ra

Niederkofler, V., Asher, T.E., Dymecki, S.M., 2015. Functional interplay between dopaminergic and serotonergic neuronal systems during development and adulthood. ACS Chem Neurosci 6 (7): 1055–1070.

Niederkofler, V., Asher, T.E., Okaty, B.W., Rood, B.D., Narayan, A., Hwa, L.S., Beck, S.G., Miczek, K.A., Dymecki, S.M., 2016. Identification of serotonergic neuronal modules that affect aggressive behavior. Cell Rep. 17, 1934–1949.

Nylen, E.L., Wallisch, P., 2017. Neural Data Science: A Primer with MATLAB® and PythonTM. Academic Press.

Ogawa, S.K., Cohen, J.Y., Hwang, D., Uchida, N., Watabe-Uchida, M., 2014. Organization of monosynaptic inputs to the serotonin and dopamine neuromodulatory systems. Cell Rep. 8, 1105–1118.

Ogawa, S.K., Watabe-Uchida, M., 2018. Organization of dopamine and serotonin system: Anatomical and functional mapping of monosynaptic inputs using rabies virus. Pharmacol. Biochem. Behav. 174, 9–22.

Ohno, Y., Shimizu, S., Tokudome, K., Kunisawa, N., Sasa, M., 2015. New insight into the therapeutic role of the serotonergic system in Parkinson's disease. Prog. Neurobiol. 134, 104–121.

Okaty, B.W., Commons, K.G., Dymecki, S.M., 2019. Embracing diversity in the 5-HT neuronal system. Nat. Rev. Neurosci. 20, 397–424. https://doi.org/10.1038/s41583-019-0151-3

Pachitariu, M., Steinmetz, N., Kadir, S., Carandini, M., Kenneth D., H., 2016. Kilosort: realtime spike-sorting for extracellular electrophysiology with hundreds of channels. bioRxiv 61481. https://doi.org/10.1101/061481

Palacios, J.M., 2016. Serotonin receptors in brain revisited. Brain Res. 1645, 46–49. https://doi.org/10.1016/j.brainres.2015.12.042

Perkel, D.H., Gerstein, G.L., Moore, G.P., 1967. Neuronal spike trains and stochastic point processes: II. Simultaneous spike trains. Biophys. J. 7, 419–440.

Pinault, D., 1996. A novel single-cell staining procedure performed in vivo under electrophysiological control: morpho-functional features of juxtacellularly labeled thalamic cells and other central neurons with biocytin or Neurobiotin. J. Neurosci. Methods 65, 113–136.

Pollak Dorocic, I., Fürth, D., Xuan, Y., Johansson, Y., Pozzi, L., Silberberg, G., Carlén, M., Meletis, K., 2014. A Whole-Brain Atlas of Inputs to Serotonergic Neurons of the Dorsal and Median Raphe Nuclei. Neuron 83, 663–678. https://doi.org/https://doi.org/10.1016/j.neuron.2014.07.002

Pollock, E., Jazayeri, M., 2020. Engineering recurrent neural networks from task-relevant manifolds and dynamics. PLOS Comput. Biol. 16, e1008128.

Prouty, E.W., Chandler, D.J., Waterhouse, B.D., 2017. Neurochemical differences between target-specific populations of rat dorsal raphe projection neurons. Brain Res. 1675, 28–40.

Puig, M.V., Gulledge, A.T., 2011. Serotonin and Prefrontal Cortex Function: Neurons, Networks, and Circuits. Mol. Neurobiol. 44, 449–464. https://doi.org/10.1007/s12035-011-8214-0

Puig, M.V., Watakabe, A., Ushimaru, M., Yamamori, T., Kawaguchi, Y., 2010. Serotonin Modulates Fast-Spiking Interneuron and Synchronous Activity in the Rat Prefrontal Cortex through 5-HT_{1A} and 5-HT_{2A} Receptors. J. Neurosci. 30, 2211 LP – 2222. https://doi.org/10.1523/JNEUROSCI.3335-09.2010

Puig, M. V, Artigas, F., Celada, P., 2005. Modulation of the activity of pyramidal neurons in rat prefrontal cortex by raphe stimulation in vivo: Involvement of serotonin and GABA. Cereb. Cortex 15, 1–14. https://doi.org/10.1093/cercor/bhh104

Ranade, S.P., Mainen, Z.F., 2009. Transient firing of dorsal raphe neurons encodes diverse and specific sensory, motor, and reward events. J. Neurophysiol. 102, 3026–3037. https://doi.org/10.1152/jn.00507.2009

Ren, J., Friedmann, D., Xiong, J., Liu, C.D., Ferguson, B.R., Weerakkody, T., DeLoach, K.E., Ran, C., Pun, A., Sun, Y., 2018. Anatomically defined and functionally distinct dorsal raphe serotonin sub-systems. Cell 175, 472–487.

Ren, J., Isakova, A., Friedmann, D., Zeng, J., Grutzner, S.M., Pun, A., Zhao, G.Q., Kolluru, S.S., Wang, R., Lin, R., 2019. Single-cell transcriptomes and whole-brain projections of serotonin neurons in the mouse dorsal and median raphe nuclei. Elife 8, e49424.

Renart, A., Brunel, N., Wang, X.-J., 2004. Mean-field theory of irregularly spiking neuronal populations and working memory in recurrent cortical networks. Comput. Neurosci. A Compr. approach 431–490.

Richards, C.D., Shiroyama, T., Kitai, S.T., 1997. Electrophysiological and immunocytochemical characterization of GABA and dopamine neurons in the substantia nigra of the rat. Neuroscience 80, 545–557. https://doi.org/10.1016/S0306-4522(97)00093-6

Ritter, J., Lewis, L., Mant, T., Ferro, A., 2008. A textbook of clinical pharmacology and therapeutics. CRC Press.

Rosenberg, J.R., Amjad, A.M., Breeze, P., Brillinger, D.R., Halliday, D.M., 1989. The Fourier approach to the identification of functional coupling between neuronal spike trains. Prog. Biophys. Mol. Biol. 53, 1–31. https://doi.org/10.1016/0079-6107(89)90004-7

Ross A McDevitt and John F Neumaier, 2011. Regulation of dorsal raphe nucleus function by serotonin autoreceptors: a behavioral perspective. J chem Neuroanat 41, 234–246. https://doi.org/10.1109/TMI.2012.2196707.Separate

Rossant, C., Kadir, S.N., Goodman, D.F.M., Schulman, J., Hunter, M.L.D., Saleem, A.B., Grosmark, A., Belluscio, M., Denfield, G.H., Ecker, A.S., Tolias, A.S., Solomon, S., Buzski, G., Carandini, M., Harris, K.D., 2016. Spike sorting for large, dense electrode arrays. Nat. Neurosci. 19, 634–641. https://doi.org/10.1038/nn.4268

Roth, B.L., 2016. DREADDs for neuroscientists. Neuron 89, 683–694.

Sakai, K., 2011. Sleep-waking discharge profiles of dorsal raphe nucleus neurons in mice. Neuroscience 197, 200–224.

Samaranayake, S., Abdalla, A., Robke, R., Nijhout, H.F., Reed, M.C., Best, J., Hashemi, P., 2016. A voltammetric and mathematical analysis of histaminergic modulation of serotonin in the mouse hypothalamus. J. Neurochem. 138, 374–383.

Saulin, A., Savli, M., Lanzenberger, R., 2012. Serotonin and molecular neuroimaging in humans using PET. Amino Acids 42, 2039–2057.

Scarr, E., Gibbons, A.S., Neo, J., Udawela, M., Dean, B., 2013. Cholinergic connectivity: it's implications for psychiatric disorders. Front. Cell. Neurosci. 7, 55.

Scheffel, U., Dannals, R.F., Suehiro, M., Ricaurte, G.A., Carroll, F.I., Kuhar, M.J., Wagner Jr, H.N., 1994. Development of PET/SPECT ligands for the serotonin transporter. NIDA Res. Monogr. 138, 111.

Schultz, W., Dayan, P., Montague, P.R., 1997. A neural substrate of prediction and reward. Science 275, 1593–1599.

Schweimer, J. V., Mallet, N., Sharp, T., Ungless, M.A., 2011. Spike-timing relationship of neurochemically-identified dorsal raphe neurons during cortical slow oscillations. Neuroscience 196, 115–123. https://doi.org/10.1016/j.neuroscience.2011.08.072

Sengupta, A., Bocchio, M., Bannerman, D.M., Sharp, T., Capogna, M., 2017. Control of amygdala circuits by 5-HT neurons via 5-HT and glutamate cotransmission. J. Neurosci. 37, 1785–1796.

Sharp, T., Barnes, N.M., 2020. Central 5-HT receptors and their function; present and future. Neuropharmacology 108155.
Shaw, J.C., 1981. An introduction to the coherence function and its use in EEG signal analysis. J. Med. Eng. Technol. 5, 279–288. https://doi.org/10.3109/03091908109009362
Shea-Brown, E., Josić, K., De La Rocha, J., Doiron, B., 2008. Correlation and synchrony transfer in integrate-and-fire neurons: basic properties and consequences for coding. Phys. Rev. Lett. 100, 108102.
Siegle, J.H., Lopez, A.C., Patel, Y.A., Abramov, K., Ohayon, S., Voigts, J., 2017. Open Ephys: an open-source, plugin-based platform for multichannel electrophysiology. J. Neural Eng. 14, 45003. https://doi.org/10.1088/1741-2552/aa5eea
Smythies, J., 2005. Section V. Serotonin system. Int. Rev. Neurobiol. 64, 217–268.
Snyder, A.C., Morais, M.J., Willis, C.M., Smith, M.A., 2015. Global network influences on local functional connectivity. Nat. Neurosci. 18, 736–743.
Spies, M., Knudsen, G.M., Lanzenberger, R., Kasper, S., 2015. The serotonin transporter in psychiatric disorders: insights from PET imaging. The Lancet Psychiatry 2, 743–755.
Sprouse, J., Reynolds, L., Braselton, J., Schmidt, A., 2004. Serotonin-induced phase advances of SCN neuronal firing in vitro: a possible role for 5-HT5A receptors? Synapse 54, 111–118. https://doi.org/10.1002/syn.20070
Sprouse, J.S., Aghajanian, G.K., 1987. Electrophysiological responses of serotoninergic dorsal raphe neurons to 5-HT1A and 5-HT1B agonists. Synapse 1, 3–9. https://doi.org/10.1002/syn.890010103
Srejic, L.R., Wood, K.M., Zeqja, A., Hashemi, P., Hutchison, W.D., 2016. Modulation of serotonin dynamics in the dorsal raphe nucleus via high frequency medial prefrontal cortex stimulation. Neurobiol. Dis. 94, 129–138. https://doi.org/10.1016/j.nbd.2016.06.009
Stauffer, W.R., Lak, A., Yang, A., Borel, M., Paulsen, O., Boyden, E.S., Schultz, W., 2016. Dopamine neuron-specific optogenetic stimulation in rhesus macaques. Cell 166, 1564–1571.
Steffensen, S.C., Svingos, A.L., Pickel, V.M., Henriksen, S.J., 1998. Electrophysiological characterization of GABAergic neurons in the ventral tegmental area. J. Neurosci. 18, 8003–8015.
Steffensen, S.C., Walton, C.H., Hansen, D.M., Yorgason, J.T., Gallegos, R.A., Criado, J.R., 2009. Contingent and non-contingent effects of low-dose ethanol on GABA neuron activity in the ventral tegmental area. Pharmacol. Biochem. Behav. 92, 68–75.
Steriade, M., 2000. Corticothalamic resonance, states of vigilance and mentation. Neuroscience 101, 243–276. https://doi.org/10.1016/S0306-4522(00)00353-5
Strogatz, S.H., 2018. Nonlinear dynamics and chaos with student solutions manual: With applications to physics, biology, chemistry, and engineering. CRC press.
Szeitz, A., Bandiera, S.M., 2018. Analysis and measurement of serotonin. Biomed. Chromatogr. 32, e4135.
Tan, K.R., Yvon, C., Turiault, M., Mirzabekov, J.J., Doehner, J., Labouèbe, G., Deisseroth, K., Tye, K.M., Lüscher, C., 2012. GABA Neurons of the VTA Drive Conditioned Place Aversion. Neuron 73, 1173–1183. https://doi.org/10.1016/j.neuron.2012.02.015
Taylor, N.E., Pei, J., Zhang, J., Vlasov, K.Y., Davis, T., Taylor, E., Weng, F.-J., Van Dort, C.J., Solt, K., Brown, E.N., 2019. The role of glutamatergic and dopaminergic neurons in the periaqueductal gray/Dorsal raphe: separating analgesia and anxiety. Eneuro 6.
Thévenot, E., Côté, F., Colin, P., He, Y., Leblois, H., Perricaudet, M., Mallet, J., Vodjdani, G., 2003. Targeting conditional gene modification into the serotonin neurons of the dorsal raphe nucleus by viral delivery of the Cre recombinase. Mol. Cell. Neurosci. 24, 139–147. https://doi.org/10.1016/S1044-7431(03)00131-3
Tian, J., Huang, R., Cohen, J.Y., Osakada, F., Kobak, D., Machens, C.K., Callaway, E.M., Uchida, N., Watabe-Uchida, M., 2016. Distributed and mixed information in monosynaptic inputs to

dopamine neurons. Neuron 91, 1374–1389.
Totah, N.K., Neves, R.M., Panzeri, S., Logothetis, N.K., Eschenko, O., 2018. The Locus Coeruleus Is a Complex and Differentiated Neuromodulatory System. Neuron 99, 1055-1068.e6. https://doi.org/10.1016/j.neuron.2018.07.037
Trudeau, L.-E., El Mestikawy, S., 2018. Glutamate cotransmission in cholinergic, GABAergic and monoamine systems: contrasts and commonalities. Front. Neural Circuits 12, 113.
Tuckwell, H.C., Penington, N.J., 2014. Computational modeling of spike generation in serotonergic neurons of the dorsal raphe nucleus. Prog. Neurobiol. 118, 59–101. https://doi.org/10.1016/j.pneurobio.2014.04.001
und Halbach, O. von B., Dermietzel, R., 2006. Neurotransmitters and neuromodulators: Handbook of receptors and biological effects. John Wiley & Sons.
Ungless, M.A., Magill, P.J., Bolam, J.P., 2004. Uniform inhibition of dopamine neurons in the ventral tegmental area by aversive stimuli. Science (80-.). 303, 2040–2042.
Valencia-Torres, L., Olarte-Sanchez, C.M., Lyons, D.J., Georgescu, T., Greenwald-Yarnell, M., Myers, M.G.J., Bradshaw, C.M., Heisler, L.K., 2017. Activation of Ventral Tegmental Area 5-HT2C Receptors Reduces Incentive Motivation. Neuropsychopharmacology 42, 1511–1521. https://doi.org/10.1038/npp.2016.264
Visser, A.K.D., van Waarde, A., Willemsen, A.T.M., Bosker, F.J., Luiten, P.G.M., den Boer, J.A., Kema, I.P., Dierckx, R.A.J.O., 2011. Measuring serotonin synthesis: from conventional methods to PET tracers and their (pre) clinical implications. Eur. J. Nucl. Med. Mol. Imaging 38, 576–591.
Wang, D.-H., Wong-Lin, K., 2013. Comodulation of dopamine and serotonin on prefrontal cortical rhythms: a theoretical study. Front. Integr. Neurosci. 7, 1–19. https://doi.org/10.3389/fnint.2013.00054
Wang, H.L., Zhang, S., Qi, J., Wang, H., Cachope, R., Mejias-Aponte, C.A., Gomez, J.A., Mateo-Semidey, G.E., Beaudoin, G.M.J., Paladini, C.A., Cheer, J.F., Morales, M., 2019. Dorsal Raphe Dual Serotonin-Glutamate Neurons Drive Reward by Establishing Excitatory Synapses on VTA Mesoaccumbens Dopamine Neurons. Cell Rep. 26, 1128-1142.e7. https://doi.org/10.1016/j.celrep.2019.01.014
Warden, M.R., Selimbeyoglu, A., Mirzabekov, J.J., Lo, M., Thompson, K.R., Kim, S.-Y., Adhikari, A., Tye, K.M., Frank, L.M., Deisseroth, K., 2012. A prefrontal cortex-brainstem neuronal projection that controls response to behavioural challenge. Nature 492, 428–432. https://doi.org/10.1038/nature11617
Watabe-Uchida, M., Eshel, N., Uchida, N., 2017. Neural Circuitry of Reward Prediction Error. Annu. Rev. Neurosci. 40, 373–394. https://doi.org/10.1146/annurev-neuro-072116-031109
Watabe-Uchida, M., Zhu, L., Ogawa, S.K., Vamanrao, A., Uchida, N., 2012. Whole-brain mapping of direct inputs to midbrain dopamine neurons. Neuron 74, 858–873.
Weissbourd, B., Ren, J., DeLoach, K.E., Guenthner, C.J., Miyamichi, K., Luo, L., 2014. Presynaptic partners of dorsal raphe serotonergic and GABAergic neurons. Neuron 83, 645–662.
Whitacre, J.M., 2010. Degeneracy: A link between evolvability, robustness and complexity in biological systems. Theor. Biol. Med. Model. 7, 1–17. https://doi.org/10.1186/1742-4682-7-6
Wilson, H.R., Cowan, J.D., 1973. A mathematical theory of the functional dynamics of cortical and thalamic nervous tissue. Kybernetik 13, 55–80.
Wilson, H.R., Cowan, J.D., 1972. Excitatory and inhibitory interactions in localized populations of model neurons. Biophys. J. 12, 1–24. https://doi.org/10.1016/S0006-3495(72)86068-5
Wittmann, M.K., Fouragnan, E., Folloni, D., Klein-Flügge, M.C., Chau, B.K.H., Khamassi, M., Rushworth, M.F.S., 2020. Global reward state affects learning and activity in raphe nucleus and anterior insula in monkeys. Nat. Commun. 11, 1–17.
Wong-Lin, K., Joshi, A., Prasad, G., McGinnity, T.M., 2012. Network properties of a computational model of the dorsal raphe nucleus. Neural Networks 32, 15–25.

https://doi.org/10.1016/j.neunet.2012.02.009
Wong-Lin, K., Prasad, G., McGinnity, T.M., 2011. A spiking neuronal network model of the dorsal raphe nucleus, in: The 2011 International Joint Conference on Neural Networks. pp. 1591–1598. https://doi.org/10.1109/IJCNN.2011.6033414
Wong-Lin, K., Wang, D.-H., Moustafa, A.A., Cohen, J.Y., Nakamura, K., 2017. Toward a multiscale modeling framework for understanding serotonergic function. J. Psychopharmacol. 026988111769961. https://doi.org/10.1177/0269881117699612
Wong, K.-F., Wang, X.-J., 2006. A recurrent network mechanism of time integration in perceptual decisions. J. Neurosci. 26, 1314–1328.
Xu, P., He, Y., Cao, X., Valencia-Torres, L., Yan, X., Saito, K., Wang, C., Yang, Y., Hinton Jr, A., Zhu, L., 2017. Activation of serotonin 2C receptors in dopamine neurons inhibits binge-like eating in mice. Biol. Psychiatry 81, 737–747.
Yamaguchi, T., Qi, J., Wang, H., Zhang, S., Morales, M., 2015. Glutamatergic and dopaminergic neurons in the mouse ventral tegmental area. Eur. J. Neurosci. 41, 760–772.
Yang, H., Thompson, A.B., McIntosh, B.J., Altieri, S.C., Andrews, A.M., 2013. Physiologically relevant changes in serotonin resolved by fast microdialysis. ACS Chem. Neurosci. 4, 790–798.
Yegenoglu, A., Denker, M., Grun, S., Phan, L.D., Davison, A., Holstein, D., 2015. Elephant - Open-Source Tool for the Analysis of Electrophysiological Data Sets, in: INM Retreat 2015. 17 Sep 2015 - 18 Sep 2015, Juelich (Germany), p. 26.
Zhang, F., Tsai, H.-C., Airan, R.D., Stuber, G.D., Adamantidis, A.R., de Lecea, L., Bonci, A., Deisseroth, K., 2015. Optogenetics in freely moving mammals: dopamine and reward. Cold Spring Harb. Protoc. 2015, pdb-top086330.
Zhong, W., Li, Y., Feng, Q., Luo, M., 2017. Learning and stress shape the reward response patterns of serotonin neurons. J. Neurosci. 37, 8863–8875.
Zhou, H., Wong-Lin, K., Wang, D.-H., 2018. Parallel Excitatory and Inhibitory Neural Circuit Pathways Underlie Reward-Based Phasic Neural Responses. Complexity 2018.